PERFORMANCE ENHANCEMENT OF MICROWAVE DEVICES USING METAMATERIAL BASED SUB-WAVELENGTH RESONATORS

S. S. Karthikeyan

PERFORMANCE ENHANCEMENT OF MICROWAVE DEVICES USING METAMATERIAL BASED SUB-WAVELENGTH RESONATORS

A

Thesis submitted

for the award of the degree of

DOCTOR OF PHILOSOPHY

By

S. S. KARTHIKEYAN

DEPARTMENT OF ELECTRONICS AND ELECTRICAL ENGINEERING

INDIAN INSTITUTE OF TECHNOLOGY GUWAHATI

GUWAHATI - 781 039, ASSAM, INDIA

JUNE 2011

Certificate

This is to certify that the thesis entitled "**PERFORMANCE ENHANCEMENT OF MICROWAVE DEVICES USING METAMATERIAL BASED SUB-WAVELENGTH RESONATORS**", submitted by **S. S. Karthikeyan** (06610207), a research scholar in the *Department of Electronics and Electrical Engineering, Indian Institute of Technology Guwahati*, for the award of the degree of **Doctor of Philosophy**, is a record of an original research work carried out by him under my supervision and guidance. The thesis has fulfilled all requirements as per the regulations of the institute and in my opinion has reached the standard needed for submission. The results embodied in this thesis have not been submitted to any other University or Institute for the award of any degree or diploma.

Dated: 16.06.2011
Guwahati.

Dr. Rakhesh Singh Kshetrimayum
Associate Professor
Dept. of Electronics and Electrical Engg.
Indian Institute of Technology Guwahati
Guwahati - 781 039, Assam, India.

To

My dear parents

S. K. Subramanian and S. Gomathi

for their love and support

&

My wife

M. Arulvani

for her encouragement

&

My guide

Dr. Rakhesh Singh Kshetrimayum

for his guidance and inspiration

Acknowledgements

First and foremost, I feel it as a great privilege in expressing my deepest and most sincere gratitude to my supervisor Dr. Rakhesh Singh Kshetrimayum, for his excellent guidance throughout my study. His kindness, dedication, hard work and attention to detail have been a great inspiration to me. My heartfelt thanks to you sir for the unlimited support and patience shown to me. I would particularly like to thank him for all his help in patiently and carefully correcting all my manuscripts. I have no doubts that finishing my degree in a proper and timely manner was impossible without his helps, suggestions and advices.

I am also very thankful to my doctoral committee members Professor P. K. Bora, Dr. R. Bhattacharjee and Dr. P. R. Sahu for sparing their precious time to evaluate the progress of my work. I express my heartfelt thanks to Prof. A. Mahanta and Dr. Roy Paily for the guidance and support given to me in this work.

I would also like to thank the Head of the Department and the other faculty members for their kind help in carrying out this work. I am also grateful to all the members of the research and technical staff of the department without whose help I could not have completed this thesis. My special thanks to Mr. L. N. Sharma, Mr. U. K. Sarma and Mr. Sanjib Das for helping me for fabrication and measurement work during my research period.

My special thanks go to my friend Vinoth Kumar, who encouraged me to join in IIT for my research work. My friends at IITG made my life joyful and were constant source of encouragement. I have no words to express my thanks to most important persons C. Shyam Anand, Krishnamoorthy, D. Senthil Kumar, Padam Priyal, Ashoke and Sabarimalai Manikandan. My work in this remote place definitely would not be possible without their love and care that helped me to enjoy my new life in this IITG. I extremely thankful to Utkal sir, Yogi madam, Nirmala madam and Jayanna sir for the care shown and the help given to me during my stay at IITG.

My special thanks go to, Himanshu Katiyar, Dakuva, Rupaban sir, Narasimahamurthy sir, Ahmad Ali, Panda, Sanjay Mondal, Pradhan, Rajib, Kuntal, Govind, Haris, and Mishra sir for their help and the care shown during my stay.

I thank all my fellow research students and M. Tech students for their cooperation. During these four years at IITG I have had several friends that have helped me in several ways, I would like to say a big thank you to all of them for their friendship and support.

My deepest gratitude goes to my family for their continuous love and support throughout my studies. The opportunities that they have given me and their unlimited sacrifices are the reasons where I am and what I have accomplished so far.

Finally, I believe this research experience will greatly benefit my career in the future.

S. S. Karthikeyan

Abstract

Metamaterials are new artificial materials with unusual electromagnetic properties, not commonly found in nature. All natural materials have positive magnetic permeability and electric permittivity. In contrast, in metamaterials they are negative. Using these exotic properties, several high performance microwave devices/components have been developed by many researchers across the globe. In our study, many size miniaturized and performance enhanced planar microwave devices/circuits employing metamaterial based subwavelength resonators viz. complementary split ring resonator (CSRR), open slot split ring resonator (OSSRR) and open complementary split ring resonator (OCSRR) were designed, fabricated, tested and are listed below.

- Various wide bandstop filters using complementary split ring resonator (CSRR), open stub and spurline are designed and used for harmonic suppression of lowpass and bandpass filters.
- A complementary single split ring resonator (CSSRR) is used to develop a band notched ultra wideband (UWB) bandpass filter, designed using ground plane aperture technique. To filter out the undesired wireless local area network (WLAN) signals, a CSSRR is placed under the coupled lines of bandpass filter. Thus, any unwanted signals (i.e., IEEE 802.11a frequency band) that may interfere with the desired UWB frequency range are effectively removed.
- An OSSRR is introduced for the first time to realize a composite right/left handed (CRLH) transmission line (TL) structure in microstrip technology. The CRLH line is synthesized by etching OSSRR in the ground plane and interdigital capacitor in the microstrip line. The proposed method of realization of CRLH TL results in size reduction compared with the conventional CSRR based TL.
- A compact lowpass filter is constructed using periodic array of OSSRR and open stubs. Open stubs are attached on both sides of the OSSRR. The proposed filter

has sharp rejection characteristics and compact size compared with the conventional stepped impedance lowpass filter.

- A compact, wide fractional bandwidth bandpass filter, using a new resonator OSSRR and compact microstrip resonating cell (CMRC) is presented. The designed BPF has a wide fractional bandwidth of 74%, sharp passband to stopband transition, and low passband insertion loss of less than 1 dB .
- Design of a compact lowpass filter using an OCSRR and an open stub is presented. The proposed lowpass filter consists of two OCSRR connected in series with the open stubs attached on either side. At the 3 dB cut-off frequency of 1 GHz, the proposed filter offers a sharp and wide rejection bandwidth of more than 20 dB, up to six times the cut-off frequency.
- The size of the lowpass filter designed using OCSRR and open stub is further reduced by replacing the open stubs with the defected ground structures. A size miniaturized lowpass filter is designed using two cell OCSRRs connected in series and dumbbell shaped DGS placed below the OCSRRs. The proposed filter size is very small and its rejection band is up to ten times the cut-off frequency.
- By utilizing the slow-wave effect of OCSRR, size miniaturized and third harmonic suppressed T-junction power divider is designed. The proposed power divider is 47% smaller than the conventional design.
- A compact and harmonic suppressed 180^0 ring hybrid is proposed using OCSRR. It offers third harmonic suppression up to 35 dB and is 37% smaller than the conventional ring hybrid.

Contents

List of Figures

List of Tables

List of Acronyms

BLC	Branch Line Coupler
BPF	Bandpass Filter
BWM	Backward wave Material
CMRC	Compact Microstrip Resonating Cell
CPW	Co-planar Waveguide
CRLH	Composite Right/Left Handed
CSR	Complementary Spiral Resonator
CSRR	Complementary Split Ring Resonator
DGS	Defected Ground Structure
DGP	Defected Ground Plane
DNG	Double Negative
DPS	Double Positive
EBG	Electromagnetic Bandgap Structures
ENG	Epsilon Negative
FCC	Federal Communication Commission
FBW	Fractional Bandwidth
HPF	Highpass Filter
LHM	Left Handed Material
LPF	Lowpass Filter
MNG	Mu Negative
MTM	Metamaterial
NIM	Negative Index Material
OCSRR	Open Complementary Split Ring Resonator
OSRR	Open Split Ring Resonator

OSSRR	Open Slot Split Ring Resonator
PBG	Photonic Bandgap Structures
PCML	Parallel Coupled Microstrip Line
SNG	Single Negative Material
SR	Spiral resonator
SRR	Split Ring Resonator
TL	Transmission Line
UWB	Ultra Wide Band
WLAN	Wireless Local Area Network

1

Introduction

Contents

1.1 Introduction

Present day RF/microwave wireless communication systems increasingly require, microwave devices with smaller size and improved performance. Over the past decade, several researchers have attempted to reduce the size and improve the performance of various planar microwave devices. In recent years, the use of metamaterial based resonators and transmission lines has been the alternative approach to obtain size miniaturization and performance enhancement of microwave components. Metamaterials are artificial materials with unusual electromagnetic properties. They have both negative electric permittivity (ε) and negative magnetic permeability (μ) that are not observed in naturally occurring materials. The past few years have been momentous for the development of concepts and applications of metamaterials.

Metamaterials were theoretically postulated by a Russian scientist, Viktor Veselago, in 1967 [1]. He investigated the electromagnetic wave propagation in such materials and their properties. According to Maxwell′s equations, the direction of energy flow of a plane wave is given by the direction of the Poynting vector. The Poynting vector is the cross product of electric field **E** and magnetic field **H**. For plane waves propagating in a regular medium, the cross product of electric field **E** and magnetic field **H** gives the direction of energy flow, and it is in same direction with that of the wave vector (**k**). The vectors **E**, **H** and **k** follow the right-hand rule. However, Veselago predicted that in a metamaterial medium, the Poynting vector direction is opposite to that of the direction of wave propagation, which indicates that $\mathbf{E} \times \mathbf{H}$ gives the direction of energy flow, and the phase velocity (wave vector) is opposite to that of energy flow. The electric field vector, magnetic field vector and wave vector form a left-handed triplet. In addition to these left-handed (LH) characteristics, other unusual properties of metamaterials are the reversal of Snell′s law, reverse Doppler effect and reverse Cerenkov effect. However, experimental verification of such materials with the simultaneously negative ε and μ was achieved only three decades later. The first particle that exhibits negative permittivity by decreasing the plasmon frequency into microwave range was proposed in [2]. Shortly after that, a particle called split ring resonator (SRR), which provided negative permeability at microwave frequencies was introduced [3]. By combining these two structures, the existence of LH metamaterial was experimentally proved in 2001 [4]. With these new artificial materials, new kinds of miniaturized antennas and microwave components/devices can be created for the RF/wireless application. In metamaterials, the wave propagation is opposite to that of energy flow. Hence metamaterials are also

known as left-handed materials (LHM) or backward-wave materials (BWM). The metamaterials can also be termed as negative index materials (NIM), since the refractive index is negative, or as double negative material (DNM) because both ε and μ are negative.

1.2 Electromagnetic metamaterials

Any material response to applied electromagnetic energy can be characterized by its magnetic permeability and electric permittivity. In metamaterials, these two material properties are negative. Electromagnetic metamaterials are defined as artificial, effectively homogeneous electromagnetic structures with unusual properties not readily available in nature [5]. An effectively homogeneous structure is a structure with average cell size much smaller than the guided wavelength. If the condition of effective homogeneity is satisfied, the structure behaves as a real material and has the same constitutive parameters, defined as the permittivity ε and the permeability μ, which are related to the refractive index n by,

$$n = \pm\sqrt{\varepsilon_r \mu_r} \tag{1.1}$$

where ε_r and μ_r are the relative permittivity and permeability related to the free space permittivity and permeability. From equation (1.1) it can be observed that there are four possible sign combinations for ε_r and μ_r, (+ +), (+ -), (- +) and (- -). A medium with positive permittivity and permeability (ε_r, μ_r >0), which constitutes most naturally occurring media (e.g., dielectrics) is called a double positive (DPS) medium. A medium with positive permittivity and negative permeability ($\varepsilon_r > 0$, $\mu_r < 0$), (e.g., ferrimagnetic materials) is called mu-negative (MNG) medium. A medium with negative permittivity and positive permeability ($\varepsilon_r < 0$, $\mu_r > 0$) is referred as epsilon negative (ENG) medium. The medium with simultaneously negative permittivity and negative permeability ($\varepsilon_r < 0$, $\mu_r < 0$) is called as double negative medium (DNG) or left-handed (LH) material. The graphical representation of the above properties is shown in Fig. 1.1.

1.2.1 Wave propagation in left-handed medium

The four Maxwells equations which describe the electromagnetic wave are

$$\nabla \bullet \mathbf{D} = \rho_v \tag{1.2}$$

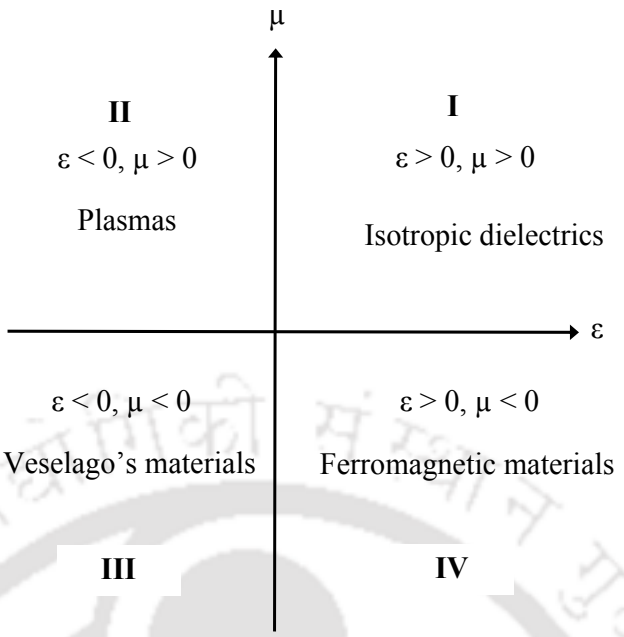

Figure 1.1: Permittivity-permeability and refractive index diagram.

$$\nabla \bullet \mathbf{B} = 0 \tag{1.3}$$

$$\nabla \times \mathbf{E} = -\frac{\partial \mathbf{B}}{\partial t} \tag{1.4}$$

$$\nabla \times \mathbf{H} = J + \frac{\partial \mathbf{D}}{\partial t} \tag{1.5}$$

for a plane monochromatic wave, the last two equations can take the form

$$k \times \mathbf{E} = \frac{\omega}{c}\mu \mathbf{H} \tag{1.6}$$

$$k \times \mathbf{H} = -\frac{\omega}{c}\varepsilon \mathbf{E} \tag{1.7}$$

It can be seen from the equation that if $\varepsilon_r > 0$ and $\mu_r > 0$ then **E**, **H** and **k** form a right-handed triplet of vectors and if $\varepsilon_r < 0$ and $\mu_r < 0$ they from a left-handed triplet. In left-handed medium, the permittivity and permeability are negative and the phase velocity will be anti-parallel to the direction

of wave propagation or energy flow; in other words the wave has a negative phase velocity in that medium. Since the direction of energy flow is always from the transmitter to the receiver, the phase moves in the opposite direction. As illustrated in Figure 1.2 in a right-handed medium, the Poynting vector (**S**) and wave vector (**k**) both are in the same direction. But in left-handed medium, these two vectors are antiparallel to each other.

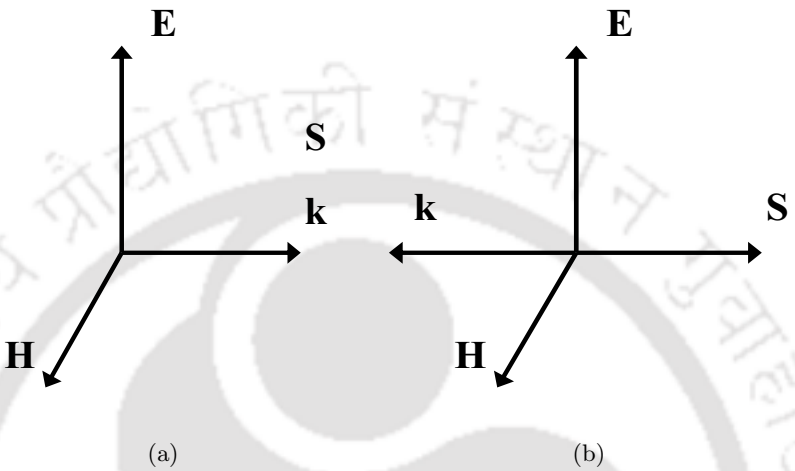

Figure 1.2: The wave propagation in a) Right-handed medium b) Left-handed medium.

1.2.2 Experimental verification of metamaterial

Following Veselago's prediction, it took more than 30 years to experimentally verify the existence of metamaterials. In 1996, J. B. Pendry [2] introduced the plasmonic type negative ε / positive μ structure consists of a mesh of very thin metal wires arranged in a periodic lattice as shown in Fig. 1.3(b). If the excitation electric field is parallel to the axis of the wires, this structure exhibits negative permittivity. Further, he proposed another structure known as split ring resonator that exhibits positive ε / negative μ when excited by magnetic field. Fig. 1.3(b) shows the array of SRR structure exhibiting negative permeability. Inspired by Pendry's work, the first left-handed material was proposed by Smith and colleagues at University of California, San Diego, which simultaneously exhibited negative permittivity and negative permeability. It is a combination of Pendry's two structures, metal wires and SRRs. In 2001, R.A. Shelby and colleagues proposed the two dimensional left-handed metamaterials and experimentally verified the negative refraction. The structure developed by these authors consisted of a square shaped SRR printed on one side of the dielectric substrate with metal

strips on the other side.

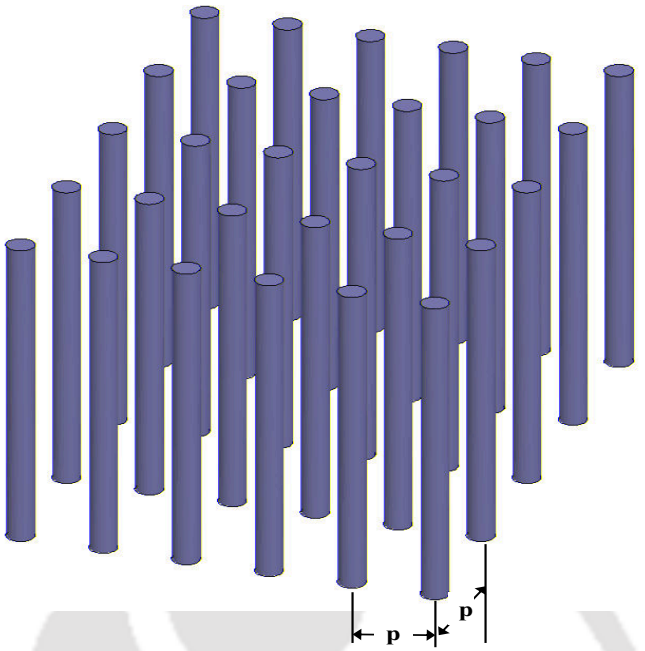

(a)

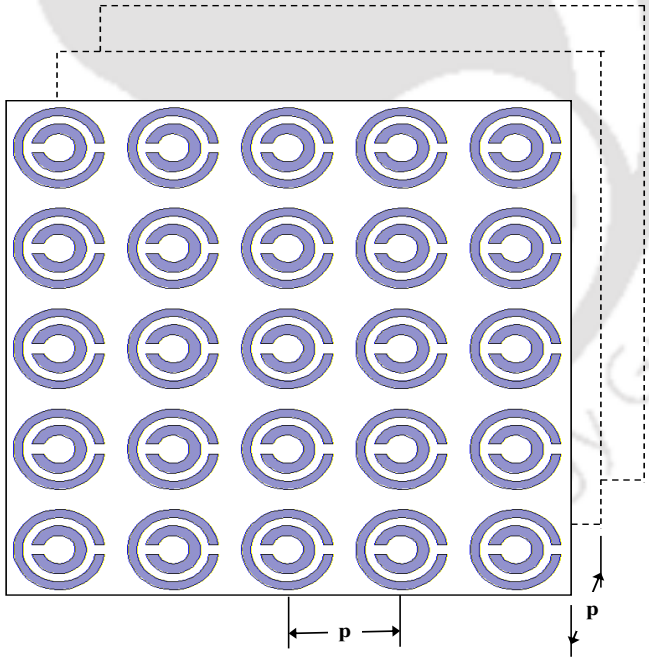

(b)

Figure 1.3: Pendry's structure a) Thin wire (negative ε / positiveμ) b) Split ring resonator array (positive ε / negative μ).

1.2.3 Implementation of left-handed line

Generally, in a planar medium, the left-handed transmission line can be synthesized using two approaches: a) Transmission line approach and b) Resonant type approach. In transmission line approach, the host line is loaded with series capacitances and shunt inductances [6–8]. In resonant type approach, the host line is loaded with the various resonating structures such as split ring resonator, spiral resonator, omega type resonator, etc. Some of the structures proposed earlier are shown in Fig. 1.4. In our study, the focus is mainly on resonant type approach.

1.3 Literature review and motivation

A planar structure exhibiting negative permeability called as split ring resonator (SRR), first proposed by J. B. Pendry [3] opened the way for size reduction and performance improvement of various devices using metamaterials. By applying the duality and complementarity principle another interesting resonator exhibiting negative permittivity known as complementary split ring resonator (CSRR) [9] is obtained. This is a negative image of the SRR. The CSRR behaves as a resonant element which is able to produce negative effective permittivity at resonance. The size of such resonators is much smaller than the wavelength at resonance; hence they are known as sub-wavelength resonator. Because of their size and characteristics, SRR and CSRR are highly useful for the size miniaturization of planar microwave devices such as filters, couplers and diplexers, and for the improvement for their performance. They can also be applied in antennas to reduce the higher order resonant effect and increase the antenna gain. Several research studies [10–12], showed that SRR and CSRR can be used as stopband filter for removing the unwanted spurious passband of the conventional bandpass and lowpass filters. By properly tuning the resonant frequency of these particles, multiple harmonic suppression can be achieved [11, 13]. It has also been demonstrated that CSRR can be used for designing compact lowpass, highpass and bandpass filters [14–19]. A lowpass filter, which exhibits a wide stopband and sharp rejection with small size, using CSRR and rectangular patch was proposed in [20]. A dual band filter with CSRR and interdigital capacitor was discussed in [21].

Apart from the filter applications, CSRR can be used for other applications as well. By etching CSRR beneath the coupled lines, the coupling effect of the coupler can be increased, and it can serve to maintain a comfortable distance of separation between the two parallel lines, which provides more flexibility in the fabrication process [22,23]. Compact microwave power dividers with several topologies

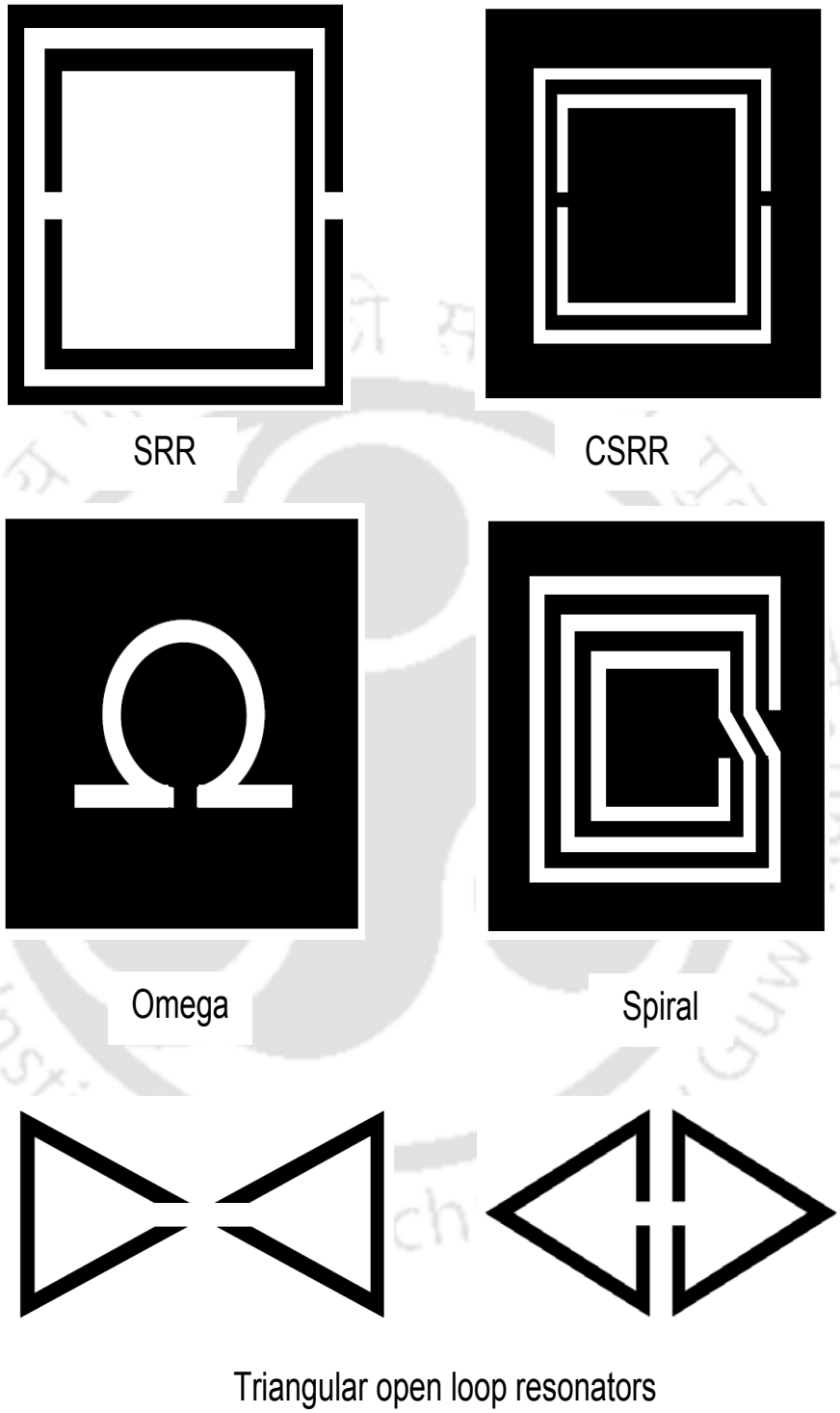

Figure 1.4: Various resonating structures exhibiting metamaterial properties.

are designed in microstrip technology by using artificial left-handed lines implemented by means of SRRs and CSRRs [24, 25]. A 90^0 impedance inverter is first designed using CSRR and etched gap in the microstrip line then; it is applied for the design of narrow band power dividers. A new type of left-handed transmission line, implemented by means of CSRR etched on the microstrip line, was proposed [26] to design a compact power divider and bandpass filter. Yet, this method involves via holes for the realization of devices. Hybrid rings are crucial structures in microwave engineering. However, the main limitation of a conventional hybrid ring is its large size because of the 270^0 branch line. To overcome this, Itoh and co-workers proposed a left-handed transmission line hybrid ring, realized by lumped elements, which has reduced size and enhanced bandwidth [27]. A novel miniaturized hybrid ring was presented, which replaced the 270^0 branch line of the conventional hybrid ring with a -90^0 left-handed branch line realized by complementary split ring resonators (CSRRs). Thus, a 60% size reduction was achieved [28]. In [29], a composite right/left handed transmission line was used for dual-band coupler design. However, the design procedures for the realization of composite right/left handed transmission line in [29] were complicated, they also degraded the performance of the coupler.

A novel dual-band branch line coupler (BLC) [30, 31] was presented by the LH-RH transmission line composed of strip-shaped CSRRs and series gap. The proposed BLCs operates in the GSM band frequencies (900 MHz & 1800 MHz). Recently a dual band compact BLC using complementary spiral resonator (CSR) was proposed in [32]. Compared with the CSRR, the resonant frequency of the CSR was half the resonant frequency of the CSRR; hence, size reduction was achieved. Recently, a new compact resonator called as open split ring resonator (OSR) [33] and open complementary split ring resonator (OCSRR) [34] were introduced by some of the authors for designing size miniaturized microwave components [35]. By periodic arrangement of OCSRR a sharp cut-off lowpass filter was implemented in microstrip technology [36]. In [34], a wideband bandpass filter was designed using OCSRR in coplanar wave guide technology. The synthesis of composite right/left-handed transmission line designed using a combination of SRR and OCSRR was reported in [35]. Due to the small dimensions of these resonators, the resulting lines were very compact. It was shown that these artificial lines can be applied to the synthesis of dual-band components and bandpass filter in coplanar wave guide (CPW) technology.

In addition, etching of CSRR in the radiating element of ultra wideband (UWB) antenna produces, notch characteristics and make the antenna coexistence with the wireless local area networks [37, 38].

By placing a patch antenn in the ground plane, containing a number of CSRRs, the patch antenna size reduction was possible without major changes in the bandwidth [39].

In spite of wide applications of left-handed materials, improvement is still needed in some cases. To obtain a wide rejection bandwidth from CSRR, a large number of CSRRs is needed, which increases the device length unnecessarily. Hence, in our work, by combining the CSRR with other stopband structures, a wide rejection band filter is designed for obtaining a spurious passband free lowpass filter (LPF) or bandpass filter (BPF). The size reduction for a few of the reported devices (power divider using CSRR and CSR) has been achieved at the expense of bandwidth reduction. Thus, this approach is limited to narrowband devices. The ever expanding wireless and consumer electronics market require the integration of more components, and there is an increasing demand for size reduction and high performance circuits. To meet this demand, a new resonator exhibiting the same characteristics as CSRR with a reduction in size is required. Therefore, a new structure called as an open slot split ring resonator (OSSRR) is introduced in this thesis. Even though the size of the OCSRR is much smaller than the size of the CSRR for the same resonant frequency, most of the applications reported are in CPW technology. The fabrication of such devices is difficult because it involves via holes and bonding wires for connecting the different ground regions. By considering this, we contribute some works related to the size miniaturization and performance improvement of microwave devices using CSRR and other sub wavelength resonators.

1.4 Contribution of this thesis

The key contributions of the present study are as follows,

- Various wide bandstop filters, using complementary split ring resonator (CSRR), open stub and spurline are designed and harmonic suppression of lowpass (LPF) and bandpass filters (BPF) are demonstrated both by simulation as well as through experimental results.

- Using a single complementary split ring resonator, a notch in the UWB bandpass filter response is created for suppression of WLAN signals. The fabricated notched UWB BPF is tested using vector network analyzer and shows the desirable notch filter characteristics.

- Novel resonators, named open split ring resonator (OSRR) and open slot split ring resonator (OSSRR) exhibiting negative material parameters at the vicinity of the resonant frequency are

investigated.

- An open slot split ring resonator is introduced to a host microstrip line to realize composite right/left handed (CRLH) transmission line structure in microstrip technology. It is experimentally verified with the fabricated results.
- A wide fractional bandwidth BPF and compact lowpass filter are designed, fabricated and tested using OSSRR.
- A wide rejection bandwidth and compact lowpass filters are proposed using OCSRR. It is verified from simulation as well as experimental results.
- A compact and harmonic suppressed T-junction power divider for wireless application is designed, fabricated and tested.
- Size miniaturized and harmonic suppressed rat-race coupler is proposed, designed and verified with the fabricated prototype.

1.5 Thesis organization

This thesis is organized into six chapters. The first chapter is an introduction that gives an overview of the study. Chapter 2 discusses the theory and applications of complementary single split ring resonator (CSSRR). The modeling, material parameter extraction and detailed parametric study of CSSRR are presented in this chapter. The applications of CSSRR as performance improvement of microwave filters are validated through several examples.

Chapter 3 presents a study of CSRR stopband characteristics. To support this study, a parametric analysis has been performed and presented. Multiple harmonic rejection of conventional parallel coupled microstrip line bandpass filter using CSRR based bandstop filter is further discussed.

The new sub-wavelength resonators OSRR and OSSRR are discussed in Chapter 4. Methods for obtaining the frequency response and material parameter extraction of the composite substrate are also presented here. The modeling of OSSRR has been carried out and the extraction of equivalent circuit parameters are also included. With the help of complete parametric study, the relation between the OSSRR dimensions and the resonant frequency is explained. Different applications of OSSRR also presented in this chapter.

Chapter 5 discusses performance enhancement of microwave devices using OCSRR. The lumped element model of OCSRR is presented and model parameters are extracted. Various performance enhanced microwave devices, such as size-miniaturized lowpass filters, T-Junction power divider and 180^0 hybrid coupler design using OCSRR in microstrip technology are demonstrated in this chapter.

Conclusion arising from this study and scope for further research directions are discussed in Chapter 6.

2

CSSRR and its applications in performance enhancement of microstrip filters

Contents

2.1 Introduction

Size miniaturization and performance improvement of microwave filters are in much demand in today's rapidly changing communication world. Since the microwave filters are distributive in nature, they have such shortcomings as suffering from spurious passband, poor roll-off rate, etc. Therefore, researchers are working toward designing high performance filters with spurious free stopbands and compact size. Many microstrip filter designs have been proposed in the past few decades, but there is still room for improvement. Over the past few years, metamaterials have been gaining a lot of interest among researchers across the globe because such artificial materials produce negative-ε and negative-μ electromagnetic properties, which do not occur in naturally available electromagnetic materials. Split ring resonators (SRRs) and complementary split ring resonators (CSRRs) are the key particles for such exotic artificial materials. These two types of resonators can also be called as sub-wavelength resonator, due to their smaller size compared with the wavelength at resonance. Several applications of SRRs and CSRRs were demonstrated in the literature. In this chapter, we introduce one such metamaterial structure, called complementary single split ring resonator (CSSRR), exhibiting negative permittivity. As a first step, single split ring resonator (SSRR) and its characteristic are studied followed by the introduction of CSSRR. A Detailed parametric study and closed form formula for the resonant frequency of the CSSRR are presented. Finally, a few of the applications of the CSSRR for performance improvement of microstrip filters are discussed.

2.2 Split ring resonator (SRR)

A split ring resonator (SRR) is a well-known structure exhibiting negative permeability, first reported by Pendry [3]. Various studies of SRRs have been carried out so far. A SRR consists of two metallic concentric rings separated by a split gap on the opposite sides of the rings. When a time varying magnetic field is applied to the SRR, the current is introduced in the split ring. Due to the split in the SRR, the current in the SRR does not find a closed path but still flows due to the capacitance between the rings. The amount of the current is determined by the inductance of the SRR and capacitance of the gap. If the quality factor of the SRR is sufficiently high, the permeability can be made negative. So far, various kinds of SRRs have been proposed by many researchers. In this chapter, however, we mainly concentrate on a single split ring resonator.

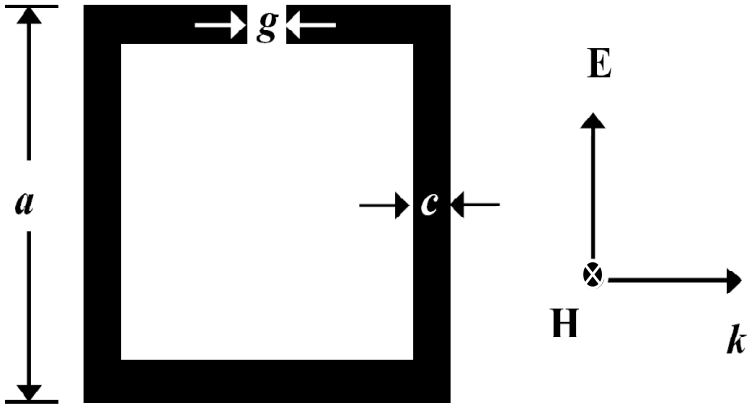

Figure 2.1: Schematic representation of SSRR.

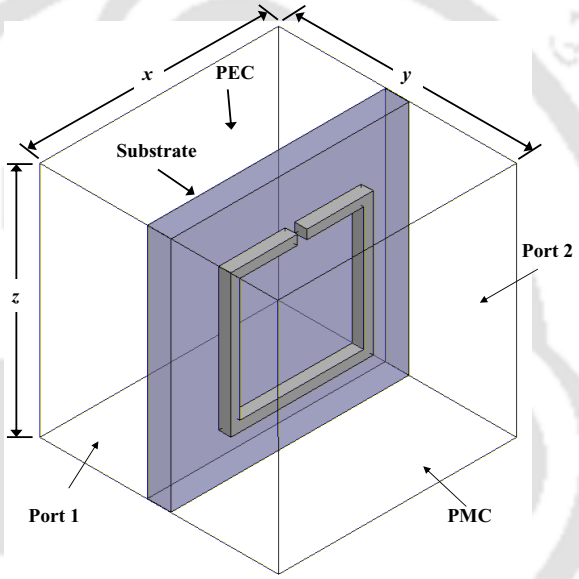

Figure 2.2: Simulation setup for parameter extraction of SSRR.

2.3 Single split ring resonator (SSRR)

Fig. 2.1 shows the structure of a single SRR. It has a square copper ring with a small split gap on one side. Circular shaped SRRs are also used in practice. Here, however, we are concentrating only on square SRR because most of our work is related to square SRR and our fabrication facility is available for such SRR only. To support our study, the parameter extraction of SRR is also performed and presented. By applying the effective medium theory, from the simulated S-parameters, the permittivity and permeability of SSRR are calculated. The simulation setup for extracting the material parameter

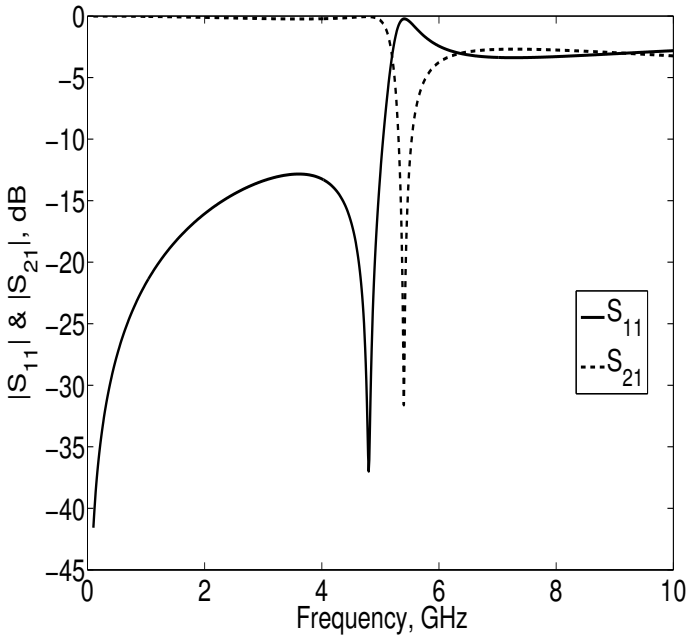

Figure 2.3: Scattering parameters of SSRR.

is shown in Fig. 2.2. The unit cell is cubic with a cell dimension of x = y = z = 5 mm. The perfect electric conductor (PEC) boundary condition is applied to the top and bottom walls of the waveguide,

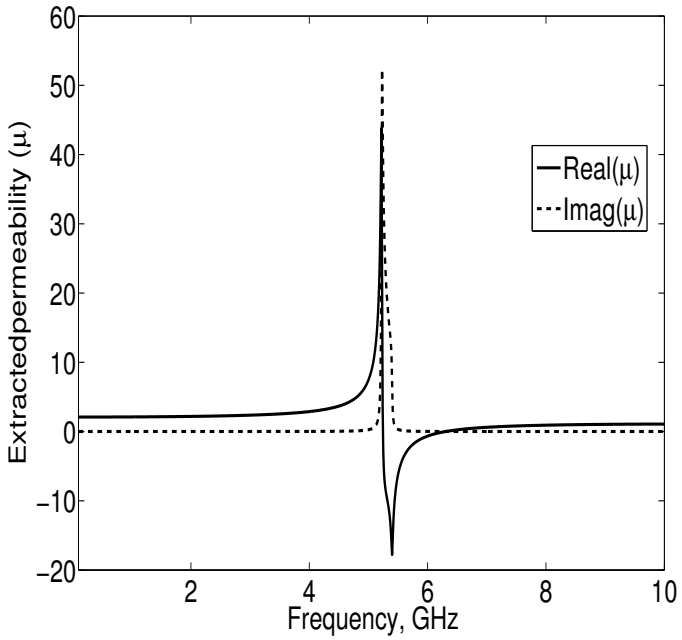

Figure 2.4: Extracted permeability of SSRR.

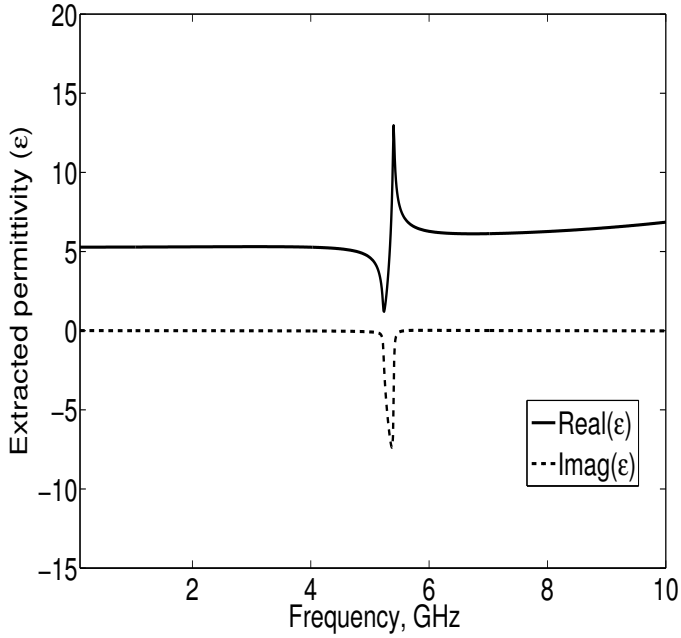

Figure 2.5: Extracted permittivity of SSRR.

and the perfect magnetic conductor (PMC) boundary condition is applied to the side walls of the waveguide. The other two sides are assigned as wave ports. A copper SSRR with $a = 4$ mm, $c = 0.2$ mm, and $g = 0.2$ mm is printed on one side of the RT/Duroid substrate with dielectric constant $\varepsilon_r = 2.33$ and height $h = 0.5$ mm. The thickness of the SSRR is taken as 0.5 mm. The S-parameters of the unit cell are computed using a full-wave simulator and plotted in Fig. 2.3. At the resonance frequency $f_r = 5.4$ GHz, a sharp narrow stopband is observed. The material parameters of the SSRR are retrieved using the following equations [40].

$$z = \sqrt{\frac{(1+S_{11})^2 - S_{21}^2}{(1-S_{11})^2 - S_{21}^2}} \tag{2.1}$$

$$n = \frac{1}{kd}\cos^{-1}\left(\frac{1}{2S_{21}}(1 - S_{11}^2 + S_{21}^2)\right) \tag{2.2}$$

$$\varepsilon = n/z \tag{2.3}$$

$$\mu = nz \tag{2.4}$$

where z is the wave impedance of the dielectric slab, d is the size of the cell, and k is the wave vector. The retrieved material parameters are illustrated in Fig. 2.4 & Fig. 2.5. It is shown that around the resonant frequency of the SSRR, the real part of permeability of the medium is negative, proving that the SSRR is a μ-negative material.

2.4 Complementary single split ring resonator (CSSRR)

Complementary single split ring resonator (CSSRR) or slotted split ring resonator contains a slot having the shape of a split ring resonator in the ground plane. By applying the property of duality and complementarity, CSSRR can be derived from SSRR. CSSRR essentially behaves as an electric dipole that can be excited by an axial time varying electric field rather than a magnetic field as in the case of SSRR. Hence, negative permittivity is expected from a CSSRR based medium. Both SSRR and CSSRR with the same dimensions resonate at the same frequency. However, CSSRR occupies less area than SSRR. Since complementary split ring resonators are etched in the ground plane, unlike SRRs that are etched in the same plane of the microstrip line, CSSRRs are mostly preferable for size miniaturization and performance enhancement of microwave devices. To verify its ε-negative property (ENG), the CSSRR is placed in the ground plane exactly below the center of a 50 Ω microstrip line of 3.06 mm width for the FR4 dielectric substrate of $\varepsilon_r = 4.4$ and height $h = 1.6$ mm as shown in Fig. 2.6. The dimensions of the CSSRR structure chosen for the simulation are: $a = 12$ mm, $c = 0.5$ mm, and $g = 0.5$ mm. Fig. 2.7 shows the simulated scattering parameters of CSSRR. Fig. 2.8

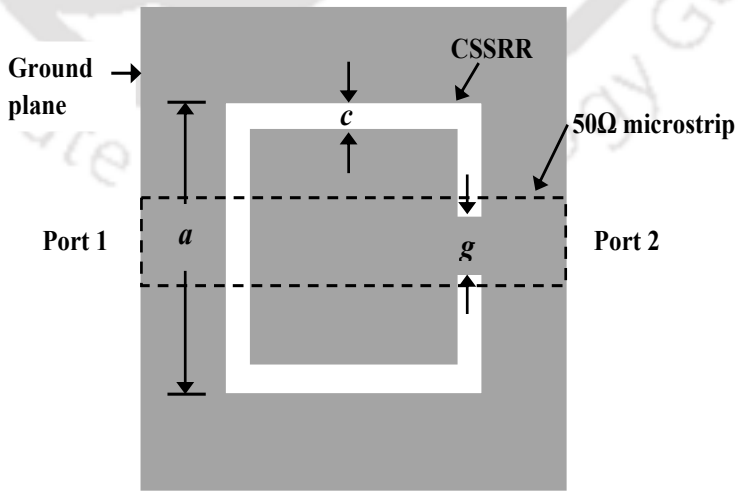

Figure 2.6: Structure of the CSSRR showing the physical dimensions.

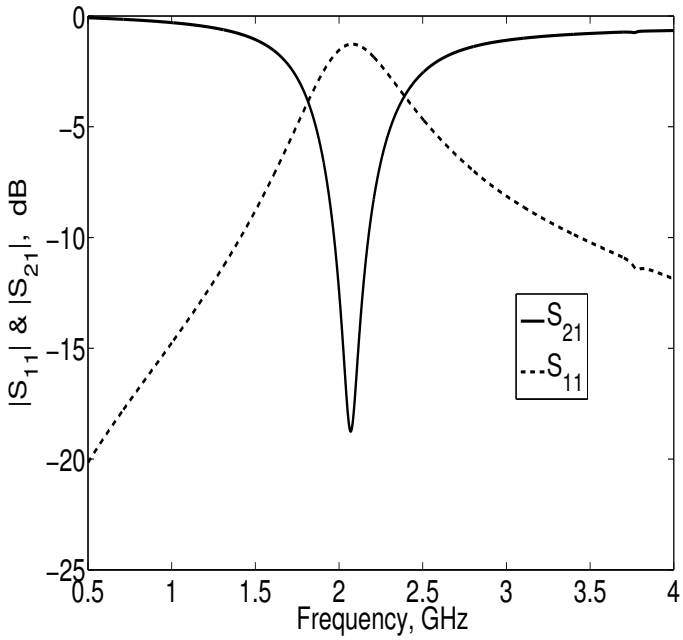

Figure 2.7: Simulated scattering parameters of CSSRR.

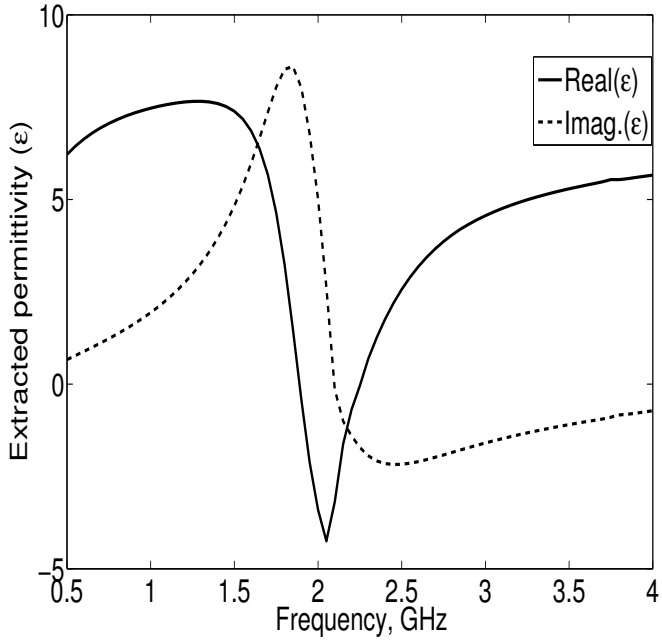

Figure 2.8: Extracted permittivity of CSSRR.

& Fig. 2.9 depict the extracted material parameters for a CSSRR loaded microstrip line using the eqns. (2.1)-(2.4). The scattering parameters illustrate that a stopband characteristic is present at the resonant frequency (f_r) of 2.09 GHz with a maximum rejection of 25 dB. Examining the extracted

parameters, one can see that the reason for the stopband characteristic is the presence of negative ε at resonance.

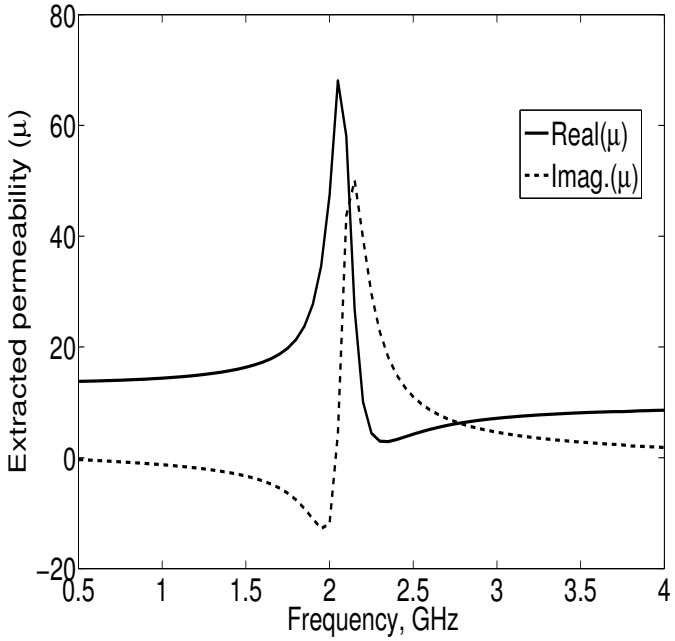

Figure 2.9: Extracted permeability of CSSRR.

2.5 Lumped element model of CSSRR

Since CSSRR is etched in the ground plane, we can consider this as a defected ground structure (DGS) or defected ground plane (DGP). The frequency response of a conventional DGS and its equivalent circuit have been studied in [41]. The equivalent lumped element model of CSSRR is obtained using [42]. For a better illustration, it is shown in Fig. 2.10. CSSRR is considered as a parallel RLC resonant circuit. L and C are the inductance and capacitance of the CSRR, and R_1 represents the losses in the resonant circuit. The nonuniform current distribution effects on the ground plane are modeled using R_2. The equivalent circuit parameters are easily obtained from the simulated scattering parameters with the help of the following equations [42],

$$A = \frac{(1+S_{11})(1-S_{22})+S_{12}S_{21}}{2S_{21}} = 1 + \frac{Y_1}{Y_2} \tag{2.5}$$

$$B = Z_0 \frac{(1+S_{11})(1+S_{22})-S_{12}S_{21}}{2S_{21}} = \frac{1}{Y_2} \tag{2.6}$$

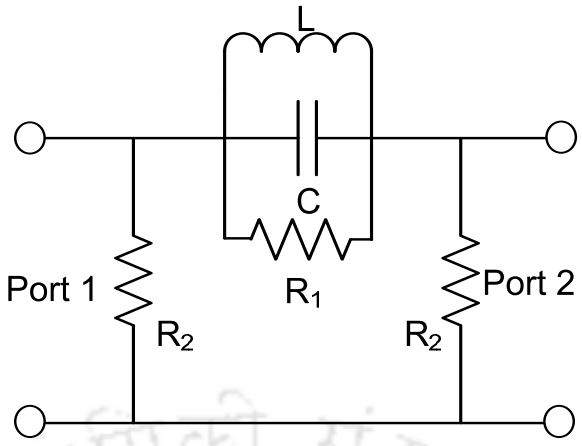

Figure 2.10: Lumped element model of CSSRR.

where Y_1 and Y_2 are the parallel and series admittances of the Π - type symmetrical two port network. Z_0 is the characteristics impedance of the microstrip line. A and B are the elements corresponding to the ABCD matrix. The relation between the equivalent circuit parameters and the Π - type two port network are given by,

$$Y_1 = \frac{A-1}{B} = \frac{1}{R_1} + jB_1 \tag{2.7}$$

$$Y_2 = \frac{1}{R_2} + jB_2 \tag{2.8}$$

Since the simulated scattering parameters of the CSSRR are complex, the resulting equivalent circuit parameters is also complex. From which the lumped element values of CSSRR are obtained using eqns. 2.9 and 2.10.

$$C = \frac{B_2}{2\pi f_0(\frac{f_0}{f_c} - \frac{f_c}{f_0})} \tag{2.9}$$

$$L = \frac{1}{4\pi^2 f_0^2 C} \tag{2.10}$$

where f_0 and f_c are attenuation pole frequency and cut-off frequency of CSSRR respectively. The extracted lumped element values of the structure are $L = 2.0325$ nH, $C = 2.9114$ pF, $R_1 = 0.9$ KΩ, and $R_2 = 1.25$ KΩ at the resonant frequency, 2.09 GHz. The equivalent circuit of CSSRR is simulated using Ansoft Designer SV and compared with the electromagnetic simulation (EM). The result is

shown in Fig. 2.11. As expected, EM simulated results are well matched with the circuit simulation. Small differences found may be due to the negligence of fringe field capacitance in the model.

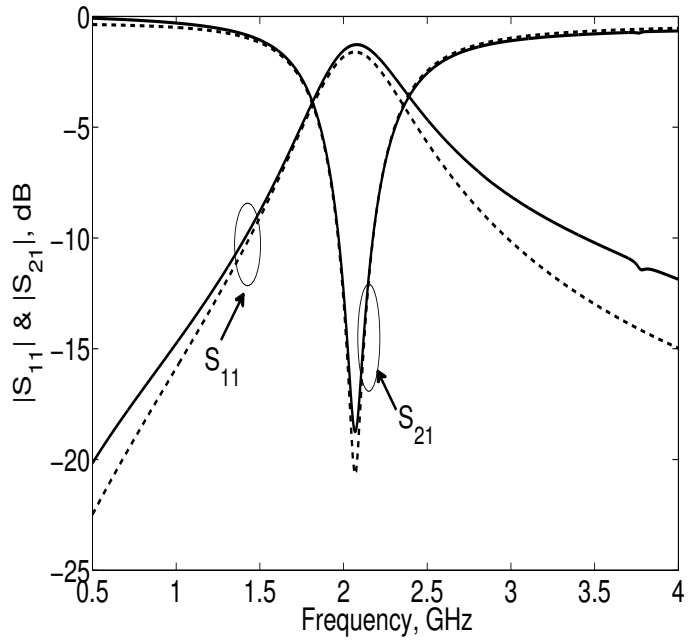

Figure 2.11: Scattering parameters of CSSRR - EM simulation (Solid line), Circuit simulation (Dashed line).

2.6 Parametric study of CSSRR

To investigate the influence of the CSSRR dimensions on the changes in its resonant frequency, we have simulated the CSSRR with different dimensions. By keeping the slot width c and gap width g constant, the side length a of the CSSRR was varied in increments of 2 mm. Similarly, the other dimensions of the structure are also varied and its frequency response is plotted in Fig. 2.12 to Fig. 2.14. The corresponding lumped element values are also extracted and tabulated in Table 2.1 to Table 2.3. By examining the plots, we can see that as the side length a of the CSSRR increases, the effective inductance value is increased, which, in turn, leads to a lower resonant frequency, or attenuation pole frequency. Similarly, the increase in slot width and split gap decreases the capacitance value with less change in inductance, so that the attenuation pole frequency moves toward the higher end. Therefore, it is concluded that for a fixed split gap value, the resonant frequency of CSSRR can be easily tuned to the desired value by changing the side length of the structure.

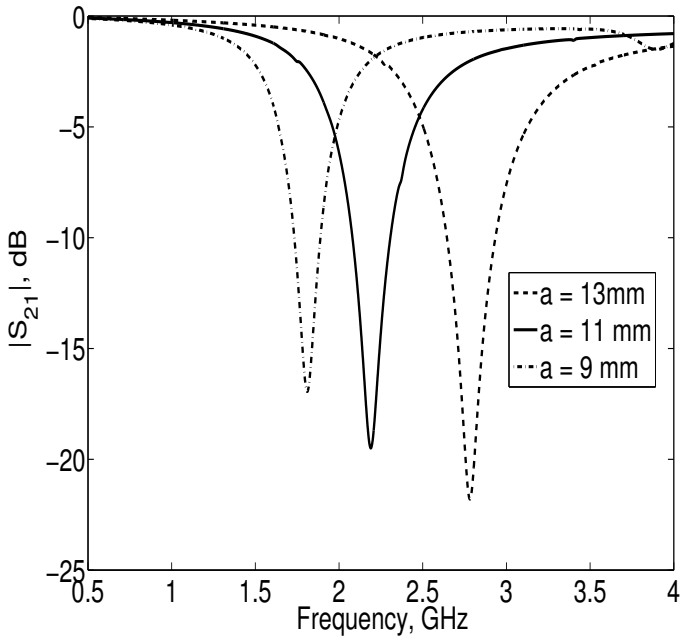

Figure 2.12: Frequency response of CSSRR for variation of side length 'a'.

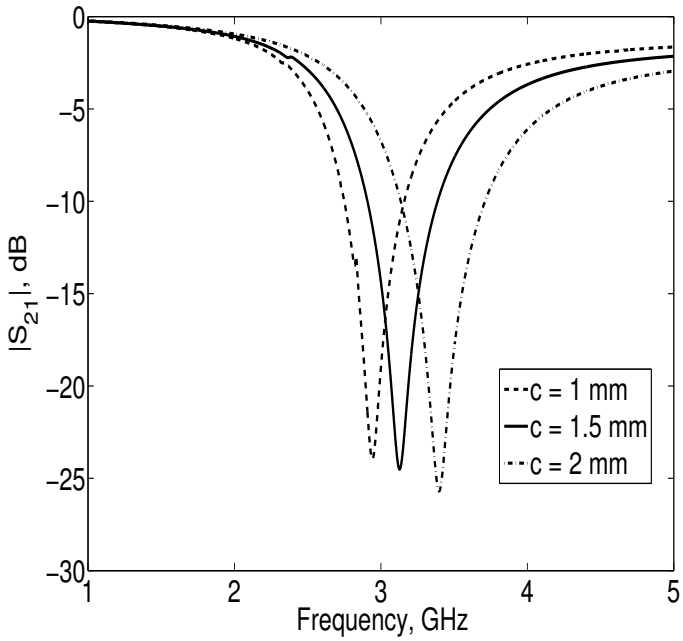

Figure 2.13: Frequency response of CSSRR for variation of slot width 'c'.

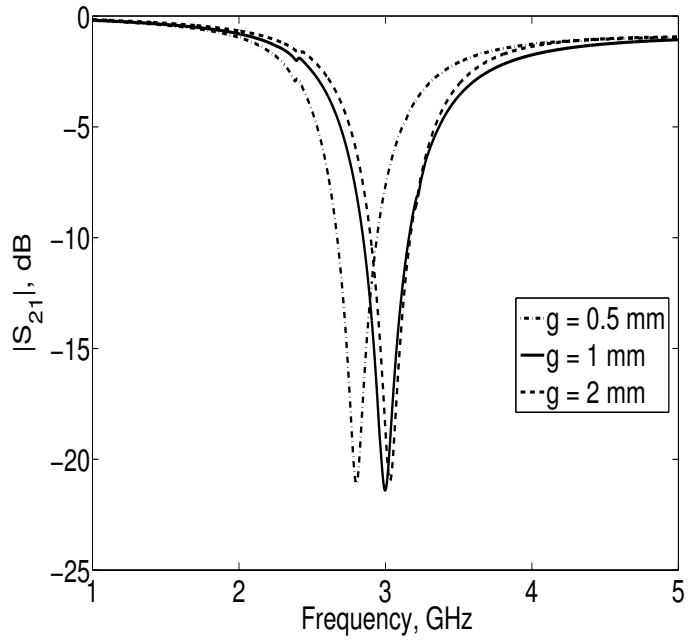

Figure 2.14: Frequency response of CSSRR for variation of split gap 'g'.

Table 2.1: Equivalent circuit values of CSSRR for various split gap 'a'

a (mm)	c (mm)	g (mm)	f_c (GHz)	f_0 (GHz)	L (nH)	C (pF)	$R_1(K\Omega)$	$R_2(K\Omega)$
9	0.5	0.5	2.38	2.78	1.4178	2.314	1.428	0.833
11	0.5	0.5	1.86	2.19	2.039	2.5928	1	1.2
13	0.5	0.5	1.56	1.81	2.1875	3.5382	0.714	1.429

Table 2.2: Equivalent circuit values of CSSRR for various slot width 'c'

a (mm)	c (mm)	g (mm)	f_c (GHz)	f_0 (GHz)	L (nH)	C (pF)	$R_1(K\Omega)$	$R_2(K\Omega)$
9	1	0.5	2.41	2.94	1.748	1.6782	2	0.909
9	1.5	0.5	2.52	3.13	1.778	1.4554	2	0.833
9	2	0.5	2.67	3.4	1.8585	1.1802	2	0.833

Table 2.3: Equivalent circuit values of CSSRR for various split gap 'g'

a (mm)	c (mm)	g (mm)	f_c (GHz)	f_0 (GHz)	L (nH)	C (pF)	$R_1(K\Omega)$	$R_2(K\Omega)$
9	0.5	0.5	2.38	2.78	1.4178	2.314	1.428	0.833
9	0.5	1	2.53	2.99	1.3303	2.132	1.67	0.769
9	0.5	2	2.54	3.09	1.6943	1.5674	1.67	1

Table 2.4: Parametric study of CSSRR

a (mm)	c (mm)	g (mm)	ε_r	Simulated f_r (GHz)	Calculated f_r (GHz)
10	0.4	0.5	4.4	2.42	2.4
10	0.6	0.5	4.4	2.54	2.46
10	0.7	0.5	4.4	2.62	2.487
10	0.5	0.4	4.4	2.53	2.427
10	0.5	0.5	4.4	2.55	2.43
10	0.5	0.6	4.4	2.75	2.44
11	0.5	0.5	4.4	2.27	1.69
12	0.5	0.5	4.4	2.0	2.19
13	0.5	0.5	4.4	1.78	2.0
10	0.5	0.5	4.4	2.55	2.43
10	0.5	0.5	6.15	2.22	2.11
10	0.5	0.5	10.2	1.79	1.69

2.6.1 Close form formula for resonant frequency of CSSRR

The conventional method [43] for calculating the resonant frequency of the CSSRR is a tedious process. To make this process easy, the length of the current path for the SSRR is first calculated, from which the resonant frequency is computed as follows,

$$f_r = \frac{v}{2 \times \{4 \times (a-c) - g\}\sqrt{\frac{\varepsilon_r+1}{2}}} \tag{2.11}$$

where v is the speed of light in vacuum. Since CSSRR is a dual counterpart of SSRR, the computed formula is applicable to the CSSRR also. To verify this formula, a detailed parametric study on the resonant frequency of CSSRRs has been carried out based on the CSSRR's side length, slot width, split gap, and substrate on which it is printed. The results are tabulated in Table 2.4. Such a detailed investigation will be useful for the proper selection of CSSRR dimensions for designing CSSRRs for various applications. It should be noted, however, that the formula is useful only for the rough estimate of initial dimensions of the CSSRR. The final dimensions should be obtained using optimization process.

2.7 Harmonic suppression of microwave filters using CSSRR

2.7.1 Objectives

The main limitation of microwave filters implemented using distributed components is the presence of unwanted spurious passbands, occurring at the harmonics of the cut-off frequency of the filter. These undesired passbands degrade the performance of the filter in certain applications that require a wide rejection bandwidth. For example, in the case of parallel coupled microstrip line (PCML) bandpass filter (BPF), the presence of a spurious passband at twice the fundamental (f_0) frequency is a major limitation of the filter. Similarly, stepped impedance lowpass filter is also seriously affected by the presence of a spurious passband near its resonance frequency. As a result, the suppression of the spurious passband in microwave filters is a challenging job for the designers. Our intention is to develop a harmonic suppression technique or device that can be used in conjunction with the existing conventional filters such as the lowpass filter (LPF) or bandpass filter to improve their filtering performance. In this section, we investigate the CSSRR-stub filter as a harmonic suppression device or technique for PCML BPF and stepped impedance lowpass filters. It should be noted, however, that this harmonic suppression technique can also be used for improving filtering characteristics of other types of filters.

2.7.2 Harmonic suppression of bandpass filter using CSSRR

Bandpass filters have been widely employed in microwave and wireless communication system for permitting desired band of frequencies while rejecting all other bands. In microstrip technology, PCML BPFs are commonly used because of their planar structure and simple design procedure. The required design parameters can be obtained from various literatures [44–46]. However, the presence of the spurious passband at twice the fundamental frequency ($2f_0$) is a major limitation of this filter. This is mainly due to the unequal even and odd mode phase velocities of parallel coupled lines. Several techniques have been proposed [10, 47–50] to suppress the spurious passband of the PCML filter at $2f_0$. Using the continuous modulation pattern, which employs a sinusoidal law in the strip widths of parallel coupled line filter, is effective in suppressing the spurious response [47]. In [48], corrugated coupled microstrip lines are designed to equalize the odd and even mode phase velocities for obtaining a wide upper stopband. Based on Bragg reflection, periodic grooves are etched in the microstrip lines to eliminate the spurious passband at $2f_0$ [49]. Recently, split ring resonators (SRR) and complementary

split ring resonators (CSRR) have been established as a solution for the suppression of harmonics in microstrip and CPW technologies [10, 50]. The bandstop filter using open stub and spurline can be adopted for suppressing the second harmonic in open loop ring bandpass filter [51]. In this work, the presence of the spurious passband at the second harmonic of center frequency is eliminated by cascading the bandstop filter, designed using CSSRR, with the PCML BPF. The bandstop filter (BSF) using open stub employs several cascaded stages to obtain a wide rejection bandwidth and high rejection ratio. On the other hand, the CSSRR has a narrow stopband and good rejection level. Placing a CSSRR under the stub filter results in a wider stopband and high rejection level. The undesired second harmonic of the conventional parallel coupled microstrip line bandpass filter is eliminated by cascading this BSF with the PCML BPF.

2.7.2.1 Design of PCML bandpass filter

A coupled line configuration consists of two transmission lines placed parallel to each other. In such a configuration, there is a continuous coupling between the electromagnetic fields of the two lines. Due to the coupling of the magnetic fields, a pair of coupled lines provides two different modes of propagation. When the coupled microstrip lines are symmetrical, the two modes of propagation are the odd mode and even mode of propagation. A detailed analysis of this phenomenon can be found in [44, 45]. The design equations for the filter are given by,

$$Z_0 J_1 = \sqrt{\frac{\pi \Delta}{2 g_1}} \tag{2.12}$$

$$Z_0 J_n = \frac{\pi \Delta}{2\sqrt{g_{n-1} g_n}} \qquad for \quad n = 2, 3, ...N \tag{2.13}$$

$$Z_0 J_{N+1} = \sqrt{\frac{\pi \Delta}{2 g_N g_{N+1}}} \tag{2.14}$$

where J_n is the admittance inverter constants, $\triangle$ is the fractional bandwidth, g is the lowpass filter prototype element values and Z_0 is the characteristic impedance of the line. To realize the J-inverters obtained above, the odd and even mode characteristics impedance of the coupled microstrip line resonators are determined by eqn. 2.15 and eqn. 2.16. With the help of these odd and even mode impedance values, width and spacing between the coupled lines have to be determined.

Table 2.5: Physical parameters of first order Chebychev BPF centered at 0.9 GHz with 10% FBW

i (mm)	Z_{0e} Ω	Z_{0o} Ω	w_i(mm)	s_i(mm)	l_i (mm)
1	70	30	1.22	0.512	46.972

$$Z_{0e} = Z_0[1 + JZ_0 + (JZ_0)^2] \tag{2.15}$$

$$Z_{0o} = Z_0[1 - JZ_0 + (JZ_0)^2] \tag{2.16}$$

As an example, a first order Chebyshev parallel coupled microstrip line filter, operating in the GSM band of frequencies in the range of 890 MHz to 960 MHz, is designed and simulated. The center frequency (f_c) of the passband is taken as 900 MHz, which covers the GSM band. The filter fractional bandwidth (FBW) is taken as 10%. The BPF is designed on the FR4 substrate of relative dielectric constant $\varepsilon_r = 4.4$ and height $h = 1.6$ mm. The physical parameters of the filter are calculated by the above equations and listed in Table 2.5. The 50 Ω access lines of 10 mm are added on both input and output ports.

The bandpass filter with the dimensions listed in Table 2.5 is simulated using a full-wave simulator. The fabricated prototype of the filter is shown in Fig. 2.15. The simulated and measured results of the conventional BPF are shown in Fig. 2.16. By observing the plots, one can see that the first passband exists from 0.83 GHz to 0.95 GHz covering the GSM band. In addition, a small spurious passband is observed around 1.8 GHz, which is twice the center frequency of the filter. This spurious passband has to be suppressed to obtain a wide rejection bandwidth. Therefore, a bandstop filter is designed using CSSRR and cascaded with the conventional BPF to improve the filter performance.

2.7.2.2 Realization of bandstop filter

The suppression of harmonics in microwave and millimeter wave system using a bandstop filter is a common practice. The conventional open stub BSF suffers from a narrow stopband and larger size. Hence, by combining the various stopband [51, 52] structures, a wide stopband can be obtained without increasing the circuit area. In our work, BSF is designed using open stub and CSSRR. As we need to suppress the second harmonic (1.8 GHz) of the GSM bandpass filter, a bandstop filter is first designed using CSSRR. Fig. 2.17(a) shows the structure of the CSSRR bandstop filter. We have

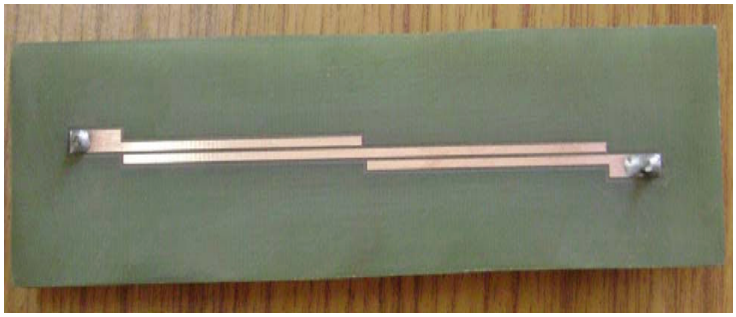

Figure 2.15: Photograph of conventional BPF.

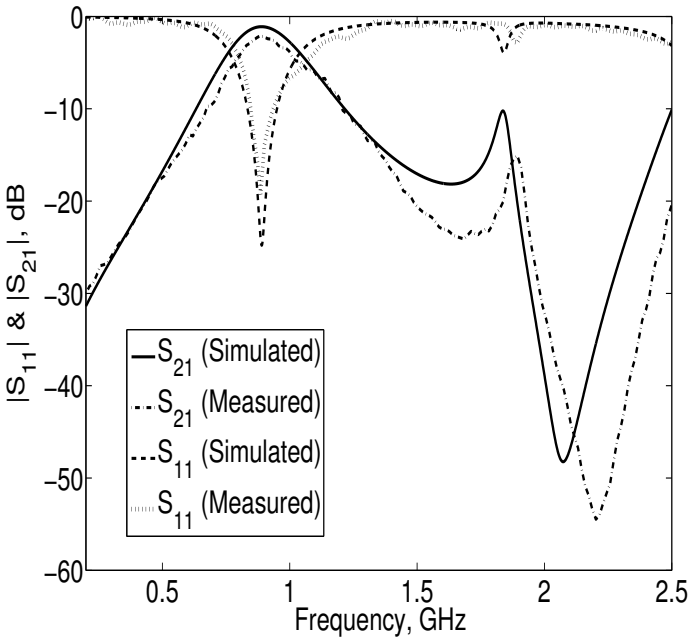

Figure 2.16: Scattering parameters of conventional BPF.

designed a CSSRR to resonate at 1.8 GHz with the following dimensions: a = 13 mm, c = 0.5 mm, and g =0.5 mm. Stop bandwidth of the designed CSSRR loaded microstrip line bandstop filter is 200 MHz. The basic configuration of the open stub filter is depicted in Fig. 2.17(b). Two open stubs of length $\lambda_g/4$ are separated by a distance of $\lambda_g/4$, where λ_g is the guided wavelength of the microstrip. A wide stopband can be obtained by cascading a greater number of open stub stages, but this results in increased circuit area. To overcome this limitation, a CSSRR is placed in the ground plane of the open stub filter as shown in Fig. 2.17(c). The open stub bandstop filter is designed for the same frequency as the CSSRR bandstop filter. The optimized dimensions of CSSRR-Stub filter are L_1 =

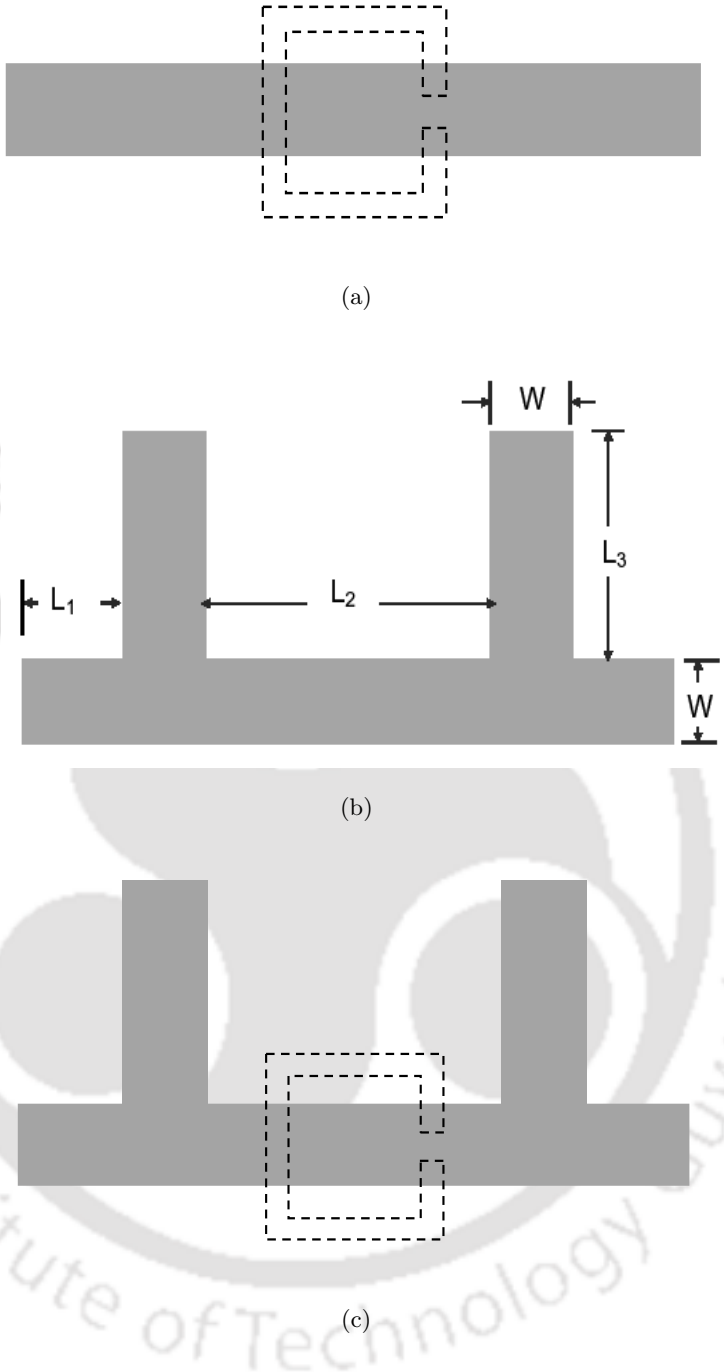

Figure 2.17: Various types of bandstop filters a) CSSRR bandstop filter b) Open stub bandstop filter c) CSSRR-Stub bandstop filter.

6.5 mm, L_2 = 23.2 mm, L_3 = 22.9 mm, and W = 3.06mm. In Fig. 2.18, simulated insertion loss of three types of bandstop filters are shown.

The stop bandwidth and rejection levels of various BSF are listed in Table 2.6. The CSSRR-

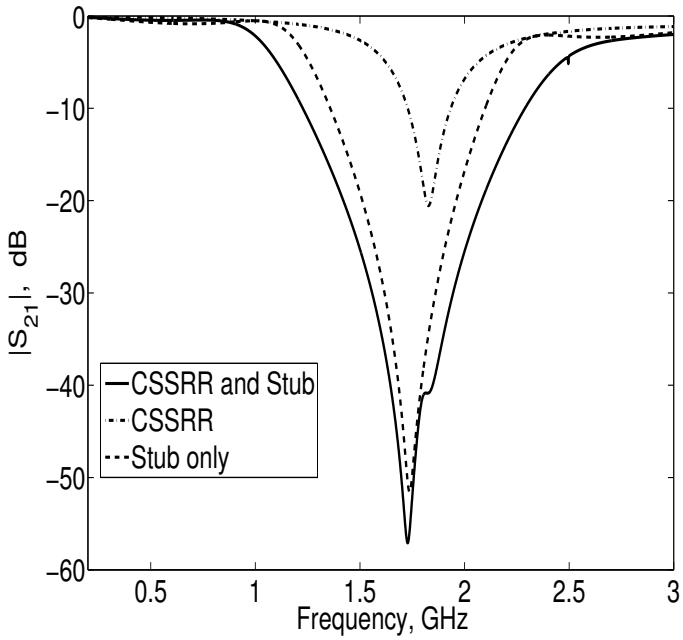

Figure 2.18: Insertion loss of various BSFs.

Stub filter has wide stop bandwidth of 1.06 GHz and a rejection level of 57.03 dB when compared with other filters, ensuring same circuit area. Compared with the conventional open stub BSF, the proposed CSSRR-Stub BSF has 40% more rejection bandwidth without increasing the number of open stub stages.

Table 2.6: Comparison of three BSFs

Filter Type	Stop bandwidth in GHz	Rejection level in dB
CSSRR	0.2	20.55
Open Stub	0.74	51.58
CSSRR-Stub	1.06	57.03

2.7.2.3 Harmonic suppressed bandpass filter

As stated earlier, the second harmonic suppression is achieved by cascading the proposed BSF with the PCML BPF. In this case, the dimensions of the BSF are optimized as follows to avoid the overlapping of desired passband of the bandpass filter and stopband of the bandstop filter. The optimized dimensions of BSF are $L_1 = 6.5$ mm, $L_2 = 18.6$ mm, $L_3 = 17.8$ mm and W = 3.06 mm. The proposed filter has been fabricated on the FR4 substrate and tested using Agilent 8753ES network

analyzer. The photograph and scattering parameters (S_{11} and S_{21}) of the proposed BPF with CSSRR-Stub filter are illustrated in Fig. 2.19. The spurious passband at twice the center frequency (1.8 GHz) of BPF is suppressed up to 40 dB without major changes in the passband. A rejection level of greater than 30 dB is obtained from 1.43 GHz to 2.53 GHz. The proposed filter offers a maximum rejection of 85 dB in the stopband and low passband insertion loss of 1.43 dB. Better results can be obtained by using the low loss substrate. Experimental results of filters are in close agreement with the simulation results. The minor differences found can be due to the tolerances in the fabrication process.

2.7.3 Harmonic suppression of lowpass filter

A simple method to implement a lowpass (LPF) filter is to use alternating sections of very high and very low characteristic impedance lines. This filter is simple in design and occupies less space than a lowpass filter implemented using stubs. As a second example of performance enhancement of a microwave filter, harmonic suppression of stepped impedance lowpass filter is presented in this section. A new wide stopband BSF is designed using open stub, CSSRR, and spurline configuration. Then, the proposed BSF is cascaded with the lowpass filter for suppressing the spurious passbands. A fifth order maximally flat response lowpass filter with a cut-off frequency of 1.0 GHz and stopband attenuation of greater than 20 dB at 2 GHz has been designed using the standard design procedure described in [44]. The low and high impedances used for the design of LPF are 20 Ω and 50 Ω respectively. The filter is designed on the FR4 substrate with $\varepsilon_r = 4.4$ and thickness of 1.6 mm. The Geometry of lowpass filter is shown in Fig. 2.20(a). The dimensions of filter are $P_1 = 6.12$ mm, $P_2 = 22.23$ mm, $P_3 = 19.8$ mm, $P_4 = 19.8$ mm, $P_5 = 11.1$ mm and $P_6 = 0.71$ mm. Fig. 2.20(b) shows the simulated scattering parameters of the low pass filter. From the plot, we observe that after the required passband, the spurious passband exists in the frequency region between 2.8 GHz to 4.6 GHz. We must suppress these harmonics of the LPF to obtain spurious free out-of-the band filter characteristics in the frequency region of interest.

2.7.3.1 Design of wide stopband BSF

Bandstop filters are widely used in microwave and wireless communication systems for prohibiting undesired signals. To date, many researchers have proposed various types of bandstop filters. A narrowband compact spurline BSF is proposed in [53]. In [51], a bandstop filter using openstub and spurline is used for harmonic suppression of the BPF. Bandstop filters with a wide rejection bandwidth

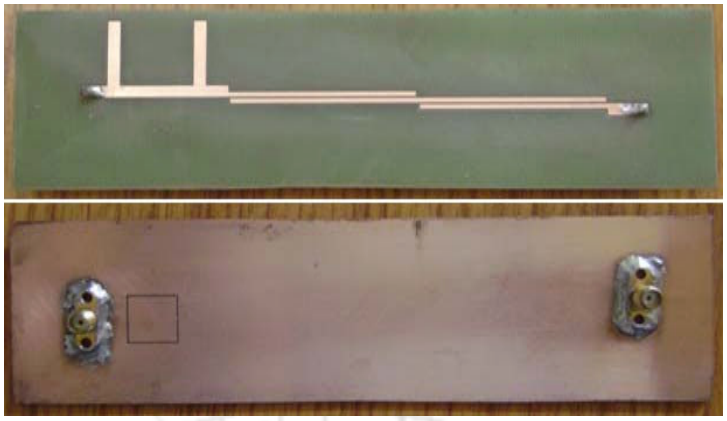

(a)

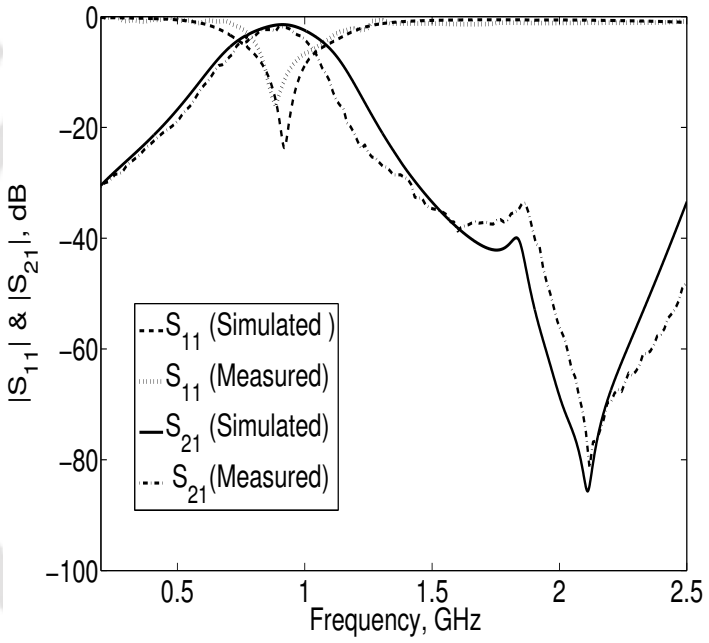

(b)

Figure 2.19: Proposed BPF with CSSRR-Stub filter a) Photograph b) Scattering parameters.

using stepped impedance resonator and spurline are investigated in [52]. A novel BSF with high Q factor using U and V shaped slot is presented in [54]. A compact bandstop filter using signal interference technique is proposed in [55]. A negative ε bandstop microstrip line filter is demonstrated in [9]. In this work, a wide bandstop filter is designed using three stopband structures such as open stub, CSSRR, and spurline. In section 2.7.2.2, a BSF is designed using open stub and CSSRR. To widen the rejection bandwidth further, additional stopband structure spurline is embedded in the

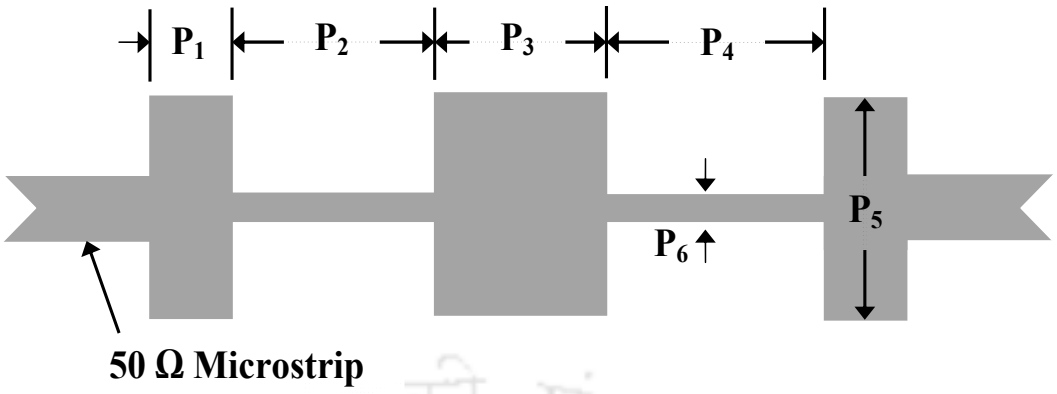

(a)

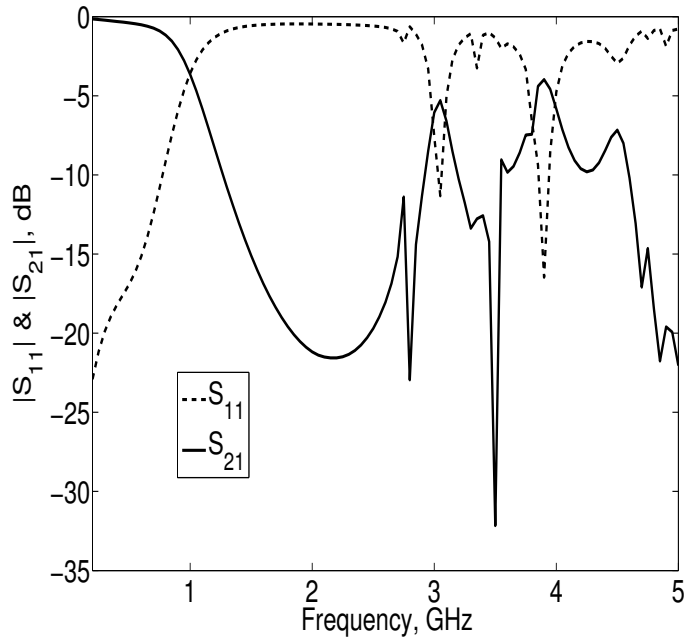

(b)

Figure 2.20: Stepped impedance lowpass filter a) Layout b) Scattering parameters.

microstrip line. To design a wide stopband BSF, we have first designed a CSSRR, using the close-form formula of equation 2.11, to resonate at 4.0 GHz. The dimensions of the CSSRR are: a = 7.0 mm, c = 1.0 mm, and g = 1.0 mm. This structure is placed in the ground plane exactly below the 50 Ω microstrip line. For all the simulations, the FR4 dielectric substrate of ε_r = 4.4 and 1.6 mm height is used. The stop bandwidth of the designed CSSRR loaded microstrip line bandstop filter is 320 MHz. A Conventional open stub filter is constructed by placing two open stubs of length L_1 =

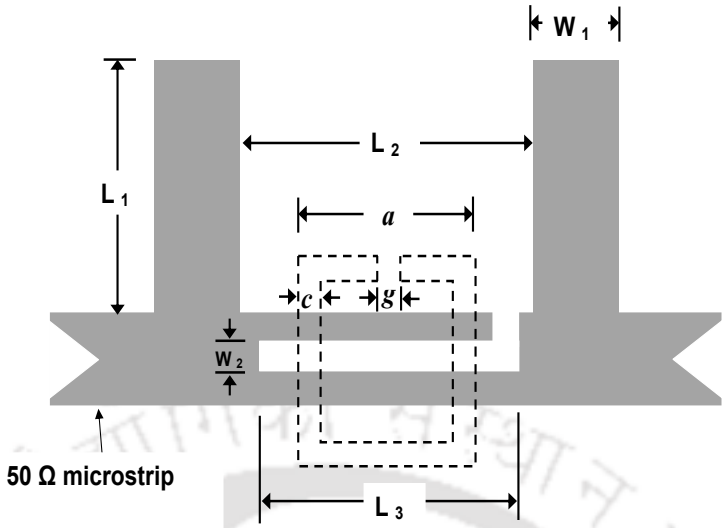

(a)

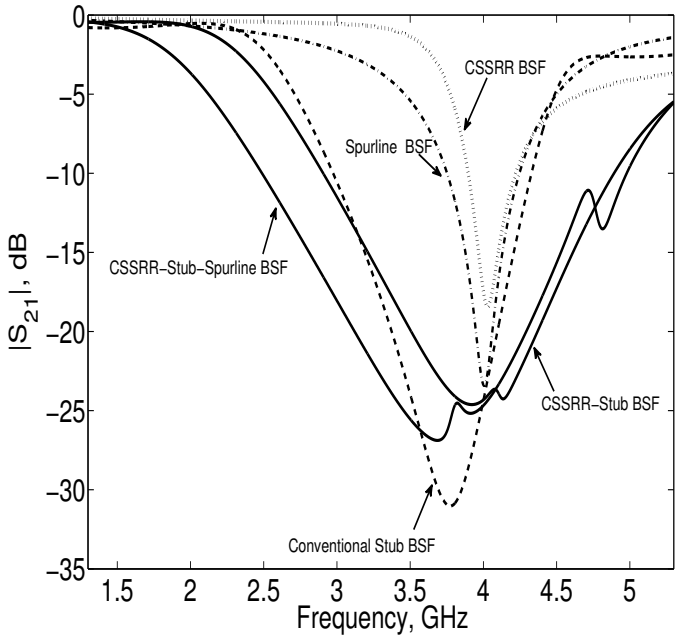

(b)

Figure 2.21: Open stub-CSSRR-Spurline BSF a) Layout b) Scattering parameters.

$\lambda_g/4$ at a distance of $\lambda_g/4$ on a microstrip line, where λ_g is the guided wavelength. We have designed the open stub filter at the center frequency of 3.6 GHz. The optimized dimensions for the filter are $L_1 = 10.23$ mm, $L_2 = 10.23$ mm, and $W_1 = 3.06$ mm. This filter gives a stop bandwidth of 1.36 GHz.

A wide stopband can be obtained by cascading more number of open stub stages, but this results in increased circuit area. To overcome this limitation, as explained earlier, the CSSRR is placed in the ground plane of the open stub filter, which results in a stop bandwidth of 1.99 GHz. To extend the rejection bandwidth further, an extra transmission zero is introduced by embedding a spurline section between the open stubs. L_3 is usually taken to be slightly less than L_2, and W_2 is chosen as approximately equal to 30% of W_1. The optimized dimensions of the spur line are L_3 = 10.0 mm and W_2 = 1.0 mm. The final layout of the proposed wide stopband BSF is shown in Fig. 2.21(a). Simulated scattering parameters of the various BSFs are depicted in Fig. 2.21(b). The CSSRR-Stub Spurline BSF has the widest stop bandwidth (2.5 GHz) in comparison with other BSFs, assuring more or less the same circuit area with the conventional open stub BSF.

2.7.3.2 Harmonic suppressed LPF using CSSRR-Stub-Spurline filter

By cascading the proposed BSF, explained in section 2.7.3.1, with the stepped impedance lowpass filter, the rejection bandwidth of the LPF is enhanced. Fig. 2.22(a) shows the photograph of top and bottom view of the fabricated lowpass filter cascaded with CSSRR-Stub-Spurline bandstop filter. In this case, the optimized dimensions of the BSF to suppress the unwanted passband in the stopband are as follows: L_1 = 10.23 mm, L_2 = 10.23 mm, L_3 = 10 mm, W_1 = 3.06 mm, W_2 = 1 mm, a = 7.5 mm, c = 1.9 mm, and g = 1.9 mm. Fig. 2.22(b) shows the simulated and measured scattering parameters of the lowpass filter cascaded with CSSRR-Stub-Spurline BSF. The spurious passbands in the frequency region from 2.8 GHz to 4.6 GHz are completely suppressed without major changes in the passband. A rejection level of greater than 25 dB is obtained from 3.2 GHz to 5 GHz. The selectivity [56] for the lowpass filter is 26 dB/GHz. All filters have been fabricated on the FR4 substrate and tested using Agilent 8753ES Network Analyzer. Experimental results of the filter are in close agreement with the simulation results. The minor differences found may be due to the tolerances in the fabrication process and connector losses.

2.8 Notched ultra-wideband BPF using CSSRR

The Federal Communication Commission (FCC) authorized the unlicensed use of the ultra-wideband (UWB) frequency spectrum (3.1-10.6GHz) in 2002 for high data rate and short range transmission. Since then, there has been a growing interest in the field of UWB communication. To utilize the required UWB frequency range, various UWB filters have been developed. However, some of the

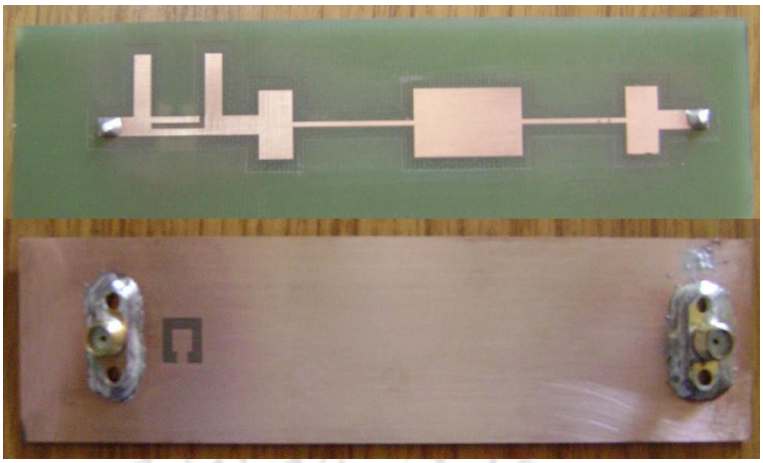

(a)

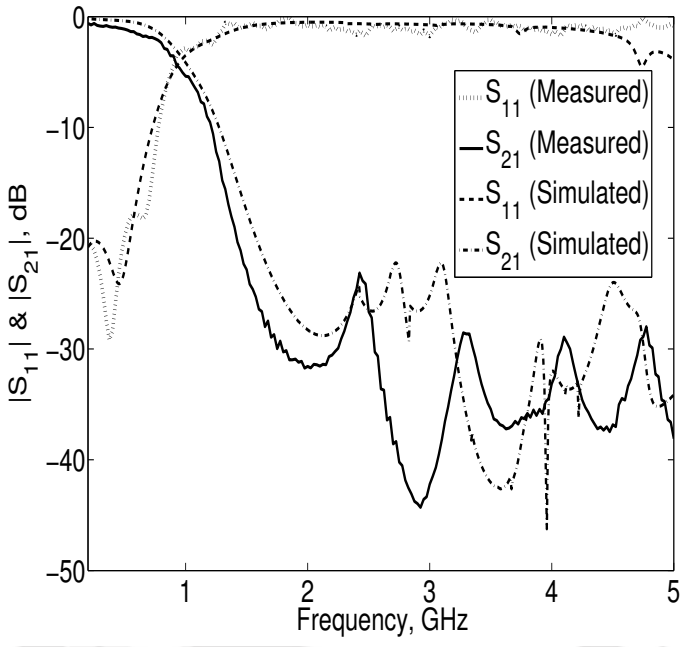

(b)

Figure 2.22: Harmonic suppressed lowpass filter a) Layout b) Scattering parameters.

frequency range within the UWB spectrum is allocated for wireless local area network (WLAN) systems. To avoid the interference between the UWB frequency spectrum and the WLAN radio signals, an UWB bandpass filter with a notch band is desirable. So far, various UWB BPFs with a notch band have been reported by many researchers [57–62]. An UWB bandpass filter with a narrow band notch characteristic using embedded open stub is demonstrated in [57] and [61]. Folded interdigital coupled lines used to create a rejection band in the UWB spectrum at 5.6 GHz are reported in [58].

A meander line slot etched in the active area of the UWB BPF effectively removed the IEEE 802.11a (5.15 GHz to 5.85 GHz) signals from the UWB passband. [59]. Recently, a metamaterial resonator has been employed to introduce wave propagation notch in the UWB bandpass filter [60]. The filters mentioned above have the disadvantage of either low performance or difficulty in fabrication due to via holes.

In this work, we present an UWB bandpass filter with notch function using CSSRR. Compared with the conventional CSRR, it has sharp cut-off and flat insertion loss. Hence, CSSRR is utilized to introduce a sharp rejection band in the UWB frequency spectrum to suppress the WLAN frequency range.

2.8.1 Comparison between CSSRR and CSRR

To compare the performance of the CSSRR with the conventional CSRR, a CSRR resonating at the same resonance frequency as the CSSRR is simulated. The layout and scattering parameters of both the CSSRR and CSRR are illustrated in Fig. 2.23. By observing the plots, we can conclude that the conventional CSRR insertion loss is high and does not have flat response after resonance. Similarly, the roll-off rate of return loss is also low after the resonant frequency. Thus the conventional CSRR performance is poor for notch function. To improve the performance of the conventional CSRR, it was slightly etched away from the host line, and an open circuited stub was employed to compensate for the increase in inductance [60]. On the other hand, by using CSSRR, we can achieve flat insertion loss in the passband of the filter and a better roll-off rate at the transition of the filter without the need for any additional structure.

2.8.2 Bandpass filter with notched band

To design the UWB bandpass filter with notch function, an UWB BPF is first designed using ground plane aperture technique [63]. Due to the aperture in the ground plane, close coupling between the microstrip lines is achieved. The layout and fabricated prototype of UWB BPF are shown in Fig. 2.24(a) and 2.24(b) respectively. A microstrip multiple mode resonator (MMR) line is used to link the two identical PCML sections with a backside aperture. A detailed design procedure of the UWB BPF can be obtained from [63]. The width and the gap between the coupled lines of a PCML are 0.2 mm each. The length of the PCML section is 6.32 mm which is equivalent to the electrical length $\phi = 180^0$. The physical length of a multi mode resonator is equal to 12.25 mm. The length of the

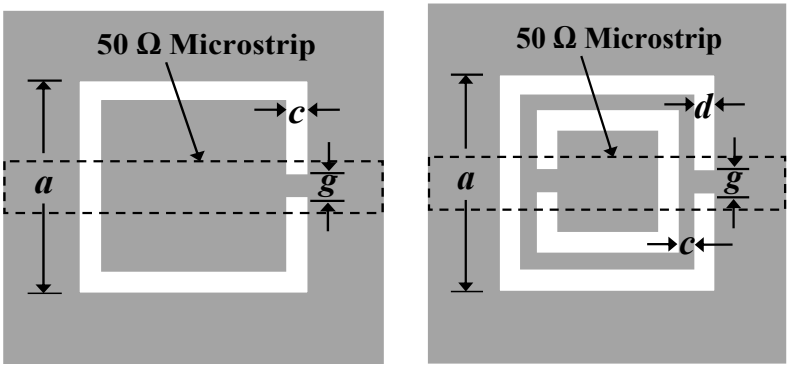

(a) (b)

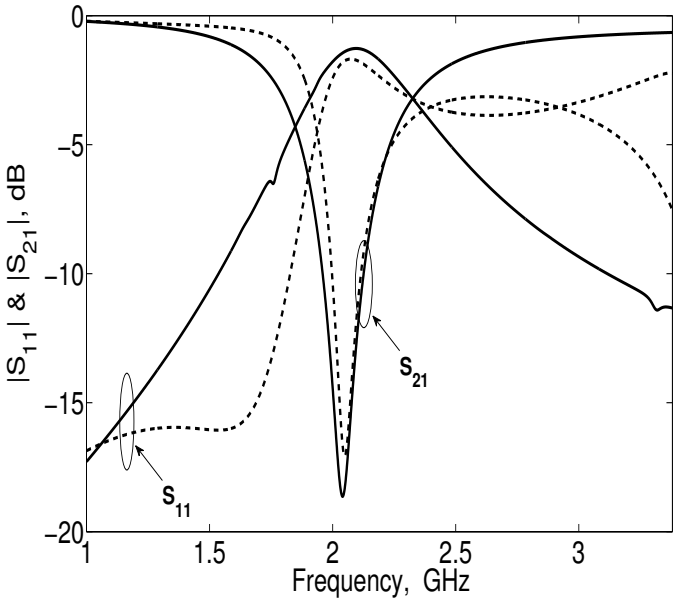

(c)

Figure 2.23: a) CSSRR geometry (a = 12 mm, $d = g$ = 0.5 mm) b) Conventional CSRR geometry (a = 10 mm, $d = c = g$ = 0.5 mm) c) Scattering parameters (CSRR - dashed line, CSSRR - solid line).

ground plane aperture is 6.42 mm and the height is 3.5 mm, both of which are optimized using EM simulation. Fig. 2.24(c) shows the simulated and measured scattering parameters of the UWB BPF. The filter passband is from 2.8 GHz to 10.6 GHz. The measured insertion loss of the conventional UWB BPF is less than 1.5 dB in the passband and return loss is more than 20 dB in the stopband.

As discussed earlier, to notch out the WLAN radio signals from the desired UWB passband, stopband characteristics of a CSSRR is utilized. A CSSRR resonating at 5.5 GHz is designed and

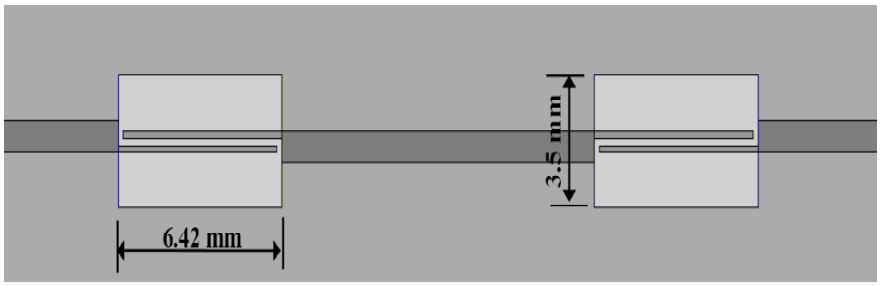

(a)

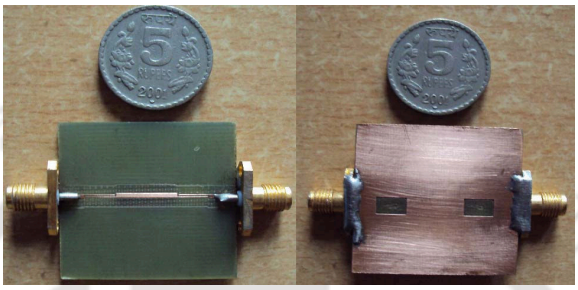

(b)

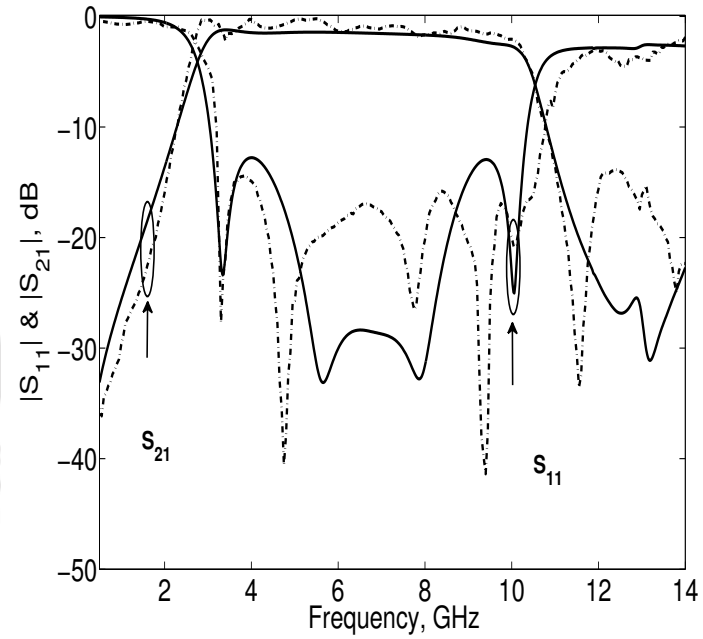

(c)

Figure 2.24: UWB BPF with aperture in the ground plane a) Geometry b) Photograph c) Simulated (solid line) and measured (dashed line) scattering parameters.

placed underneath the parallel coupled lines. The initial dimensions of the CSSRR are obtained from equation 2.11. Since the CSSRR is etched around the ground plane aperture, resonant frequency of the

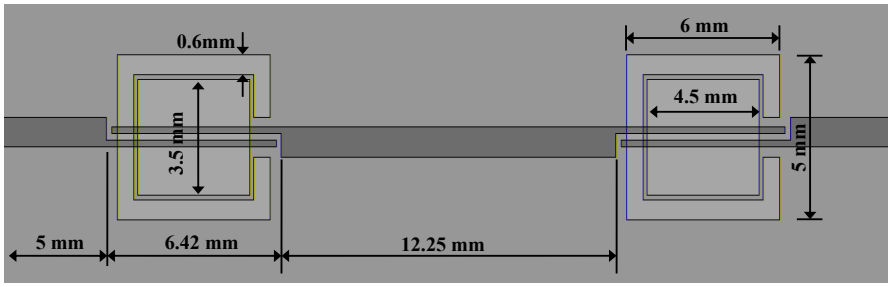

(a)

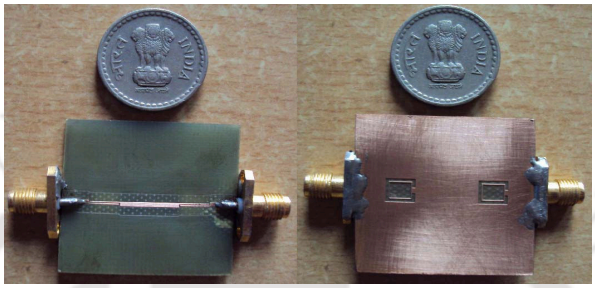

(b)

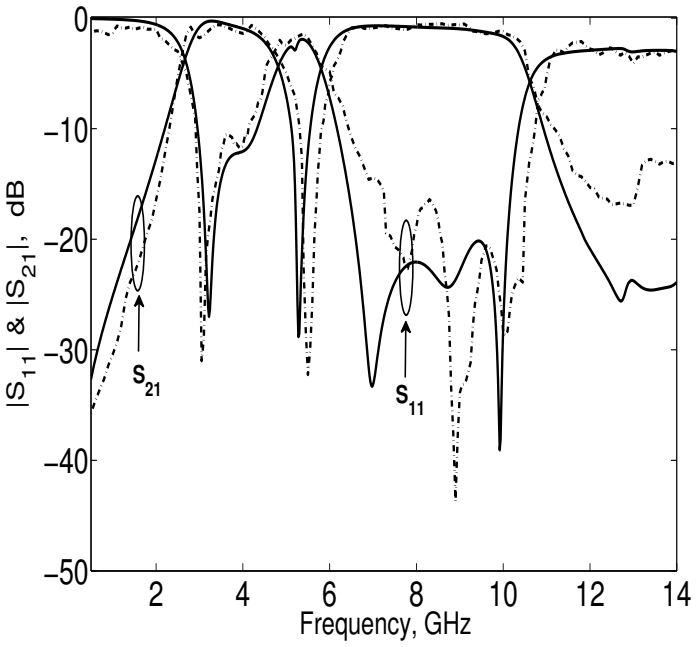

(c)

Figure 2.25: Proposed UWB BPF with notched band a) Geometry b) Photograph c) Simulated (solid line) and measured (dashed line) scattering parameters.

CSSRR does not exactly match the equation 2.11. However, the final dimensions are optimized using EM simulation. To provide room for both the aperture and CSSRR under the coupled lines, the size of

the aperture is modified. Similarly, instead of a square-shaped CSSRR, a rectangular-shaped CSSRR is used to obtain the proper notch-out behavior. All the specifications of the UWB BPF with notched band and photograph of the fabricated filter are shown in Fig. 2.25(a) and Fig. 2.25(b) respectively. Fig. 2.25(c) shows the simulated and experimental results of the UWB BPF. The fabricated UWB BPF passband is from 2.96 GHz to 10.75 GHz, exhibiting notch characteristics at 5.5 GHz with a rejection level of 32.25 dB. The lower and upper 3 dB points of notch are 4.85 GHz and 6.12 GHz respectively. Thus, the proposed filter is capable of effectively suppressing the interference from IEEE 802.11a WLAN signals. Compared with the work reported in [57] and [64], the proposed method provides better FBW in the notch band and does not require any via holes, as used in [57] and [60].

2.8.3 Summary

This chapter presented the theory and applications of single negative sub-wavelength resonator known as CSSRR. The detailed parametric study and lumped element model of the CSSRR are presented. From the parametric study, approximate close form formula for the resonant frequency of CSSRR is obtained. Two different BSFs are designed using CSSRR, open stub, and spurline combination. The proposed BSFs stop bandwidth are wider than the conventional BSF using open stubs. By cascading these BSFs with the conventional PCML BPF and stepped impedance LPF, the spurious passbands occurring at the stopband of the filters are suppressed. To demonstrate the another application of CSSRR, notched UWB BPF design using CSSRR is presented.

3

CSRR and its applications in performance enhancement of microstrip filters

Contents

3.1 Introduction

The split ring resonator (SRR) medium introduced by J. B. Pendry [3] has given us the opportunity to make materials with negative permeability, from which a left-handed medium can be constructed. This left-handed media exhibit a frequency band, where the μ value is negative, despite being made of a nonmagnetic material. They also have another component called a complementary split ring resonator (CSRR), which provides the negative ε behavior. By using the concepts of duality and complementarity, it is straightforward to derive a CSRR from the SRR structure. This CSRR structure provides a negative ε effective permittivity in any medium. Because of their small size, SRRs and CSRRs are called sub-lambda structures or sub-wavelength resonators. Due to this, a super-compact stopband structure can be implemented using SRRs and CSRRs. This chapter mainly discusses the theory and application of CSRRs for the performance improvement of microwave bandpass filter (BPF). The detailed parametric study and stopband characteristics of a CSRR are presented followed by the multiple harmonic suppression of a PCML BPF.

3.2 Topology and circuit model of SRR and CSRR

The split ring resonator consists of two concentric copper rings separated by a small slit gap on opposite sides of the rings. The layout and equivalent circuit model [43] of the SRR is illustrated in Fig. 3.1(a). In this figure, C_0 represents the total capacitance between the rings, i.e., $C_0 = 2\pi r_0 C_{pul}$, where C_{pul} is the per unit length capacitance between the between the rings. The resonant frequency of the SRR is given by,

$$f_0 = \frac{1}{2\pi\sqrt{L_s C_s}} \tag{3.1}$$

where C_s is the series capacitance due to the split gaps of the upper and lower halves of the SRR, and L_s is the inductance of a single ring with an average radius, r_0 and width, c. When excited by an axial magnetic field, the SRR behaves as a magnetic dipole and produces the stopband because of its negative permeability. If the effects of metal thickness and losses are neglected, a CSRR is a perfect dual counterpart for a SRR [65]. Therefore, when excited by an axial electric field, CSRR can be considered as an electric dipole. The layout and equivalent circuit of a CSRR is shown in Fig. 3.1(b). The capacitance C_c of a disk of radius, r_0 - $c/2$ surrounded by a ground plane at a distance c of its edge, replaces the inductance L_s of the SRR model. Similarly, the series capacitor, $C_0/2$ in the SRR model is substituted by the parallel combination of two inductances, $L_0/2$.

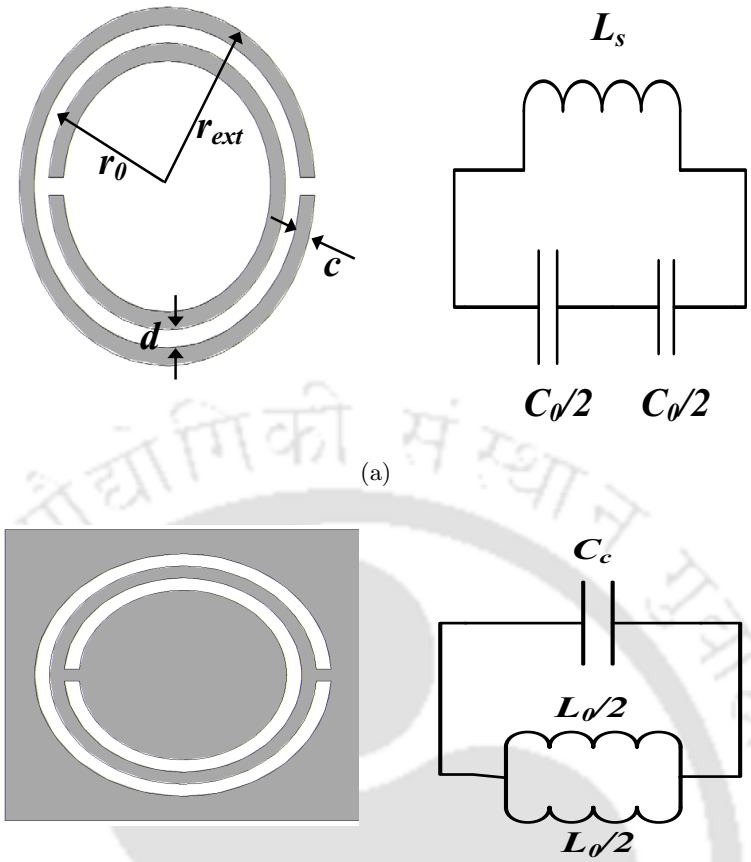

Figure 3.1: Topology and equivalent circuit of a) SRR b) CSRR (Dark portion represents the metal).

3.3 Extraction of material parameters

To verify the left-handed property of the SRR and the CSRR, the material parameters, such as effective permittivity and permeability are extracted as explained in section 2.3. Fig. 3.2(a) shows the simulation setup for parameter extraction. A copper square shaped SRR, with a side length of 4 mm, is printed on one side of the RT/Duroid substrate, with dielectric constant $\varepsilon_r = 2.33$ and height $h = 0.5$ mm. The split gap, width and spacing between the split rings are chosen as 0.2 mm. This setup is simulated using CST Microwave Studio and simulated results are shown in Fig. 3.2(a). As expected, the SRR exhibits sharp rejection characteristics around at the resonant frequency f_0 of 4.69 GHz. The effective material parameters are extracted from the simulated scattering parameters and illustrated in Fig. 3.3. Before resonance, the effective relative permeability reaches its maximum positive value of 43.55 at 4.58 GHz and crosses the zero at 4.6 GHz. At the resonant frequency, it

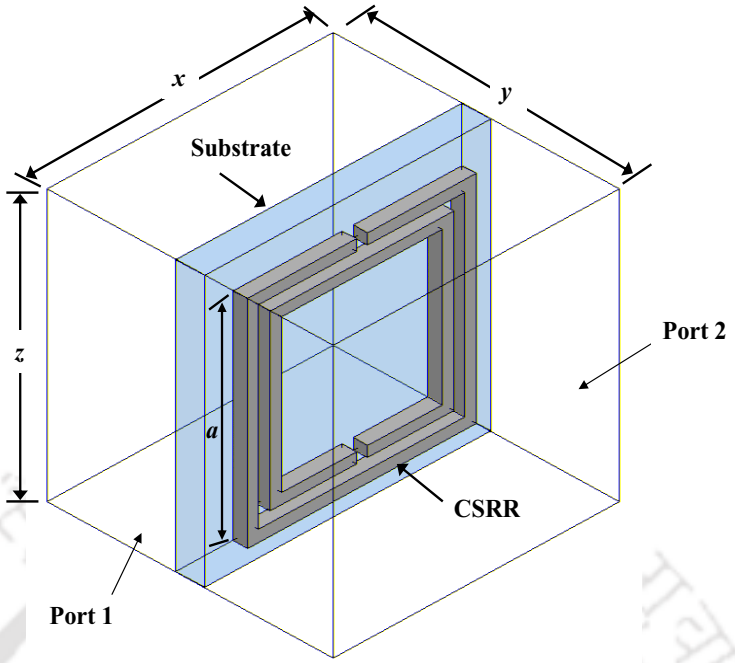

(a)

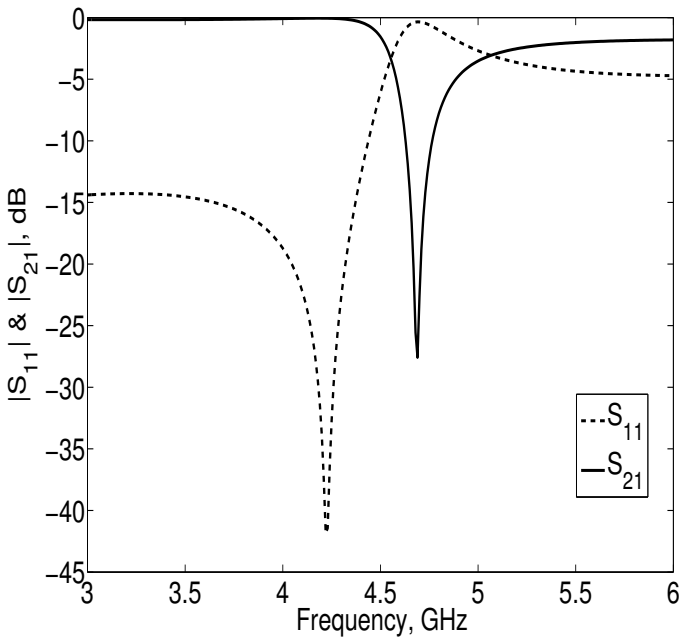

(b)

Figure 3.2: a) Simulation setup b) Scattering parameters.

reaches its negative maximum value of -22.08 and again crosses zero at 5.3 GHz. Similarly, to study the frequency response characteristic of a CSRR, a CSRR with the following dimensions, $a = 10$ mm,

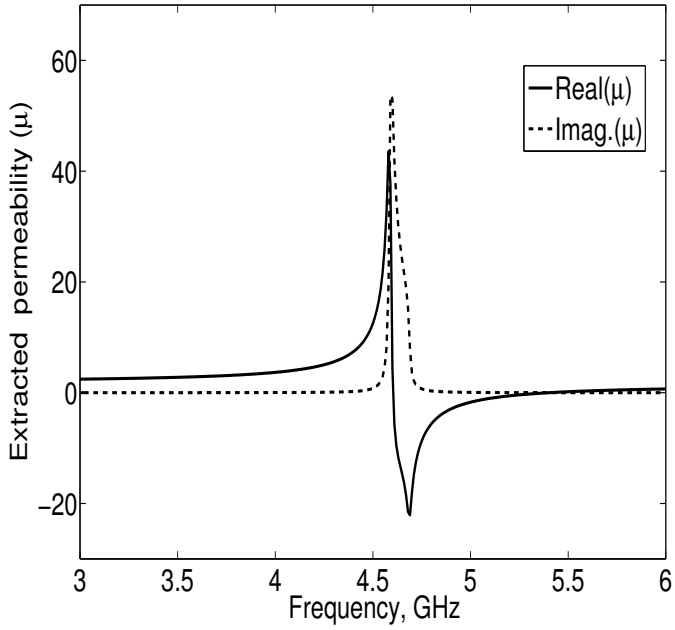

(a)

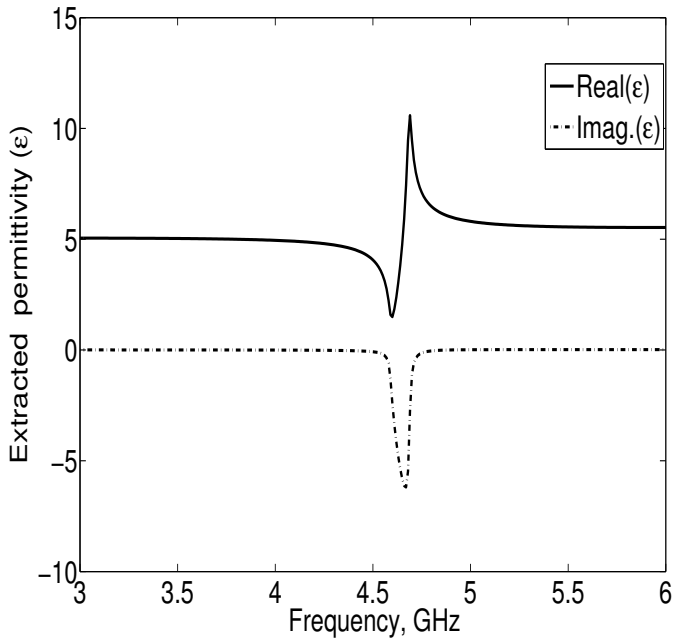

(b)

Figure 3.3: Extracted effective material parameters of SSRR a) Permeability b) Permittivity.

$c = 0.5$ mm, $d = 0.5$ mm, and $g = 0.5$ mm is placed under a 50 Ω microstrip line as Fig. 3.4(a) shows. Since the CSRR is obtained by etching out the SRR shape from the ground plane, it occupies a lesser

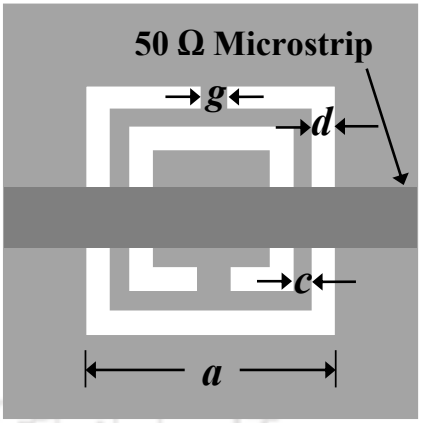

(a)

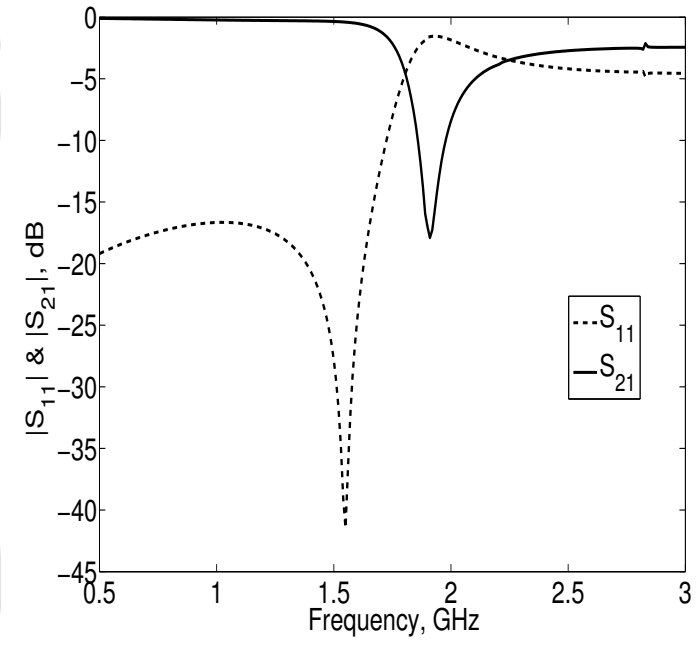

(b)

Figure 3.4: CSRR loaded microstrip line a) Layout b) Simulated scattering parameters.

area than the SRR does. The substrate used for simulation is FR4, with dielectric constant of 4.4 and thickness of 1.6 mm. Fig. 3.4(b) depicts the frequency response characteristic of a CSRR loaded microstrip line. Like the SRR, the CSRR also exhibits stopband near its resonance frequency f_0 = 1.91 GHz.

Fig. 3.5 shows the extracted material parameters of the CSRR loaded microstrip line. As expected, the effective permittivity of the structure shows a maximum negative value of -28.81 at the resonant

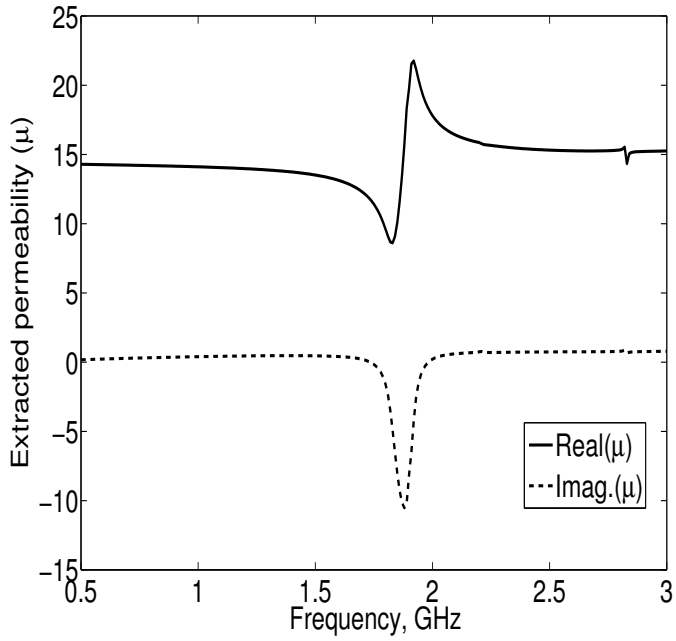

(a)

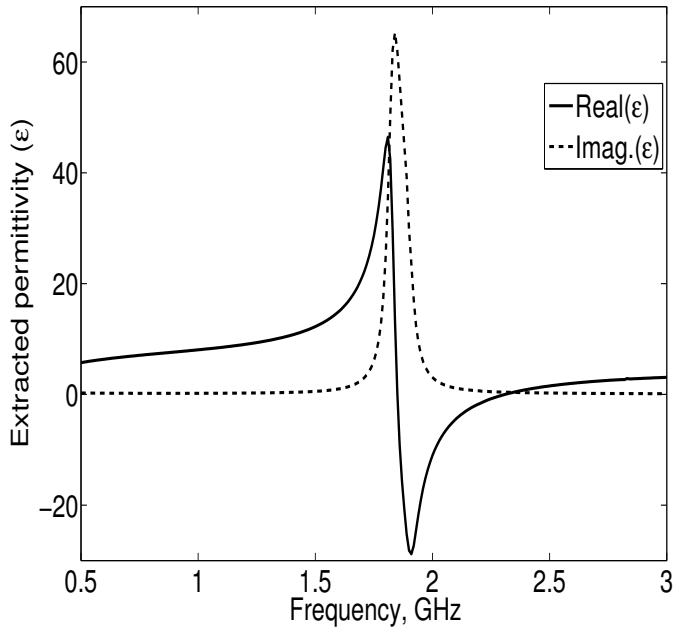

(b)

Figure 3.5: Extracted effective material parameters of CSRR a) Permeability b) Permittivity.

frequency. It reaches its positive maximum value of 46.44 at 1.85 GHz. The zero crossing points are at 1.85 GHz and 2.3 GHz respectively.

Table 3.1: Parametric study of CSRR

a (mm)	d (mm)	c (mm)	g (mm)	Simulated f_r (GHz)
9	0.5	0.5	0.5	2.23
10	0.5	0.5	0.5	1.91
11	0.5	0.5	0.5	1.7
10	0.5	0.5	0.5	1.91
10	1	0.5	0.5	2.02
10	1.5	0.5	0.5	2.36
10	0.5	0.5	0.5	1.91
10	0.5	1	0.5	2.09
10	0.5	1.5	0.5	2.17
10	0.5	0.5	0.5	1.91
10	0.5	0.5	1.5	1.98
10	0.5	0.5	2.5	2.11

3.4 Parametric study of CSRR

Many different parameters affect the resonant frequency of a CSRR, the most dominant being the permittivity of the substrate and the length of the resonator. In the following sections, we show the effect of parameters involved in the design that affect the resonant frequency and that are easy to vary practically. While varying one of the parameters, the other parameters are kept constant.

3.4.1 Influence of CSRR dimension

To investigate the influence of the CSRR side length (a), on the the resonant frequency of CSRR, CSRRs with different side length were simulated and Table 3.1 tabulates the results. As the side length of the CSRR increases, the effective inductance also increases, which in turn, shifts the resonant frequency to the lower end. Similarly, the other parameters also varied and the corresponding changes in the resonant frequency of the CSRR are tabulated. From the table, it is observed that the CSRR resonant frequency is inversely proportional to the side length of the CSRR. Increasing the other parameters of the CSRR, such as slot width (d), strip width (c), and split gap (g), also increases the resonant frequency.

3.4.2 Influence of substrate permittivity

The resonant frequency is inversely proportional to the dielectric constant of the substrate. Modifying the substrate dielectric constant (ε_r) will shift the resonant frequency accordingly. To demonstrate

Table 3.2: CSRR etched in different substrate

Substrate	Dielectric constant (ε_r)	Simulated f_r (GHz)
RT/Duroid 5880	2.33	2.815
FR4	4.4	1.79
RT/Duroid 6006	6.15	1.61

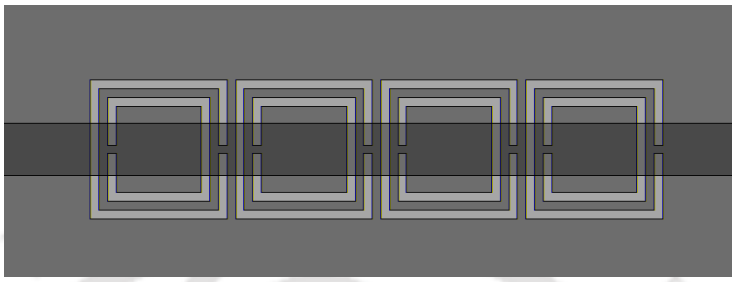

Figure 3.6: Microstrip line loaded with periodic array of CSRRs.

this effect, we simulated the CSRR using three different substrates, and Table 3.2 tabulates the results. From Table 3.2, it is evident that as ε_r increases, the resonant peak shifts toward lower frequency. As ε_r is increased, the capacitances of the CSRR also increase and hence, the resonant frequency shifts to a lower frequency.

3.5 Stopband characteristics of CSRR

In this section, we present the stopband characteristics of the microstrip line loaded with the periodic array of CSRRs. As discussed in section 3.3, the CSRR produces a narrow stopband during its resonance. Here, our concern is to enhance the stopband filter characteristics by increasing the number of CSRR structures in the ground plane. This is achieved by placing more CSRRs with the same dimensions periodically below the microstrip line. The dimensions of all CSRRs are kept as follows: $a = 8$ mm, $c = 0.5$ mm, $d = 0.5$ mm, and $g = 0.5$ mm. The distance between the two adjacent CSRRs is maintained at 0.5 mm. Fig. 3.6 shows such a stopband filter structure as having four CSRR structures, in which all the CSRRs have the same dimensions.

Fig. 3.7 shows the insertion loss of various numbers of CSRRs in the ground plane. From the figure, it is observed that, the rejection bandwidth of a single CSRR is only 170 MHz and the maximum rejection level is 19.22 dB. In order to widen the rejection bandwidth further, the number of CSRRs under the microstrip line is increased up to eight cells. The results show a large stop bandwidth

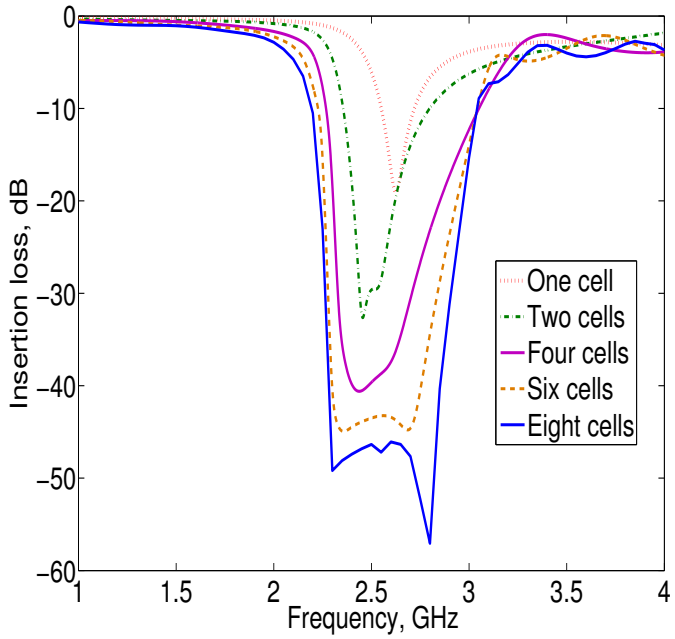

Figure 3.7: Insertion loss of microstrip line loaded with periodic array of CSRRs.

from 2.2 GHz to 3.05 GHz with a rejection bandwidth of 850 MHz. This is a significant improvement compared with the previous results of a single CSRR. The rejection level of the eight cell CSRR is also increased to 57.06 dB. Fig. 3.8 and Fig. 3.9 respectively show the rejection bandwidth and maximum rejection level of various numbers of CSRR cells.

3.6 Multiple harmonic suppression of PCML bandpass filter using CSRR

3.6.1 Introduction

Microstrip bandpass filters (BPF) have been widely employed in microwave and wireless communication systems for permitting a signal in the desired range of frequencies and rejecting all others. Different filters techniques are available for designing BPF. The PCML BPF is the most popular one because of its planar structure, readily available design formulae, and easy design procedures. However, the fundamental limitation of such BPFs is the presence of nearby out-of-band spurious passbands. This is mainly due to the difference in the odd and even mode phase velocities and the distributed nature of the microstrip line. To avoid interference with devices working in the nearby frequency spectrum, these spurious passbands should be completely removed or suppressed.

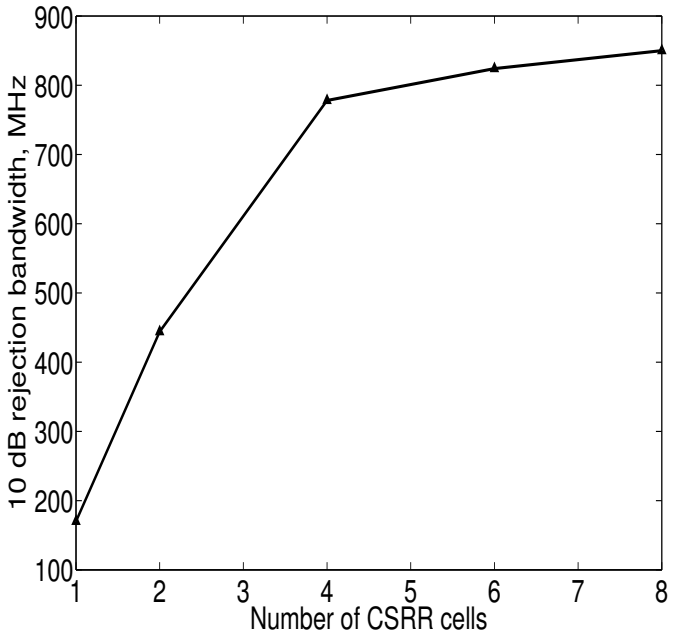

Figure 3.8: Rejection bandwidth (10 dB) of microstrip line loaded with various number of CSRRs.

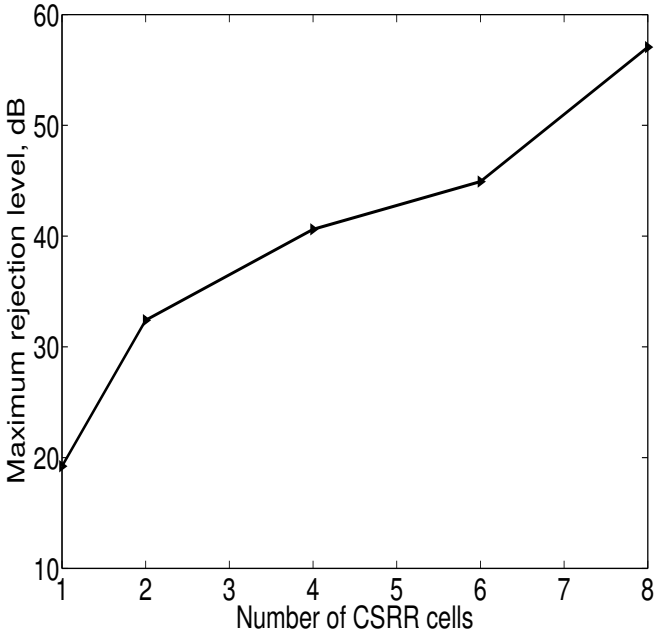

Figure 3.9: Maximum rejection level of microstrip line loaded with various number of CSRRs.

Several techniques have been reported in the literature to solve this problem. By etching periodic photonic bandgap (PBG) patterns in the ground plane, the harmonics of the PCML BPF are effectively removed in [66]. In [47], continuous perturbation of the coupled line width according to the sinusoidal

law has been suggested for suppressing the second harmonic. Corrugated coupled microstrip lines are designed to equalize the odd and even mode phase velocities for obtaining a wide upper stop band in [48]. Based on Bragg reflection, periodic grooves are etched in the microstrip lines to eliminate a spurious passband at $2f_0$ [49]. SRRs and CSRRs have been established as a means for suppression of harmonics in microstrip and CPW technologies [10], [50]. Bandstop filters using open stub and spurline can be adopted for suppressing the second harmonic in the open loop ring BPF [51]. Odd and even mode phase velocities were equalized using the substrate suspension technique [67] and by placing a dielectric overlay over the coupled lines [68] to eliminate the second harmonic. Parallel coupled microstrip sections with a slotted ground plane are proposed as building blocks of PCML BPFs for harmonic rejection in [69]. Floating strip conductors printed on the backside of the substrate are shown to be useful for suppressing second harmonics in microstrip filters [70].

But the use of PBG structures for low frequencies increases the circuit area of the filter and side by side, introduces passband ripple. As SRRs are normally placed on the upper side of the substrate close to the signal strip, it results in an increased filter size. The printing of sinusoidal and corrugated structures on the signal strip is difficult from a fabrication point of view. In this work, to reject the unwanted spurious passband, we use a traditional open stub-spurline rejection band filter. However, to enhance the rejection bandwidth, additional transmission zero is introduced by placing a CSRR under the 50 Ω microstrip line. Using this newly proposed BSF, which is constructed employing three bandstop structures, the harmonic suppression of a PCML BPF up to the fifth order harmonic ($5f_0$) is possible. It is demonstrated both from IE3D simulation results as well as experimental results.

3.6.2 Design of wide stopband BSF using CSRR

A Conventional open stub filter is first constructed by placing two open stubs of length $L_1 = \lambda_g/4$ at a distance of $L_2 = \lambda_g/4$ on a microstrip line, where λ_g is the guided wave length. We have designed the open stub filter at the center frequency of 4 GHz. The optimized dimensions of the filter are L_1= 10.23 mm, L_2 = 10.23 mm, and W_1 = 3.06 mm. This filter gives a stop bandwidth of 1.35 GHz. A wide stopband can be obtained by cascading grater number of open stub stages, however, it results in increased device area. To overcome this limitation, a spurline is embedded [51] between the open stubs. The length of the spurline is $\lambda_g/4$ and the width is chosen as 10% of the microstrip line width. The optimized dimensions of spur line are L_3 = 10 mm and W_2 = 1 mm. The stop bandwidth of stub-spurline filter is 2 GHz, which is 0.65 GHz more than the open stub BSF. To extend the rejection

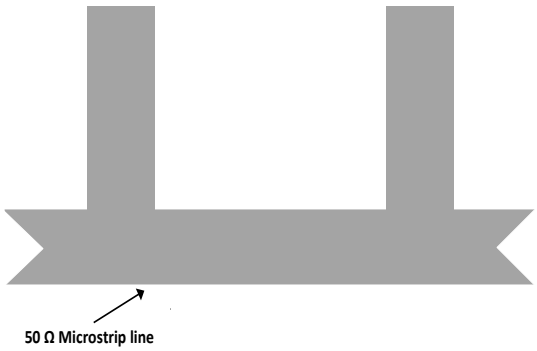

(a)

(b)

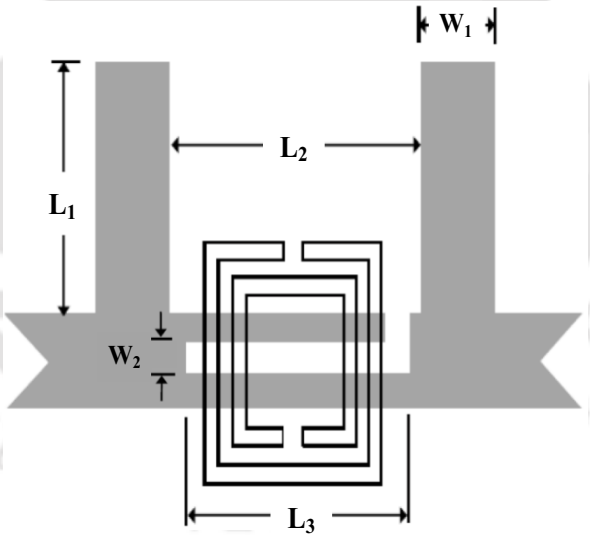

(c)

Figure 3.10: Geometry of a) Open stub b) Open stub-Spurline and c) Proposed BSFs.

bandwidth further, one more stop band structure is added by placing a CSRR below the open stub and spurline section. The CSRR is designed to resonate near the second harmonic frequency with

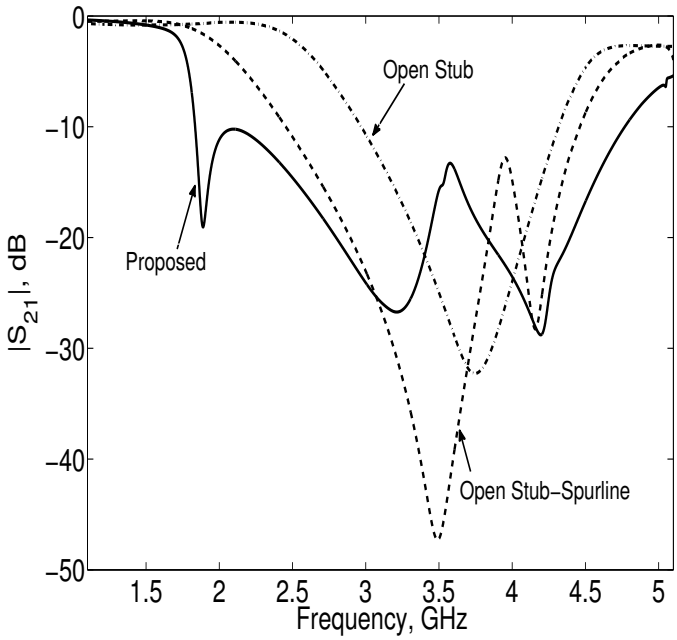

Figure 3.11: Simulated insertion loss of various BSFs.

Table 3.3: Comparison of three BSFs

Filter Type	Stop bandwidth in GHz
Open stub	1.35
Open Stub-Spurline	2
Proposed	2.93

the following dimensions $a = 10$ mm, $c = 0.5$ mm, $d = 0.5$ mm, and $g = 0.5$ mm. Due to this, stopband of the bandstop filter is enhanced up to 2.93 GHz. Fig. 3.10 and Fig. 3.11 show the various types of bandstop filter layouts and their simulated insertion losses respectively. Among them, the CSRR-Stub-Spurline filter has the widest stop bandwidth and a sharp passband to stopband transition compared with other BSFs. Table 3.3 lists the stop bandwidths of various BSFs.

3.6.3 Harmonic suppression of PCML BPF

To verify the harmonic rejection capabilities of the proposed bandstop filter, a first order Chebyshev PCML BPF centered at $f_c = 0.9$ GHz with 10% fractional bandwidth (FBW) has been designed on a FR4 substrate using the standard design procedure [44, 45]. The physical parameters of the filter are listed in Table 3.4. Fig. 3.12 shows the simulated and measured scattering parameters (S_{11}

and S_{21}) of the conventional PCML BPF. From the figure, we observe that the spurious passbands occur at multiples of the center frequency. This spurious passband will degrade out-of-the-band filter performance. So by embedding the proposed wide rejection bandwidth bandstop filter in the input port of the PCML BPF, these undesired harmonics can be eliminated effectively .

Table 3.4: Physical parameters of the first order Chebychev BPF centered at 0.9 GHz with 10% FBW

i	$Z_{0_e}\Omega$	$Z_{0_o}\Omega$	w_i(mm)	s_i(mm)	l_i(mm)
1	70	30	1.22	0.512	46.972

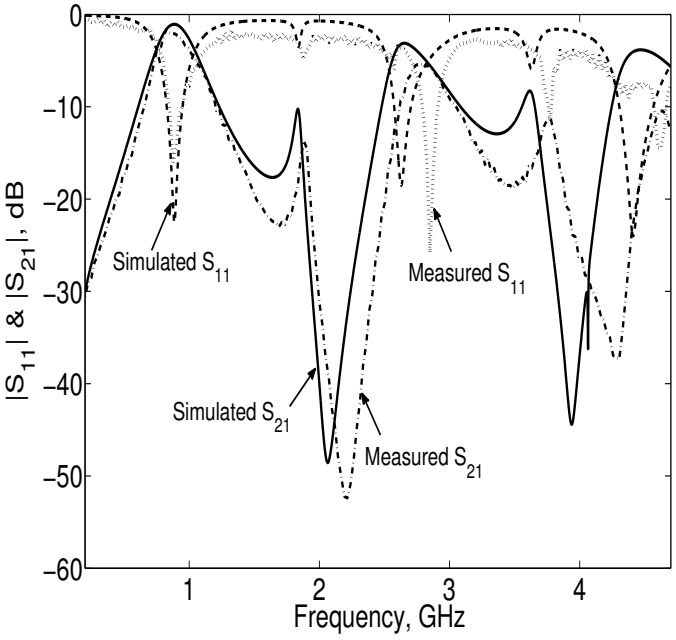

Figure 3.12: Simulated and measured scattering parameters of conventional PCML BPF.

Fig. 3.13 shows a photograph of the new harmonic suppressed PCML BPF. Fig. 3.14 shows the simulated and measured results of the proposed PCML BPF with the CSRR-Stub-Spurline section. The measured insertion loss and return loss are less than 1.43 dB and 20 dB respectively. The rejection level is more than 20 dB, up to 4.5 GHz, and that means, the harmonic suppression up to $5f_0$ has been achieved. Above 30 dB rejection level is obtained from 3 to 4.2 GHz. The differences in the simulated and experimental results are due to tolerances in the fabrication process.

In general, a third or more order BPF is used in practice. Therefore, we have simulated a third

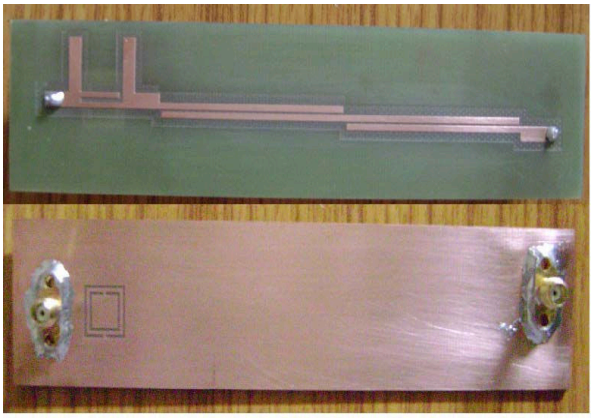

Figure 3.13: Fabricated prototype of proposed PCML BPF using CSRR-Stub-Spurline BSF (Top and Bottom view).

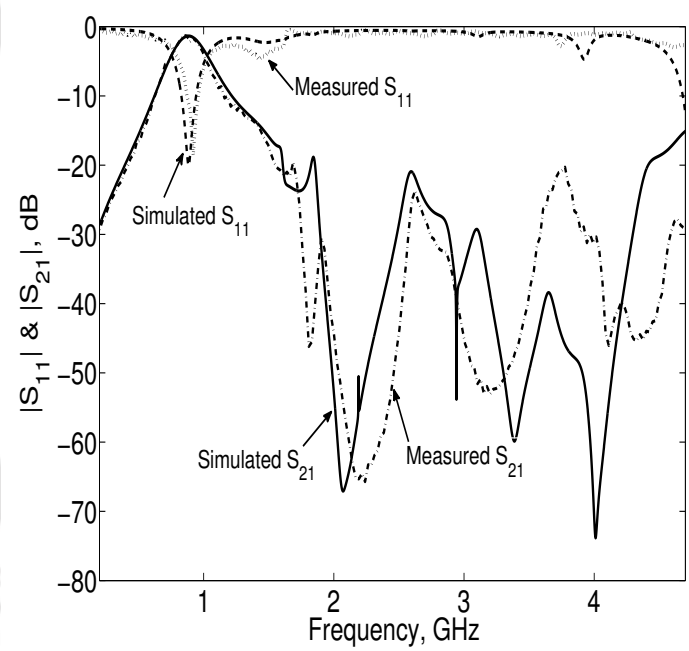

Figure 3.14: Simulated and measured scattering parameters of harmonic suppressed PCML BPF using CSRR-Stub-Spurline BSF.

order PCML BPF with the same specification and the proposed CSRR-Stub-Spurline filter is cascaded with this BPF. A better harmonic suppression is also achieved in this case. Table 3.5 shows the physical parameters of the filter. Fig. 3.15 shows the simulated scattering parameters of a conventional and a proposed third order PCML BPF. The harmonic suppression of more than a 25 dB rejection level is

Table 3.5: Physical parameters of the third order equi ripple PCML BPF centerd at 0.9 GHz with 10% FBW

i	$Z_{0_e}\Omega$	$Z_{0_o}\Omega$	w_i(mm)	s_i(mm)	l_i(mm)
1	70.61	39.24	1.22	0.4	46.684
2	56.64	44.77	1.44	1.28	46.432
3	56.64	44.77	1.44	1.28	46.432
4	70.61	39.24	1.22	0.4	46.684

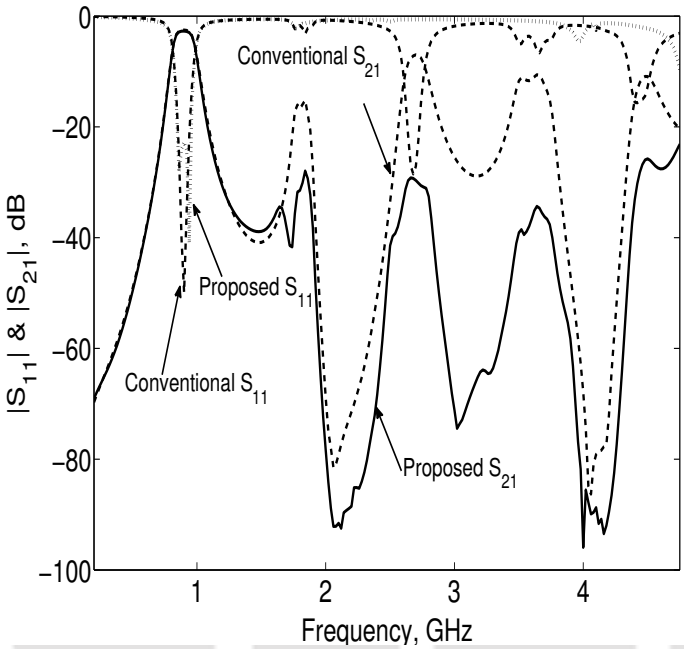

Figure 3.15: Simulated scattering parameters of harmonic suppressed third order PCML BPF using CSRR-Stub-Spurline BSF.

achieved up to $5f_0$.

3.7 Summary

In this chapter, a well-known structure SRR, exhibiting negative permeability, and its counterpart CSRR, exhibiting negative permittivity, are studied. The detailed parametric study and stopband characteristics of a CSRR in the ground plane of the microstrip line are presented. A new bandstop filter is constructed using CSRR, open stub and spurline combination. It produces a sharp passband to stopband transition and 47% more rejection bandwidth than the conventional BSF assuring the same device area. By combining this BSF with a conventional PCML BPF, the undesired harmonics

are eliminated. The proposed harmonic suppressed PCML bandpass filter operating in the 900 MHz GSM band offers more than a 20 dB rejection level up to the fifth harmonic, a maximum rejection level of 75 dB in the stop band, and a low passband insertion loss of less than 1.43 dB.

4

OSSRR and its applications in performance enhancement of microstrip filters

Contents

4.1 Introduction

Metamaterials are a special class of artificial materials simultaneously exhibiting negative permeability and permittivity. Recently, various structures exhibiting metamaterial characteristics have been proposed by various authors [71–78]. A double negative (DNG) metamaterial (MTM) cell composed of a SRR and an I shaped ring is demonstrated in [71]. A negative index material designed using an omega like structure is presented in [72] and [74]. Size miniaturized left-handed transmission lines using a multiple SRR and spiral resonator are discussed in [73]. A fractal spiral resonator exhibiting negative permeability is demonstrated in [78].

In this chapter, we introduce two new resonators exhibiting metamaterial properties, namely an open split ring resonator (OSRR) and an open slot split ring resonator (OSSRR). The OSRR exhibits negative μ and the OSSRR exhibits negative ε. Compared with the conventional SRR and CSRR structures, the proposed structures occupy a lesser area for the same resonant frequency. Hence, size miniaturization of microwave devices is possible using the new class of resonators. First, the theory and material parameter extraction of OSRR are discussed. Then the design of a single negative and double negative cell using an OSRR is presented. The rest of the chapter deals with the detailed analysis of the planar structure OSSRR, starting from material parameter extraction, equivalent circuit modeling, and is followed by the parametric study of OSSRR. Few applications of OSSRR, such as bandpass filter, lowpass filter and composite right/left handed transmission line are presented to support this study.

4.2 Open split ring resonator

Fig. 4.1 describes the structure of the OSRR. It is formed by two concentric copper rings having openings at the same side that are connected to another set of concentric copper rings. This structure is printed on one side of the RT/Duroid substrate, with dielectric constant of 2.33 and a height of 0.5 mm. This structure is placed inside a waveguide. The dimensions of the cubic cell are x = y = z = 5 mm. The perfect electric conductor (PEC) boundary condition is applied to the top and bottom walls of the waveguide, whereas a perfect magnetic conductor (PMC) boundary condition is applied to the sidewalls of the waveguide. The other two opposite sides of the waveguide are assigned as wave ports. Fig. 4.2 shows the simulation setup for acquiring the scattering parameters. This setup is simulated using commercial full-wave simulator. Fig. 4.3(a) shows a plot of the the simulated

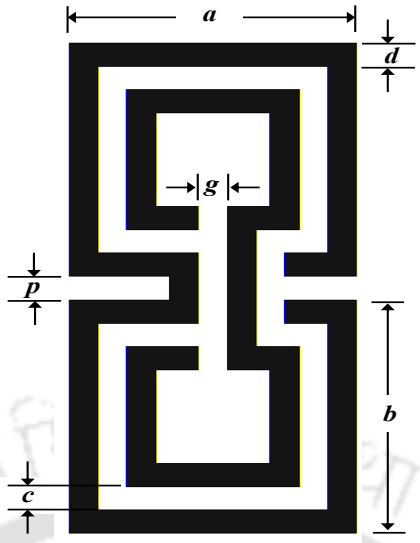

Figure 4.1: Layout of OSRR ($a = 4$ mm, $b = 2$ mm, $p = g = c = d = 0.2$ mm).

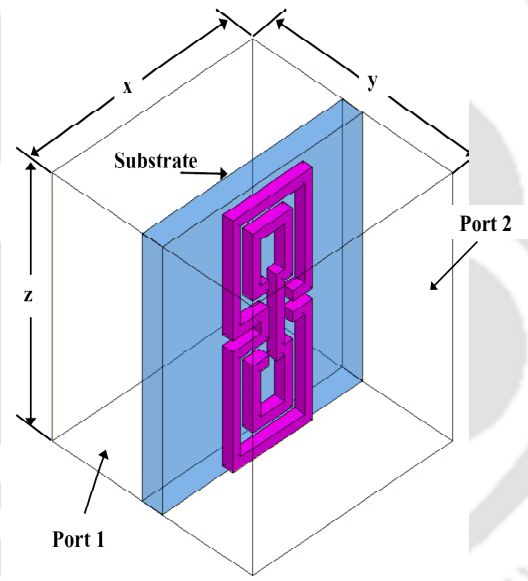

Figure 4.2: Simulation setup of OSRR.

scattering parameters of the OSRR. Similar to an SRR [50], if an array of the OSRR is excited by the magnetic field parallel to the ring axis, current loops are introduced in the ring. At resonance, these current loops are closed through the capacitance between the rings and an incident wave is reflected back to the source, causing a stopband. At a resonance frequency of 4.12 GHz, a sharp rejection band is observed.

The parameter extraction can be done using the method described in [78]. The extracted perme-

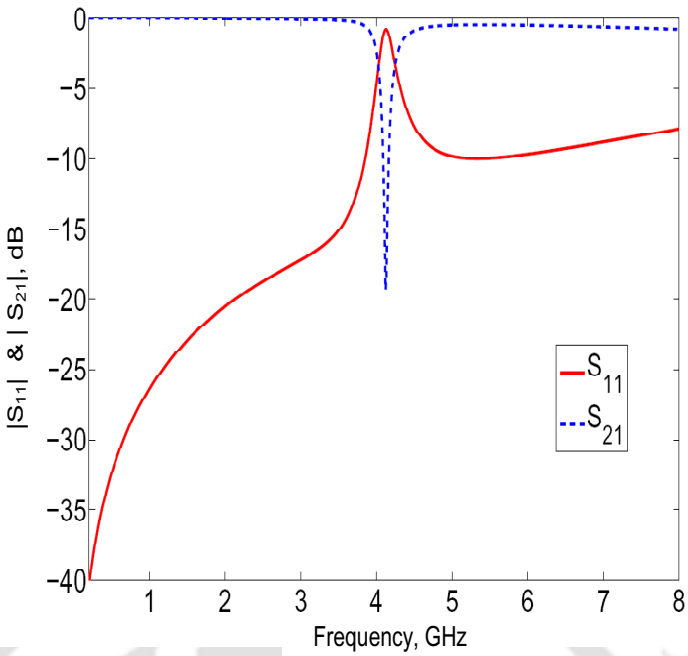

(a)

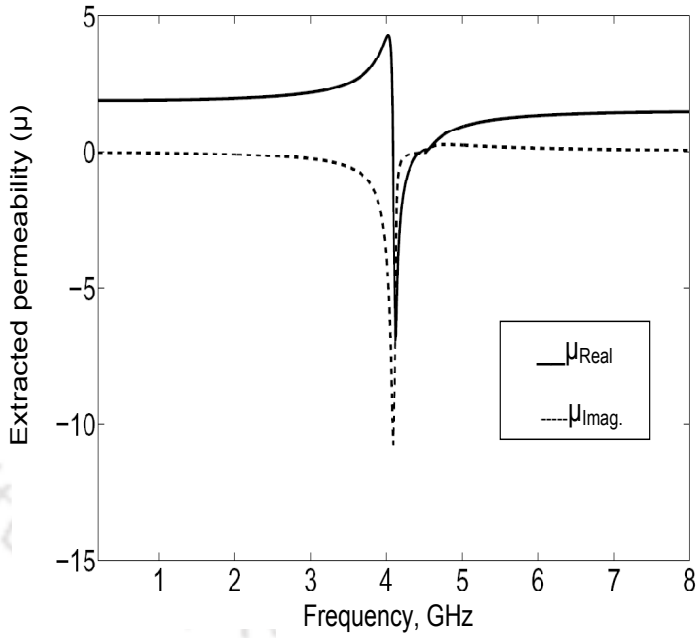

(b)

Figure 4.3: OSRR a) Simulated scattering parameters b) Extracted permeability.

ability of OSRR is shown in Fig. 4.3(b). Similar to the well-known mu-negative material (MNG) SRR, OSRR also exhibits negative permeability near its resonance frequency of 4.12 GHz. The bandwidth

of the μ negative region is 0.4 GHz.

To study the characteristics of the OSRR for different dimensions, a parametric study has been performed and Table 4.1 shows the results. When one of the OSSRR parameters was increased, all others were kept unchanged. When 'a' and 'b' are increased, the equivalent inductance of the OSRR is increased and the resonant frequency, f_r is decreased. When the split gap 'g' of the OSRR is increased, the decreased equivalent capacitance leads to an increase in f_r. Similarly, an increase in ring width 'd' also increases the resonant frequency. For comparison purposes, we also designed a SRR resonating at the same frequency as the OSRR. The simulation setup for SRR is same as described in section 4.2. Fig. 4.4 shows a plot of the comparative results of SRR and OSRR. By observing the plots and dimensions of both structures, we conclude that the OSRR is approximately 20% smaller than the SRR.

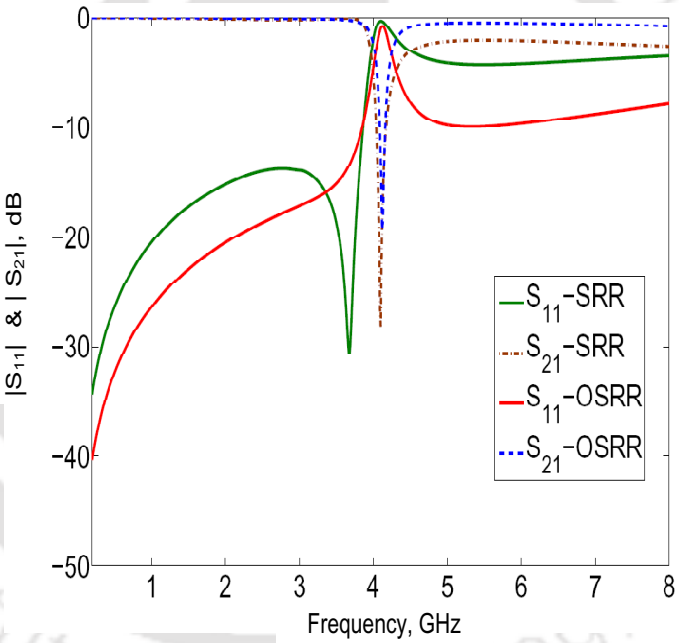

Figure 4.4: Simulated scattering parameters of SRR and OSRR.

4.2.1 Double negative MTM cell using OSRR

A double negative (DN) cell is constructed by placing the OSRR and thin copper wire on opposite sides of the substrate. Fig. 4.5 illustrates the simulation setup for the DNG cell. The width of the copper wire is 0.2 mm and it runs along the length of the cell. The material parameters are extracted from the scattering parameters, as explained in the previous section. The retrieved material

Table 4.1: Parametric study of OSRR
(all dimensions are in mm)

a	b	c	d	g	l	f_r (GHz)	μ_{real}
2.5	1.5	0.2	0.2	0.2	0.2	7.39	-1.99
3.5	1.5	0.2	0.2	0.2	0.2	5.48	-4.27
4.5	1.5	0.2	0.2	0.2	0.2	4.12	-6.97
4.5	2	0.2	0.2	0.2	0.2	3.44	-9.401
3.5	1.5	0.2	0.2	0.4	0.2	5.68	-5.68
3.5	1.5	0.4	0.2	0.2	0.2	5.86	-6.864
3.5	1.5	0.2	0.3	0.2	0.2	6.14	-3.191

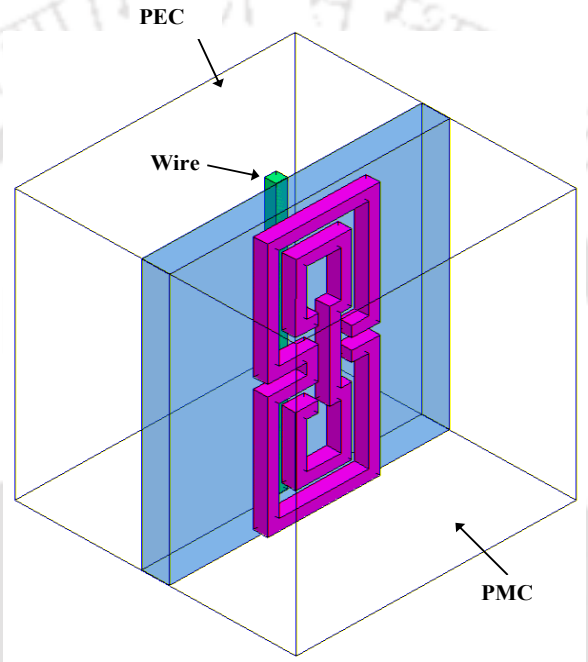

Figure 4.5: Simulation setup of DN-MTM cell.

parameters are shown in Fig. 4.6. The double negative region, where permittivity and permeability both are negative, is observed from 4.3 GHz to 4.6 GHz.

4.3 Open slot split ring resonator

An OSSRR is a negative image of the OSRR. An OSSRR is formed by two concentric square slots having openings at the same side that are connected to another set of concentric square slots. Since OSSRR is a dual counterpart of the OSRR, an axial time varying electric field is required to excite the OSSRR instead of a magnetic field as with an OSRR. As a result, the permittivity of the OSSRR loaded medium is negative. To study the frequency response characteristics of an OSSRR, an OSSRR

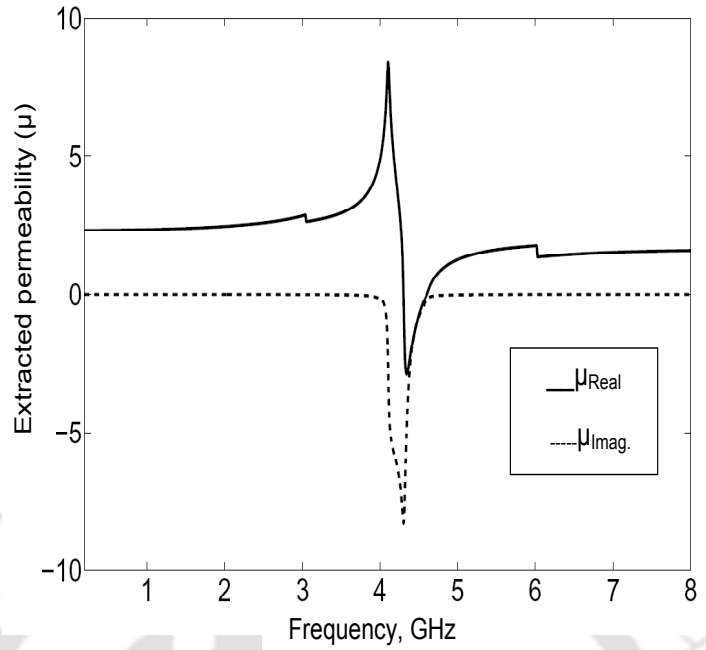

(a)

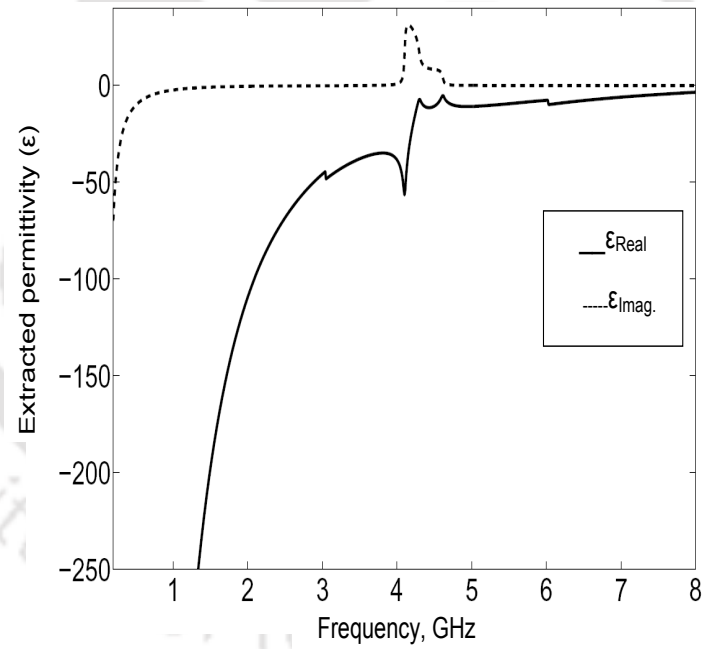

(b)

Figure 4.6: a) Extracted permeability of DN-MTM cell b) Extracted permittivity of DN-MTM cell.

with the dimensions, $a = 12$ mm, $c = 0.5$ mm, $d = 0.5$ mm, $g = 0.5$ mm, and $l = 3$ mm is placed under a 50 Ω microstrip line and simulated using a full-wave simulator. A FR4 substrate, with the

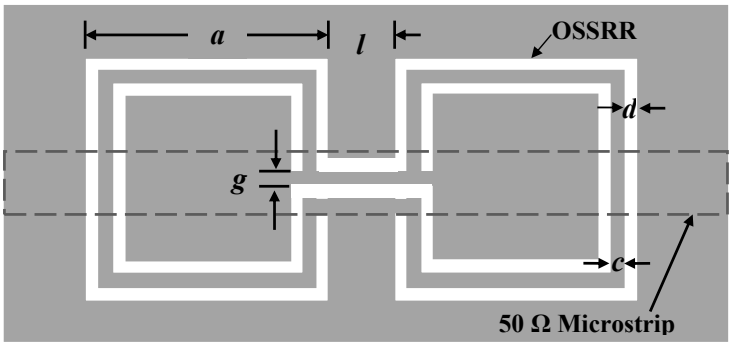

(a)

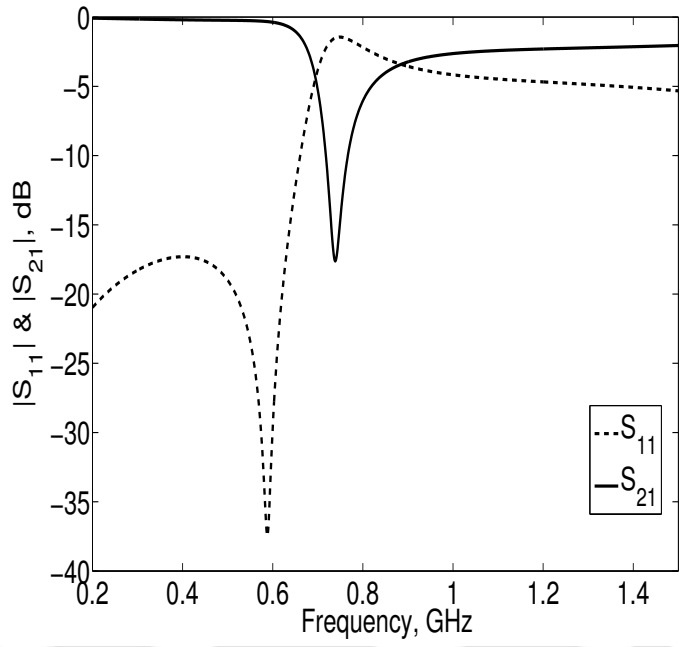

(b)

Figure 4.7: Open slot split ring resonator a) Layout b) Simulated scattering parameters.

dielectric constant $\varepsilon_r = 4.4$ and height $h = 1.6$ mm is used for all simulations. Fig. 4.7 depicts the layout and scattering parameters of the OSSRR. At the resonance frequency $f_r = 0.74$ GHz, a sharp stopband is observed. The values of permittivity and permeability of the OSSRR loaded transmission line are obtained from the simulated scattering parameters and plotted in Fig. 4.8. The amplitude of the real part of permittivity (ε) is negative just above the resonant frequency. It reaches its most positive value, i.e., 125.5, at 0.69 GHz, crossing the zero at 0.707 GHz, and then reaches its most negative value, i.e., -53.07, at 0.74 GHz, again crossing the zero at 0.827 GHz.

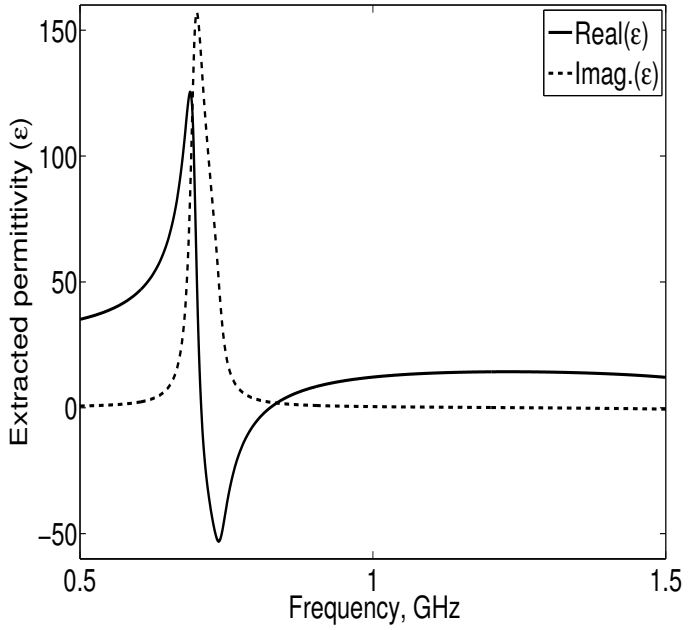

(a)

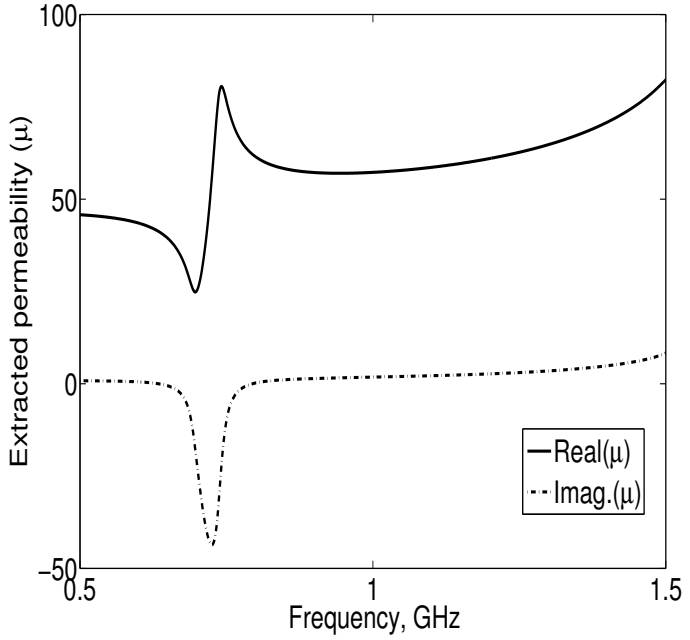

(b)

Figure 4.8: Material parameters of OSSRR a) Permittivity b) Permeability.

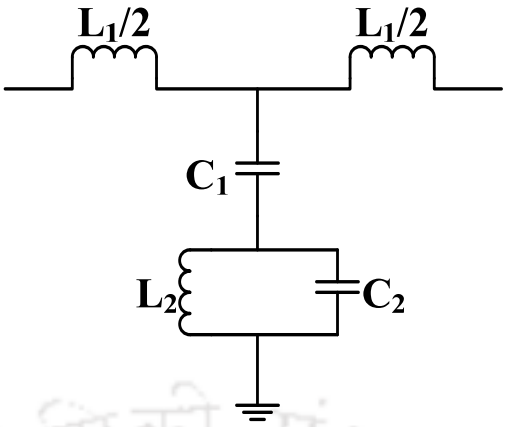

Figure 4.9: Lumped element model of OSSRR.

4.4 Lumped element model of an OSSRR

To validate the proposed OSSRR to a practical circuit design, it is necessary to model the OSSRR. So the lumped element equivalent circuit of the OSSRR is constructed and parameter values are obtained using [79]. We can model the proposed OSSRR as a parallel resonant circuit attached to the equivalent circuit of the transmission line. Fig. 4.9 shows the equivalent circuit of the OSSRR. L1 and C1 are the inductance and capacitance of the microstrip line respectively and L2 and C2 are the inductance and capacitance of the OSSRR respectively. Two frequencies can be identified from the equivalent circuit. One is the resonant frequency of the OSSRR f_r,

$$f_r = \frac{1}{2\pi\sqrt{L_2C_2}} \tag{4.1}$$

and the other is transmission zero frequency, f_z which nulls the shunt impedance.

Let

$$Z_1 = \frac{1}{j\omega C_1} \tag{4.2}$$

$$Z_2 = \frac{1}{j\omega C_2 + \frac{1}{j\omega L_2}} \tag{4.3}$$

The resonance occurs at

$$Z_1 + Z_2 = 0 \tag{4.4}$$

$$\frac{1}{j\omega C_1} + \frac{j\omega L_2}{1-\omega^2 L_2 C_2} = 0 \tag{4.5}$$

$$1 - \omega^2 L_2 C_2 = \omega^2 L_2 C_1 \tag{4.6}$$

$$\omega^2 = \frac{1}{L_2(C_1 + C_2)} \tag{4.7}$$

$$f_z = \frac{1}{2\pi\sqrt{L_2(C_1 + C_2)}} \tag{4.8}$$

The two frequencies can be obtained from the simulation. The notch in the transmission coefficient is identified as $f_z = 0.74$ GHz. To obtain f_r, the reflection coefficient is plotted on a Smith chart. At this frequency, the shunt path to the ground is opened and the input impedance seen from the port is only the series impedance of the structure. Therefore, f_r is calculated by the intersection between the simulated reflection coefficient and the unit normalized resistance circle. Fig. 4.10 illustrates the representation of the reflection coefficient on a Smith chart. The calculated f_r is 0.812 GHz. From that, the inductance 'L' of the equivalent circuit is determined. By solving the equations 4.1 and 4.8, we can compute the remaining unknowns of the lumped element model. However, the equations 4.1 and 4.8 are dependent on three unknowns, so we need an additional condition for solving. At the angular frequency $\omega_{\pi/2}$, where the phase of the transmission co-efficient is $\pi/2$,

$$Z_s(j\omega_{\pi/2}) = -Z_p(j\omega_{\pi/2}) \tag{4.9}$$

where $Z_s(j\omega_\pi)$ and where $Z_p(j\omega_\pi)$ are the series and shunt impedance of the equivalent circuit. Thus, by solving the three equations 4.1, 4.8 and 4.9, we can determine the values of the shunt branch element. By the method explained above, the lumped element values of the proposed OSSRR structure are computed and tabulated in Table 4.2. From these element's values, we have obtained the electrical simulation of the model using Ansoft Designer SV. The comparison between the circuit simulation and the EM simulation results are plotted in Fig. 4.11. The discrepancy between the results may be due to the negligence of losses in the circuit.

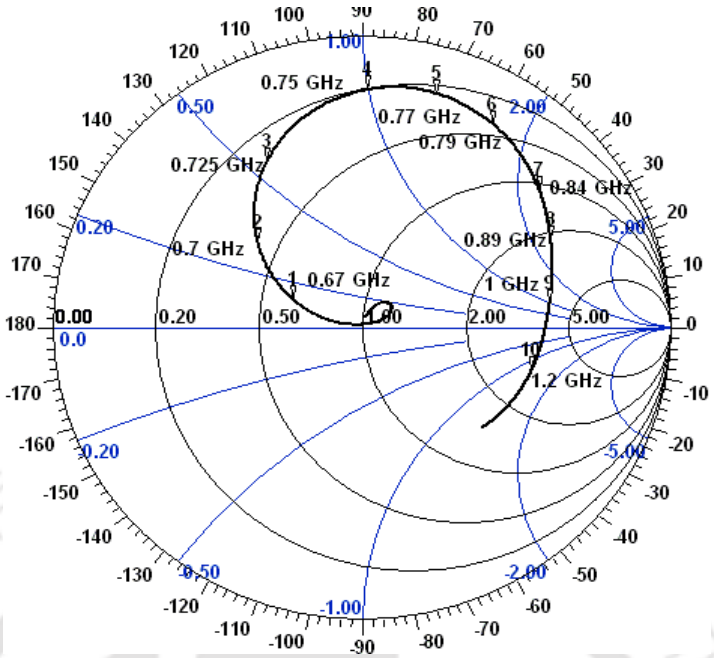

Figure 4.10: Representation of reflection co-efficient (S_{11}) on the Smith chart.

Table 4.2: Extracted equivalent circuit parameters of the OSSRR

L_1 (nH)	C_1 (pF)	L_2 (nH)	C_2 (pF)
22.04	1.9584	4.3538	8.6949

4.5 Parametric study of OSSRR

The effect of varying different dimensions of the OSSRR on the resonant frequency is investigated. Any of the parameters of the OSSRR, such as side length (a), slot width (d), strip width (c) or split gap (g) is varied, while the other parameters are kept constant. The side length of the OSSRR is varied from 12-14 mm and the other parameters are (d, c and g), varied from 0.5 mm-1.5 mm. The resonant frequency of the OSSRR loaded microstrip line with different OSSRR dimensions is shown in Fig. 4.12. From the results, it is evident that the transmission zero frequency is varied with respect to the OSSRR dimensions.

Similarly, the dependence of the lumped element values upon the OSSRR dimensions are also studied using the equivalent circuit extraction method [79]. Fig. 4.13 illustrates the variation of extracted lumped element values with respect to the OSSRR dimensions. From the plots, we observe

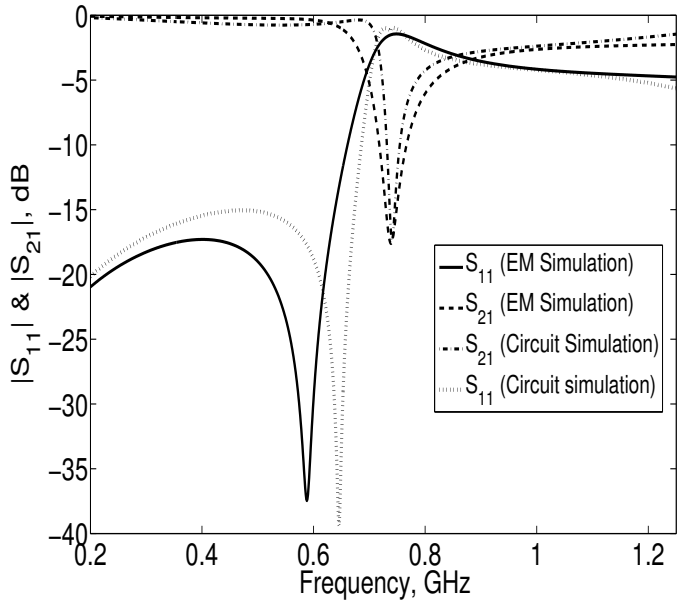

Figure 4.11: Comparison between OSSRR EM and EC simulation.

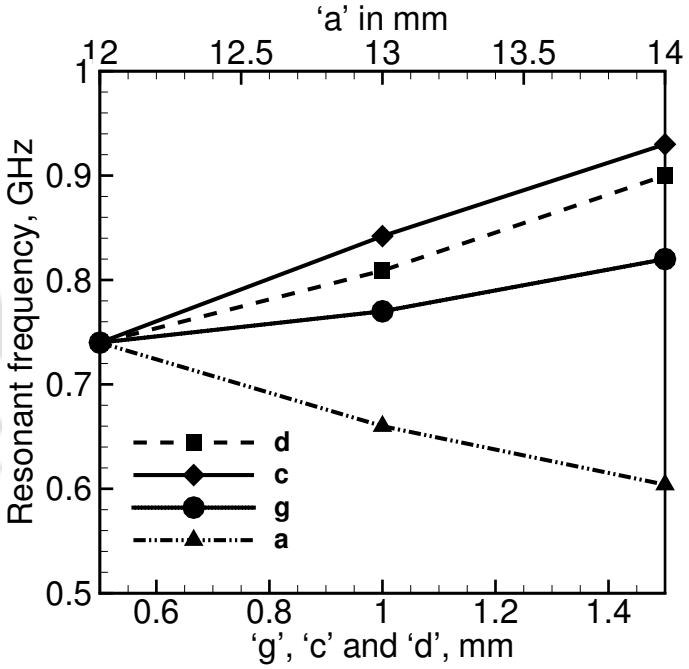

Figure 4.12: Variation of resonance frequency vs dimensions of OSSRR.

that the increase in side length of the OSSRR decreases its transmission zero frequency due to the increase in effective inductance. An increase in slot width decreases the effective capacitance of OSSRR, which leads to an increase in transmission zero frequency. Increases in strip width and split

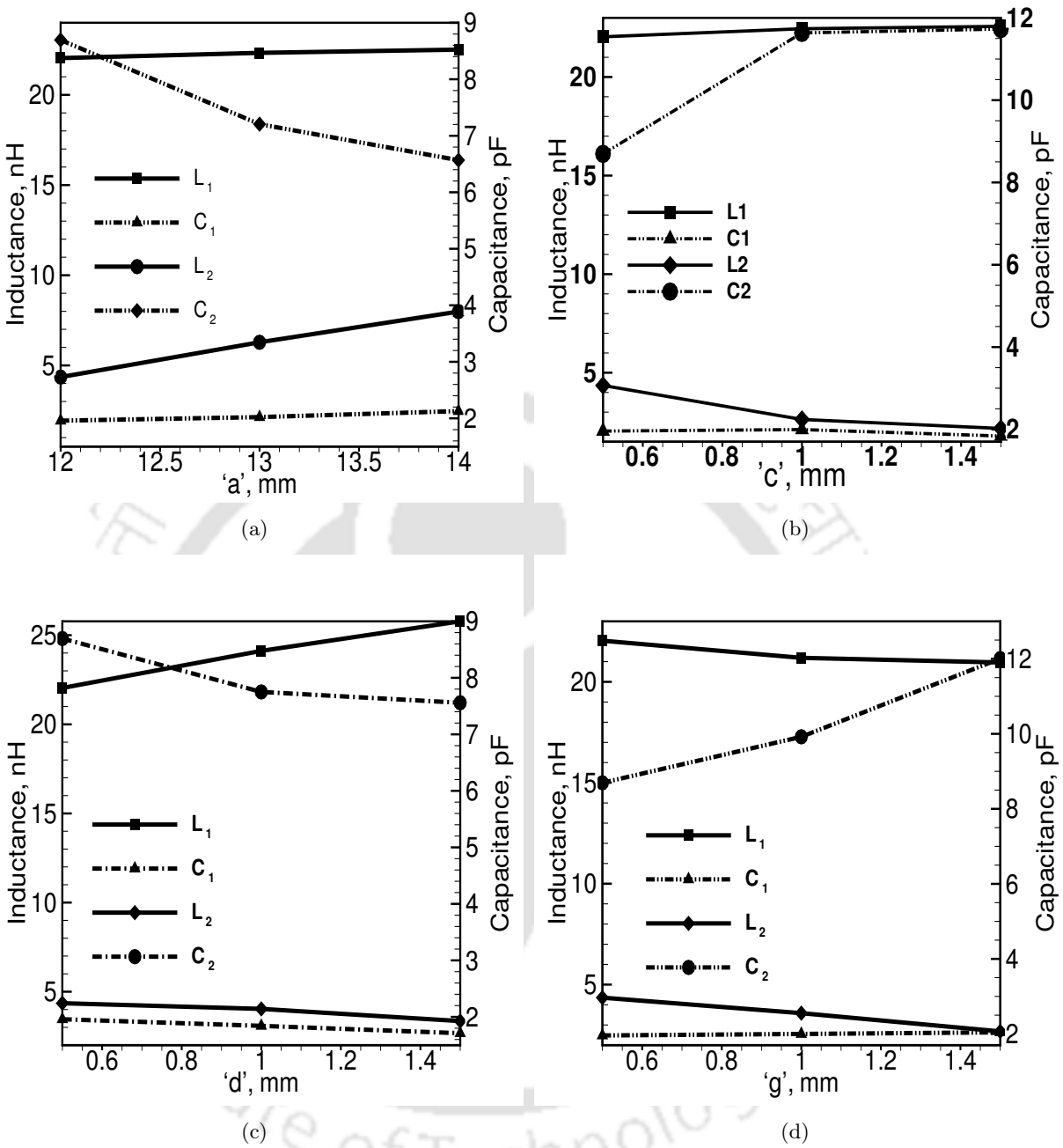

Figure 4.13: Extracted equivalent circuit values vs different a) Side length 'a' b) Strip width 'c' c) Slot width 'd' and d) Split gap 'g'.

gap decrease the inductance of the OSSRR, hence, the resonant frequency is increased. So the desired resonant frequency can be easily obtained by tuning the dimensions of OSSRR.

4.6 Composite right/left handed transmission line based on open slot split ring resonator

4.6.1 Introduction

In metamaterials, the wave propagation is governed by the left-hand rule instead of right-hand rule. Therefore, these artificial materials are also called as left-handed (LH) materials or backward-wave (BW) materials. In LH material, the electromagnetic wave propagation is opposite to that of energy flow. As a result, the electromagnetic waves propagating through the metamaterials have both phase and group velocities opposite to each other. The left-handed materials can be realized by either using transmission line approach (TL) or resonant type approach. In resonant type approach, the host line is loaded with various types of resonant structures and series gap to exhibit left-handed property. In [73] and [80], complementary split ring resonator (CSRR) is used to realize the composite right/left handed (CRLH) transmission line. A Planar transmission line medium with negative refractive index based on complementary omega like structure is proposed in [74]. Recently, a negative index metamaterial composed of triangular open-loop resonator and wire structure is demonstrated in [76]. In [81], a composite right/left handed (CRLH) transmission line is implemented by combining open split ring resonators (OSRRs) and open complementary split ring resonators (OCSRRs) using CPW technology. Very recently, a compact CRLH transmission line is synthesized using complementary spiral resonator (CSR) by M. D. Sindreu et al. [32]. In our work, we propose a new, compact planar composite right/left handed transmission line using an OSSRR for microstrip technology.

4.6.2 CRLH line using OSSRR

A Composite right/left handed planar transmission line can be synthesized by an OSSRR and an interdigital capacitor. An OSSRR is a modified and negative image of the open split ring resonator [33]. The shape of the OSRR is slightly modified, and its negative image is etched out from the ground plane to obtain an OSSRR. Similar structure in coplanar wave guide technology is proposed for design of wide bandpass filter [34]. However, for the first time in microstrip technology, an OSSRR is utilized to synthesize a CRLH transmission line. Before realizing the CRLH transmission line, to understand the propagation characteristics of OSSRR, the OSSRR with the dimensions mentioned in section 4.3 is simulated and its attenuation constant, phase constant and characteristic impedance are plotted in Fig. 4.14 & Fig. 4.15 respectively using the following equations [82].

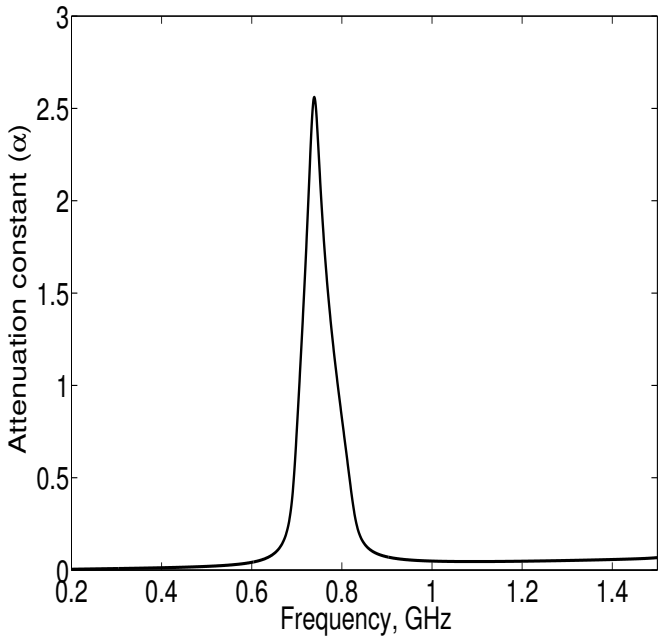

(a)

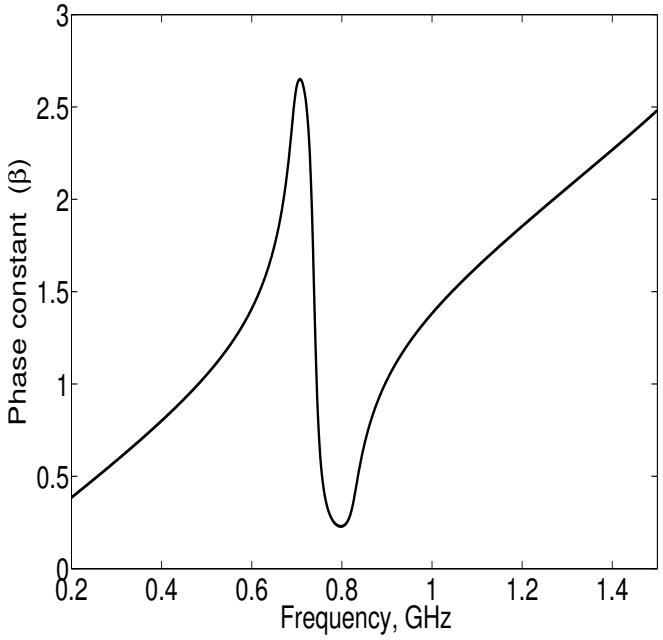

(b)

Figure 4.14: Propagation characteristics of OSSRR a) Attenuation constant b) Phase constant.

$$\gamma = \frac{1}{\Lambda}\cosh^{-1}\{\frac{[(1+S_{11})(1-S_{22})+S_{12}S_{21}]+\frac{Z_{01}}{Z_{02}}[(1-S_{11})(1+S_{22})+S_{12}S_{21}]}{4S_{21}}\} \tag{4.10}$$

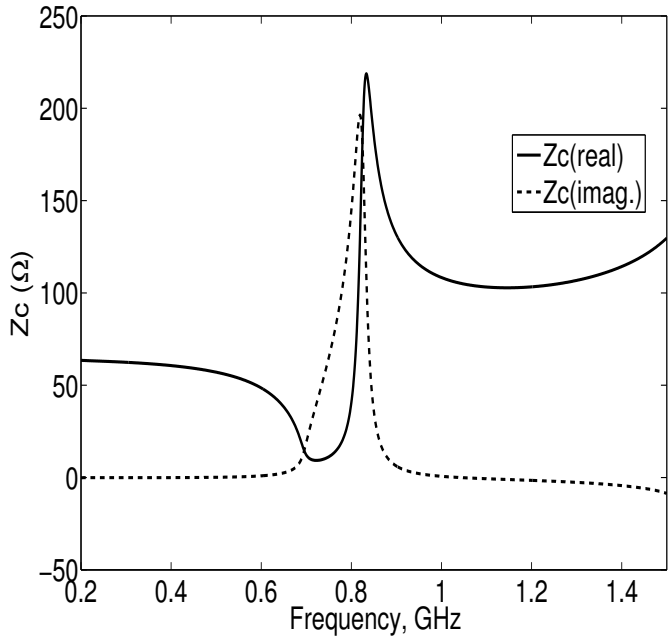

Figure 4.15: Characteristic impedance of OSSRR.

$$Z_c = z_0\sqrt{\frac{(1+S_{11})(1+S_{22})-S_{12}S_{21}}{(1-S_{11})(1-S_{22})-S_{12}S_{21}}} \tag{4.11}$$

where Z_{01} and Z_{02} are the port impedances and l is the length of the cell. The real part of γ is attenuation constant and imaginary part is phase constant. From the figures, it is observed that within the stopband, attenuation constant is dominant and the real part of the characteristic impedance is diminishing.

Fig. 4.16 shows the layout and photograph of CRLH line realized using OSSRR and interdigital capacitor. A two finger interdigital capacitor is embedded in the microstrip line to introduce series capacitance. Fig. 4.17 shows the simulated and measured scattering parameters of the structure . To understand the wave propagation in the CRLH TL structure, the dispersion characteristic is obtained using eqn. 4.10 and plotted in Fig. 4.18. In region 1, the phase and group velocities are in the same direction and in region 2 both are opposite to each other. This indicates that region 1 is right-handed (RH) band and region 2 is left-handed (LH) band. The transition frequency between LH band and RH band is observed at 0.92 GHz. At the transition frequency, the phase constant is zero. By inspecting the dispersion relation, we observe that the proposed structure exhibits both the right-handed and left-handed characteristics. Compared with the work reported in [81], the proposed structure does not

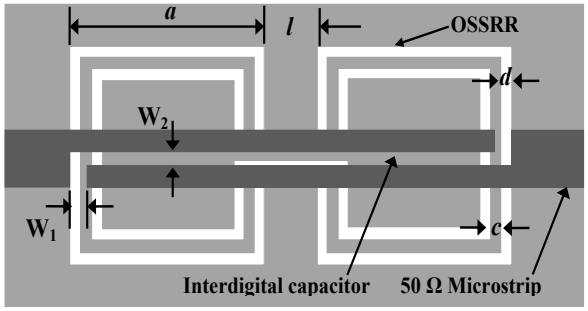

(a)

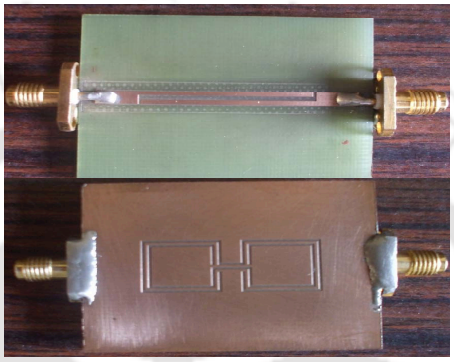

(b)

Figure 4.16: CRLH transmission line a) Schematic ($W_1 = 0.6$ mm, $W_2 = 1$ mm) b) Fabricated prototype.

involve any via holes. So complexity in fabrication process is reduced.

4.7 Compact lowpass filter design using open slot split ring resonator

4.7.1 Introduction

Over the past few years, defected ground structure (DGS) or defected ground plane (DGP) draws the attention of many researchers for size reduction and harmonic suppression of various microwave devices [41,83–90]. Due to the defects in the ground plane, change in shield current takes place, which effectively changes the value of the inductance and capacitance of the microstrip line. This produces stopband effect in certain frequency range. So far, various shapes of defected ground structures like dumbbell, spiral, arrowhead, elliptical, U-shaped and H-shaped etc. [41, 83–87] are demonstrated by various authors. Recently, a CSRR [88] DGS and OSSRR [91] DGS have been successfully applied for size reduction and performance enhancement of microwave devices. In this work, a lowpass filter

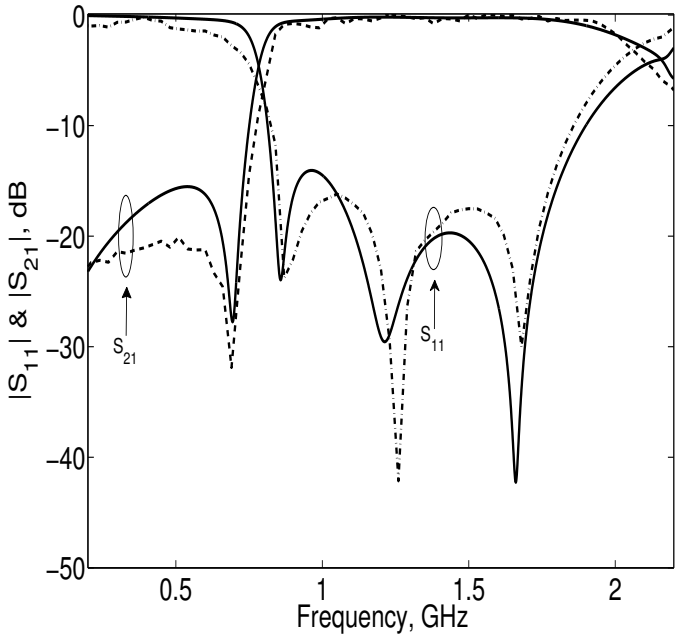

Figure 4.17: Scattering parameters of proposed CRLH transmission line.

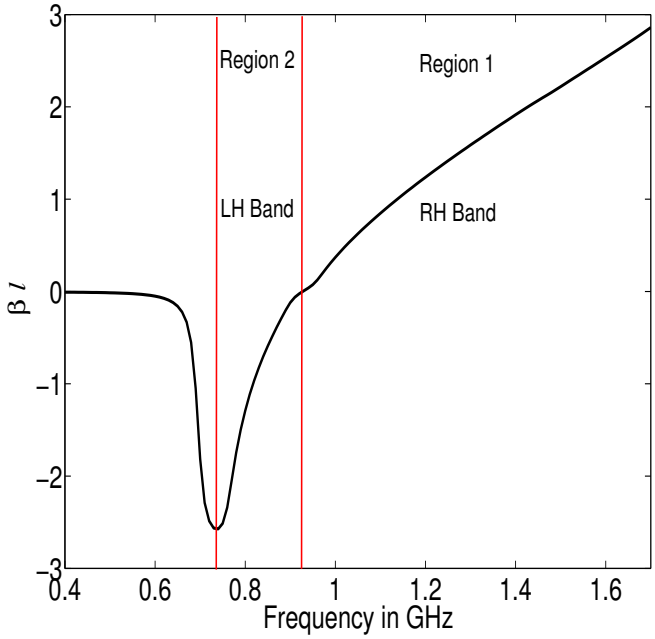

Figure 4.18: Dispersion relation of CRLH TL.

(LPF) is constructed using a periodic array of OSSRR and open stubs. The proposed filter has sharp cut-off and good outband suppression.

Since OSSRR is obtained by etching a OSRR shaped slot in the ground plane, we can consider

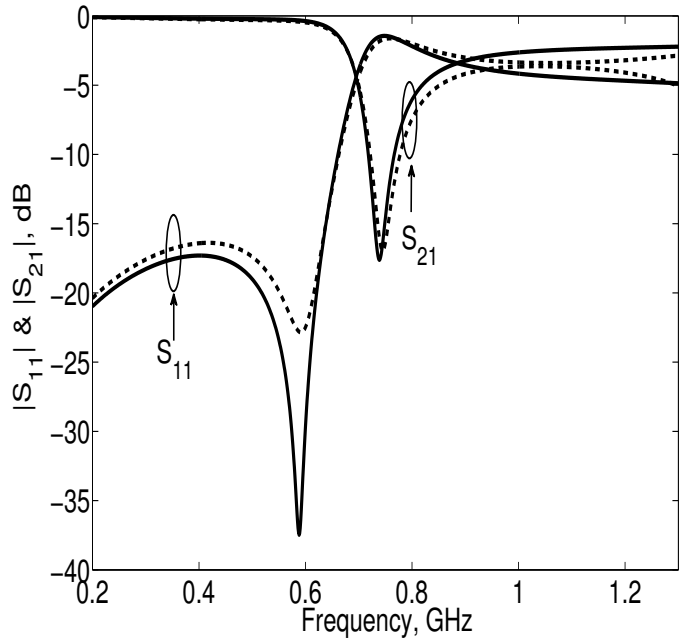

Figure 4.19: Simulated scattering parameters of OSSRR (solid line) and CSRR (dashed line).

the OSSRR as a defected ground structure. To compare the performance of the CSRR DGS with the OSSRR DGS, a CSRR resonating at the same frequency as OSSRR (explained in section 4.3) is designed and their scattering parameters are plotted in Fig. 4.19. The total defected area occupied by the OSSRR and CSRR for the same resonant frequency is 27 ×12 mm^2 and 30 ×15 mm^2 respectively. So approximately 28% area reduction is achieved for the OSSRR DGS compared with the CSRR DGS. Hence, size miniaturization is achieved using OSSRR DGS.

4.7.2 Comparison between various DGS

Lowpass filters with sharp cut-off characteristics, compact size and easy design procedures are desirable for modern microwave communication systems. Many novel types of microstrip lowpass filters have been proposed using various DGS [85–90]. However, the OSSRR DGS has sharper cut-off frequency than the conventional DGS such as dumbbell, arrowhead, elliptical etc. To compare the properties of different DGS, various DGSs having the same transmission zero frequency are simulated and their characteristics are listed in Table 4.3. Fig. 4.20 depicts the simulated transmission response of various DGSs. The sharpness factor of the lowpass (LPF) filter is given by,

$$SF = \frac{f_c}{f_0} \tag{4.12}$$

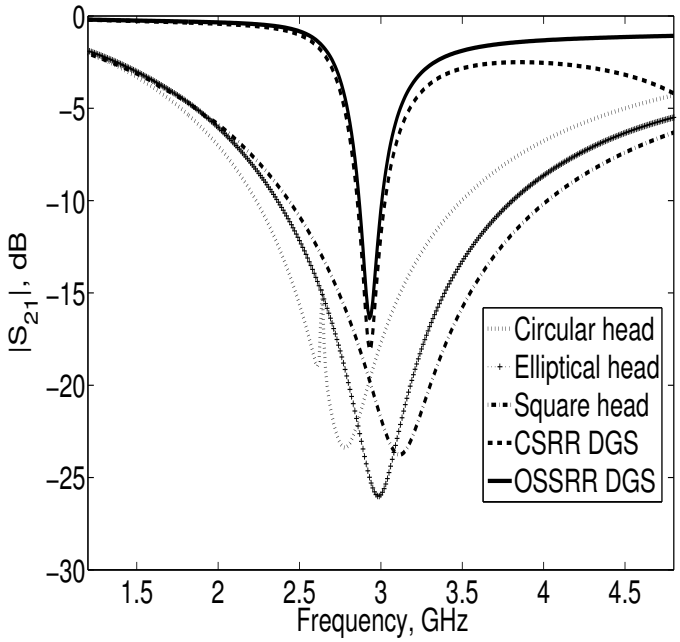

Figure 4.20: Transmission response of various DGSs.

Table 4.3: Comparison of various DGSs

DGS Type	f_c (GHz)	f_0 (GHz)	SF	Area (mm^2)
Square	1.47	3.1	0.47	100
Circular	1.45	2.8	0.5	99.71
Elliptical	1.5	2.98	0.52	95
CSRR	2.71	2.93	0.93	56.25
OSSRR	2.73	2.93	0.93	49.5

where f_0 is the attenuation pole frequency and f_c is the cut-off frequency. From Table 4.3, we observe that the transmission zero frequencies of DGSs are slightly varied and OSSRR DGS has good sharpness factor and less defected area compared with the other DGSs.

4.7.3 Lowpass filter using OSSRR

As explained in the previous section, the OSSRR has good sharpness factor and occupies less defected area, yet the rejection bandwidth of OSSRR DGS is small, so this property is not suitable for LPF application. To get the sufficient suppression in the high frequency range, open stubs are placed on both sides of the OSSRR, as shown in Fig. 4.21(a).

To obtain a 3 dB cut-off frequency of 1.5 GHz, the OSSRR dimensions are chosen as follows: a

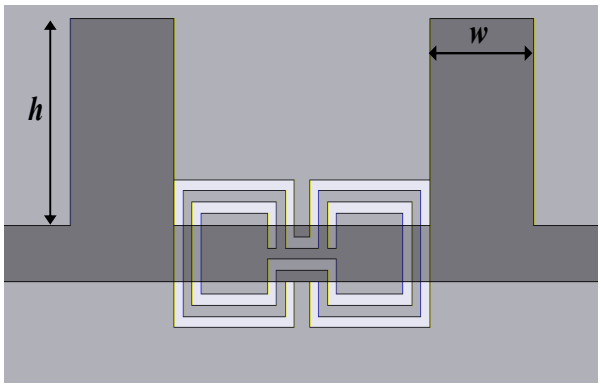

(a)

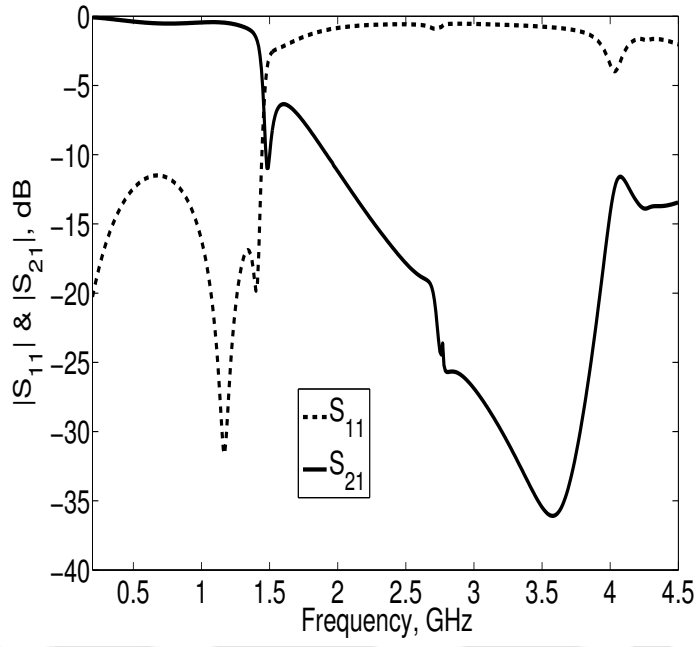

(b)

Figure 4.21: Proposed single cell lowpass filter a) Layout b) Simulated scattering parameters.

= 7 mm, $c = 0.4$ mm, $d = 0.4$ mm, $g = 0.4$ mm, and $l = 1$ mm. The length and width of the open stubs are $h = 11$ mm and $w = 4$ mm respectively. Fig. 4.21(b) shows the scattering parameters of a single OSSRR DGS LPF. From the figure, we observe that still the outband filter performance is not sufficiently good as we have expected. Therefore, cascaded stages of OSSRR DGS cells are used to obtain a good rejection band. Fig. 4.22(a) & Fig. 4.22(b) show the layout and photograph of cascaded stages of two cell OSSRR DGS respectively. Simulated and measured scattering parameters of the proposed lowpass filter are shown in Fig. 4.22(c). The proposed filter offers, a steep rejection

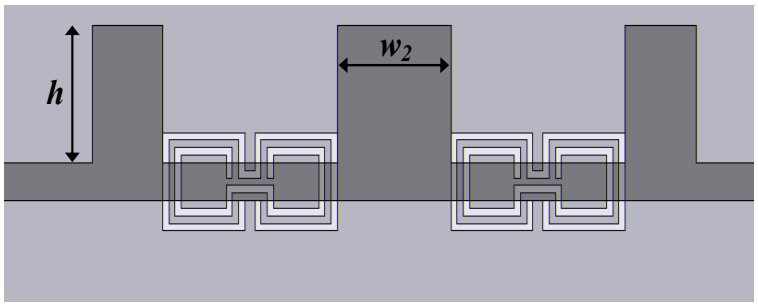

(a)

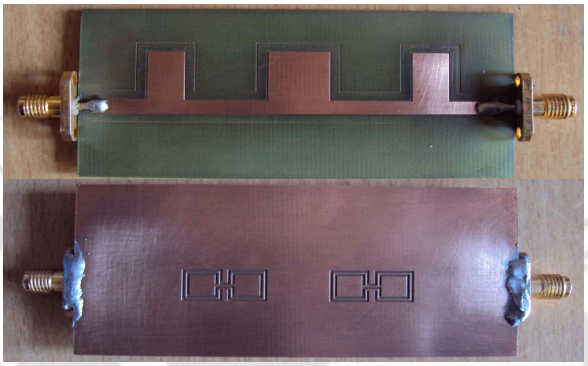

(b)

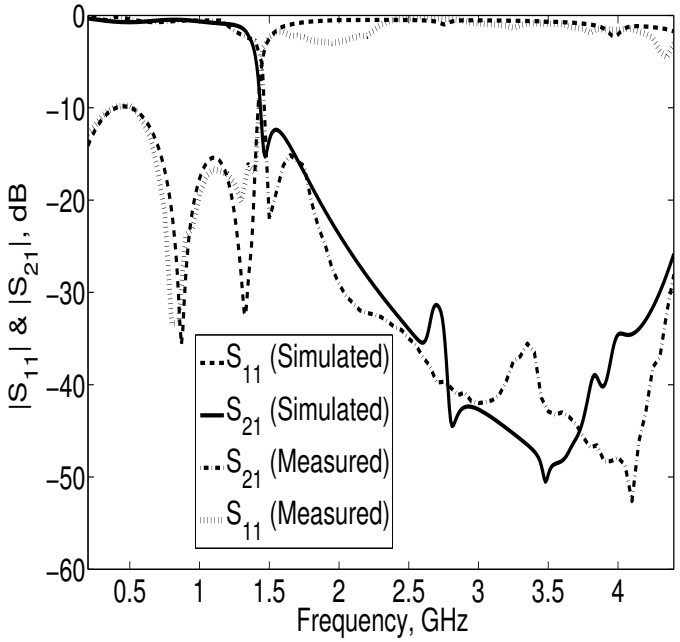

(c)

Figure 4.22: Proposed lowpass filter a) Layout (W_2 = 11.1 mm) b) Fabricated prototype c) Simulated and measured scattering parameters.

at 1.5 GHz and has more than a 20 dB rejection from 2 GHz to 4.5 GHz. We have calculated the selectivity of the filter as 35.42 dB/GHz using eqn. 4.13,

$$\xi = \frac{\alpha_{\min} - \alpha_{\max}}{f_s - f_c} \tag{4.13}$$

where ξ is selectivity of the filter, α_{min} and α_{max} are the attenuation points at 3 dB and 20 dB respectively, and f_s is the 20 dB stopband frequency.

4.8 Compact wideband bandpass filter using open slot split ring resonator and CMRC

4.8.1 Introduction

A bandpass filter (BPF) having wide fractional bandwidth is needed to cope up with, present day wideband RF/Wireless communication systems. However, the BPF implemented using parallel coupled microstrip line (PCML) is suitable for obtaining a fractional bandwidth (FBW) of only up to 20%. This is mainly due to the weak coupling between the parallel coupled lines. To achieve a large FBW, microstrip width and spacing between the coupled lines has to be very small, which is difficult to fabricate. Many researchers have proposed the various techniques to obtain a wide bandpass filter response [15,63,92–96]. A ground plane aperture technique is used to obtain the fractional bandwidth of 60% in multipole bandpass filter in [63]. A cascaded lowpass and highpass sections are utilized to construct an ultra wideband (UWB) bandpass filter in [92] and [93]. Using a complementary split ring resonator, a bandpass filter with wide controllable fractional bandwidth is designed in [15]. In [94], the authors utilized the defected ground structure and a highpass filter to obtain a wide bandpass response. However, this filter involves via holes, which are difficult to fabricate. An ultra wideband filter using DGS and fractal shape slot is reported in [95]. Recently, a wide passband of about 61% fractional bandwidth is obtained using a transversal resonator and asymmetrical interdigital coupled lines in [96].

In our work, a wide fractional bandwidth bandpass filter is designed by cascading a highpass (HPF) and lowpass (LPF) filters realized using an OSSRR and a compact microstrip resonating cell (CMRC) respectively. The FBW of the filter can be easily varied by varying the cut-off frequencies of the LPF and HPF sections. The proposed filter has a wide FBW and compact size, when compared with the conventional PCML BPF.

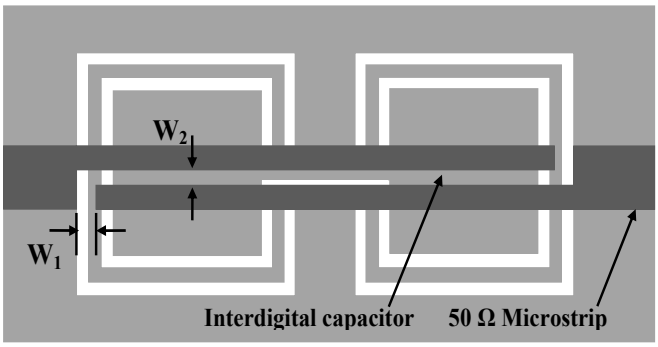

(a)

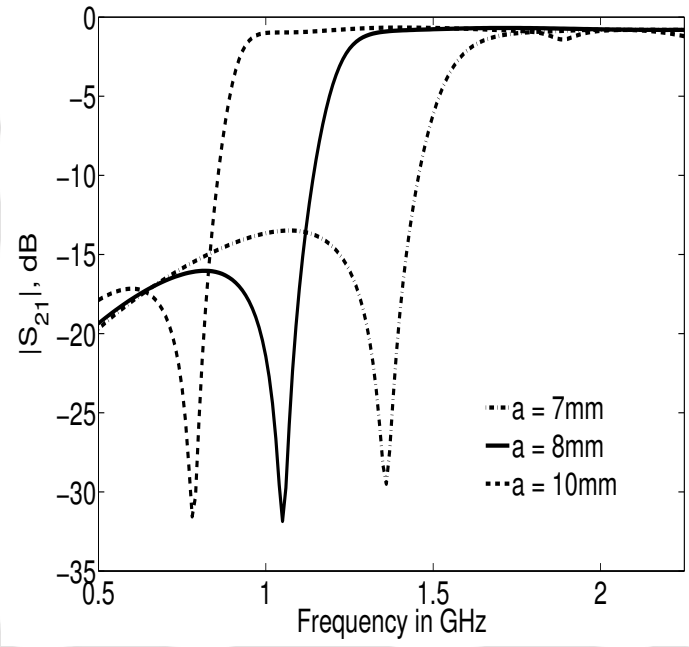

(b)

Figure 4.23: Highpass filter a) Geometry b) Transmission response for various 'a'.

4.8.2 Design of highpass filter

The stopband produced by the CSRR can be converted into a passband by introducing a interdigital capacitor in the microstrip line [97]. Similarly, the stopband of a OSSRR can also be converted into a passband. Thus, a two finger interdigital capacitor is embedded in the 50 Ω microstrip line. The geometry of highpass filter is presented in Fig. 4.23(a). The dimensions of the OSSRR are as follows: $a = 12$ mm, $c = 0.5$ mm, $d = 0.5$ mm, $g = 0.5$ mm, and $l = 3$ mm. The dimensions of the interdigital capacitor are $W_1 = 0.6$ mm and $W_2 = 1$ mm. The cut-off frequency of the HPF can be easily controlled

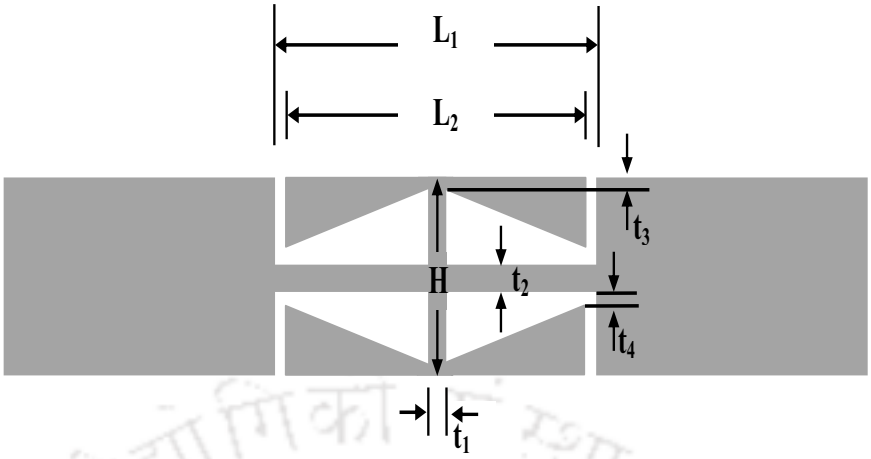

Figure 4.24: Layout of a single CMRC cell.

by the side length 'a' of the OSSRR. Fig. 4.23(b) shows the simulated transmission response for various values of 'a'. By tuning the physical parameters of the OSSRR, the desired 3 dB cut-off frequency can be easily obtained.

4.8.3 Design of lowpass filter

A Lowpass filter is constructed by a periodic arrangement of compact microstrip resonating cell (CMRC). We have utilized the structure presented in [98] for designing lowpass filters. The propagation constant of a lossless transmission line is a function of distributed shunt capacitance and series inductance. Therefore, by increasing the value of inductance and capacitance of the transmission line periodically, slow-wave effect can be achieved. Fig. 4.24 illustrates the structure of a single CMRC cell. The narrow connecting lines result in increased inductance and the gaps between the width of the lines are responsible for increased capacitance. The detailed investigation about this structure can be found in [99]. The width of the cell is equal to the width of the 50 Ω microstrip line. The dimensions of the CMRC cell are as follows, $L_1 = 10$ mm, $L_2 = 9.2$ mm, $H = 3.06$ mm, and $t_1 = t_2 = t_3 = t_4 = 0.4$ mm. By changing the size of the cell, the stopband frequency can be easily varied. Fig. 4.25(a) shows the simulated frequency response of the cell for various lengths. As the length of the cell is increased, the stopband frequency moves toward the lower end. Therefore, to avoid the increase in cell length for a lower frequency, width of the cell is increased. Fig. 4.25(b) illustrates the characteristics of a CMRC cell for various widths. As the width increases, the stopband frequency moves toward the

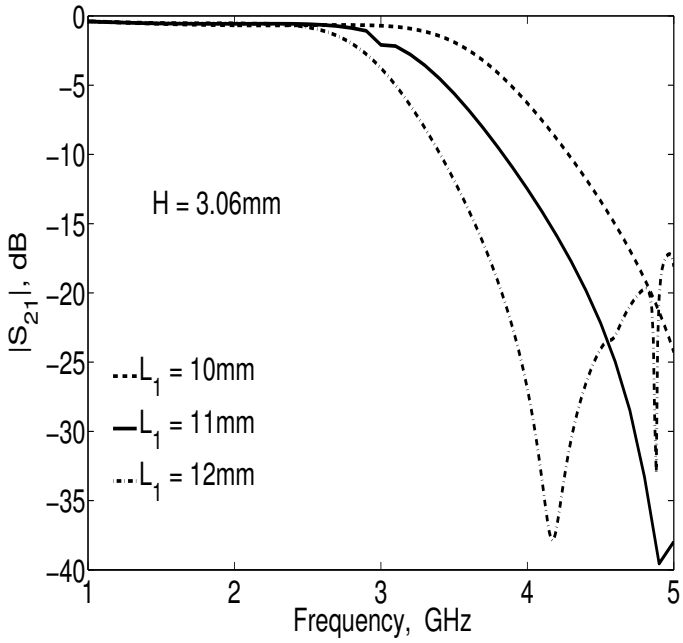

(a)

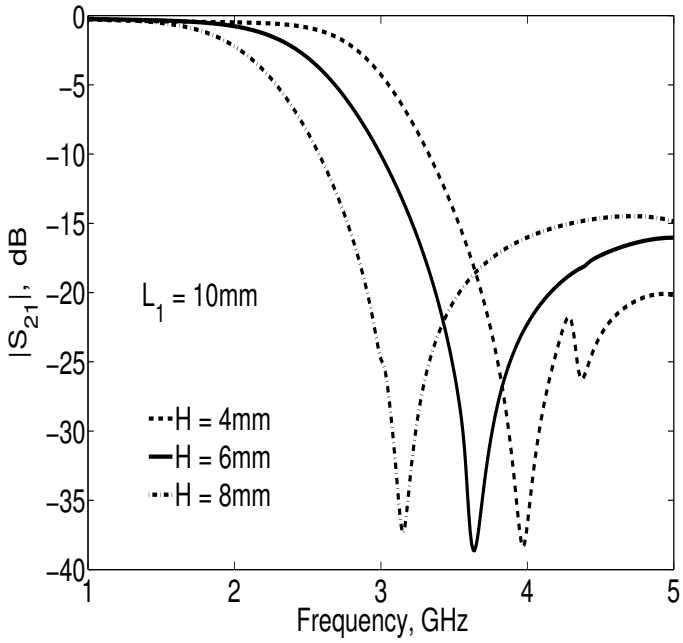

(b)

Figure 4.25: Frequency response of CMRC for a) Various lengths c) Various widths.

lower end without increasing the length of the device. A wide stopband can be achieved by cascading many cells.

Table 4.4: Physical parameters of BPFs
(all dimensions are in mm)

	a	c, d, g	l	W_1	W_2	L_1	L_2	H	t_1	t_2	t_3	t_4
Type 1	5.5	0.5	3	0.8	1.5	12	11.2	3.06	0.3	0.3	0.4	0.4
Type 2	8	0.5	3	0.6	1	8	7.2	6	0.3	0.3	0.4	0.4

4.9 Design of bandpass Filter

(a)

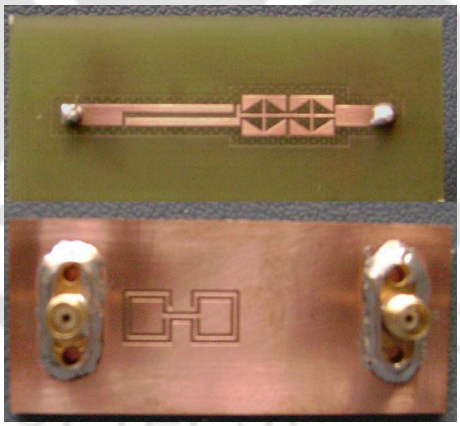

(b)

Figure 4.26: Fabricated proposed BPFs a) Type 1 b) Type 2.

As mentioned earlier, the BPF is constructed by cascading a lowpass and highpass sections. Two BPFs are designed and simulated for obtaining a different fractional bandwidth.

To obtain a sharp passband to stopband transition and a wide rejection band, two CMRC cells

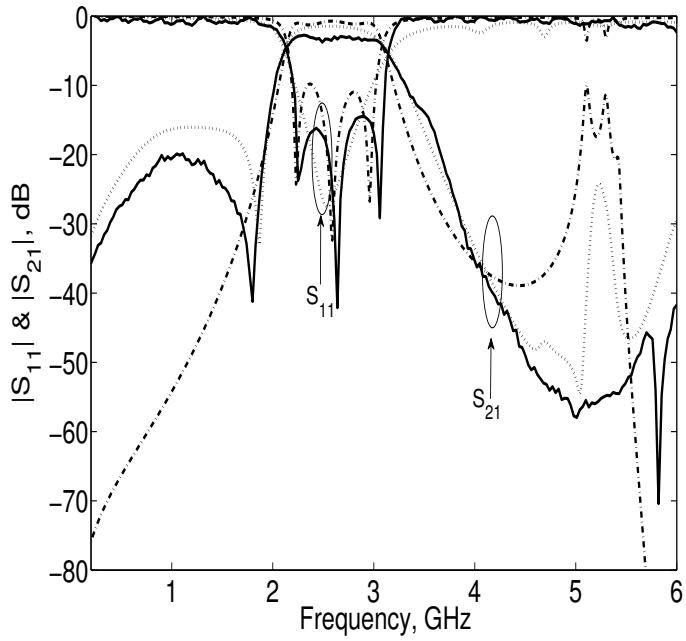

(a)

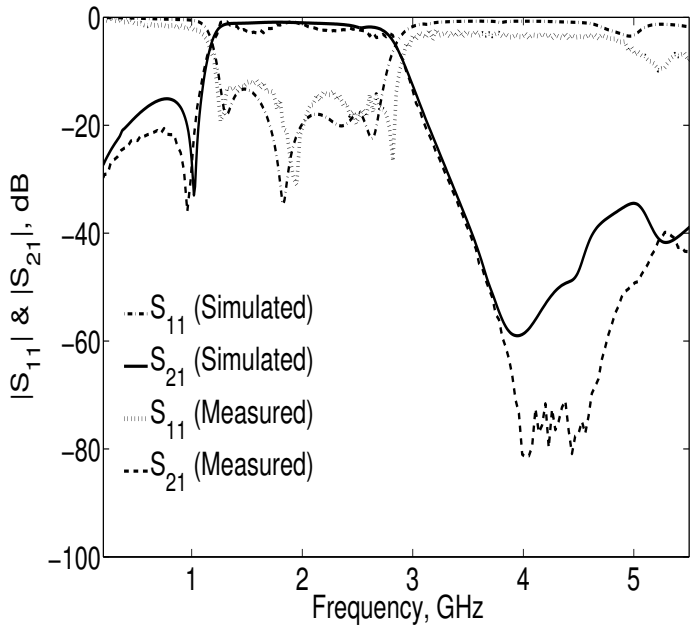

(b)

Figure 4.27: Scattering parameters of proposed BPFs a) Type 1 (Continuous line→ measurement, Dotted line→ simulation, Dashed line→ Conventional PCML BPF) b) Type 2.

are used in the LPF section. Table 4.4 lists the dimensions of two types of proposed filters. The photographs of fabricated filters are shown in Fig. 4.26. In Type 1 filter, the CMRC cell width (H) is

same as the width of the microstrip line and in Type 2 filter, the CMRC cell width is different from the microstrip line width, to reduce the length of the filter. The cut-off frequency of BPF can be either varied by changing the cut-off frequency of LPF or HPF. Fig. 4.27 shows the simulated scattering parameters of proposed BPFs. From the figures, it can be observed that the Type 1 filter has 29.2% FBW and is 20% smaller in size than the conventional third order PCML bandpass filter. The Type 2 BPF has 76% FBW and occupies 47% smaller area than the traditional PCML BPF with the same center frequency at 2 GHz. The insertion losses of Type 1 and Type 2 filters are less than 1.48 dB and 1 dB respectively. Compared with the conventional PCML BPF, proposed bandpass filters are free from second harmonic.

4.10 Summary

In this chapter, new types of resonators exhibiting metamaterial characteristics are presented. The OSRR exhibits negative permeability and its dual counterpart OSSRR exhibits negative permittivity. The lumped element model of the OSSRR is presented and verified with the parameter extraction technique. The detailed parametric study of OSSRR has been done and the relation between the OSRRR dimensions with its resonant frequency is verified. As compared with the conventional CSRR, OSSRR is smaller in size and hence, size miniaturization of microwave devices is possible. To demonstrate the applications of OSSRR, few of the planar circuit designs such as composite right/left handed transmission line, controllable wide fractional bandwidth BPF and compact lowpass filter are presented.

5

OCSRR and its applications in performance enhancement of microwave devices

Contents

5.1 Introduction

Over the past few years, left-handed transmission line based on resonant type approach is a growing field of interest in microwave research community. In transmission line approach, the host line is loaded with the various kinds of resonators [65, 73, 100–102] such as split ring resonator, complementary split ring resonator, spiral resonator (SR) and open slot split ring resonator etc., and mainly used for the implementation of planar metamaterial-inspired structures. In these implementations, the resonators are electrically or magnetically coupled to a host line, and a signal propagation is inhibited at the resonant frequency. Due to the sub-wavelength property of these resonators, several size miniaturized microwave components have been designed. Recently, a new electrically small resonator called an open complementary split ring resonator (OCSRR) [36] developed by some of the authors opens up the opportunity for synthesis of miniaturized artificial transmission line and microwave passive devices [35]. However, most of the work already reported are mainly focussed on OCSRR based devices implemented in coplanar waveguide technology (CPW) [34, 103]. The fabrication of such devices in CPW technology is difficult because it involves via holes and bonding wires for connecting the different ground regions. Hence, in our study, we are concentrating on the design of microwave passive devices in microstrip technology using OCSRR.

This chapter deals with the modeling of OCSRR and its application for size miniaturization of some of the planar microwave components such as filters, power divider and hybrid coupler. Specifically, lowpass filters with improved stopband and compact size, size miniaturized and harmonic suppressed T-junction power divider, and rat-race coupler are designed, fabricated and tested.

5.2 Conventional open split ring resonator and open complementary split ring resonator

An open complementary split ring resonator is the complementary counterpart of the open split ring resonator (OSSR). The OSRR is a modified version of the split ring resonator (SRR). It consists of two metallic concentric rings printed on the upper side of the dielectric substrate. The rings are truncated by a small slit gap on the same side of the rings and each ring is connected to the adjacent ports. Hence, we can consider the OSRR as an open resonator. As discussed in [33], it can be modeled as a series LC resonator as shown if Fig. 5.1(a), where L_s is the inductance of a closed ring of averaged radius $r_0 = r_{ext}$ - c - d / 2 and C_0 is the distributed capacitance between the inner and outer rings.

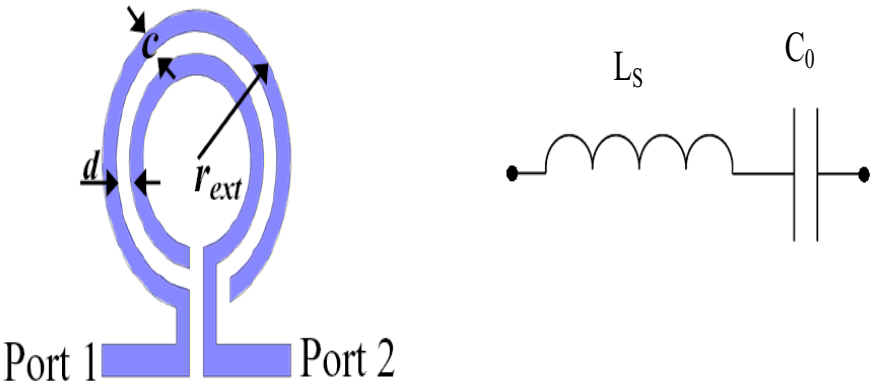

(a)

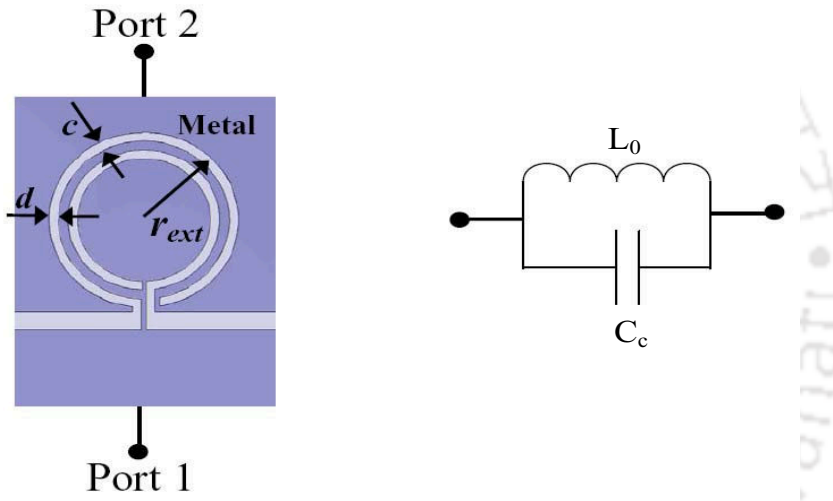

(b)

Figure 5.1: Typical topology and equivalent circuit of a) Open split ring resonator b) Open complementary split ring resonator.

The OCSRR is a negative image of the OSRR. A shown in Fig. 5.1(b), it can be modeled as an open parallel LC resonator, where L_0 is the inductance of the metallic strip between the ring slots, and C_c, is the capacitance of a disk of radius r_o - c / 2 surrounded by a metallic plane at a distance c of its edge [43]. Since OCSRRs and OSRRs are complementary structures, it is expected that their resonant frequencies are roughly the same if they have identical dimensions and substrates, which have been theoretically explained in [43].

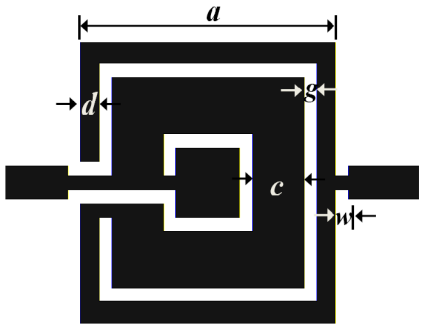

(a)

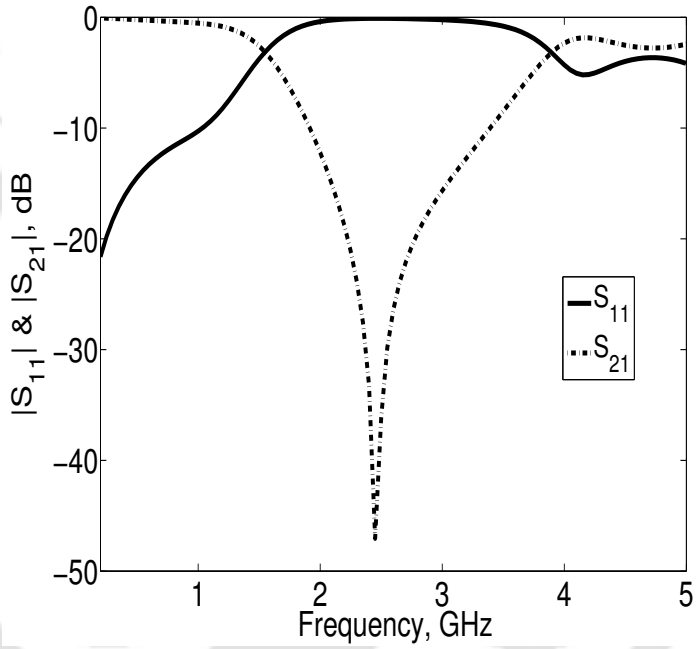

(b)

Figure 5.2: OCSRR a) Layout b) Simulated scattering parameters.

5.3 OCSRR and its modeling

A typical topology of a square-shaped OCSRR in microstrip technology is shown in Fig. 5.2(a). Here, the OCSRR is embedded in the microstrip line. The circular-shaped OCSRR is first proposed in [36] for designing a sharp cut-off lowpass filter with compact size. To study the frequency response characteristics of the OCSRR, this structure is designed on the Rogers 5880 substrate with $\varepsilon_r = 2.2$ and a substrate thickness of 0.381 mm and simulated using CST Microwave Studio. The dimensions of the OCSRR are as follows: $a = 11$ mm, $c = 3.4$ mm, $d = 0.5$ mm, $g = 0.5$ mm and $w = 0.5$ mm.

The simulated scattering parameters of the OCSRR are depicted in Fig. 5.2(b). A transmission zero is observed at the resonant frequency $f_0 = 2.46$ GHz. At the resonant frequency, the resonator is left open and the transmitted energy is reflected back to the source causing a transmission zero. The current distribution of the OCSRR at the resonant frequency is shown in Fig. 5.3. With reference

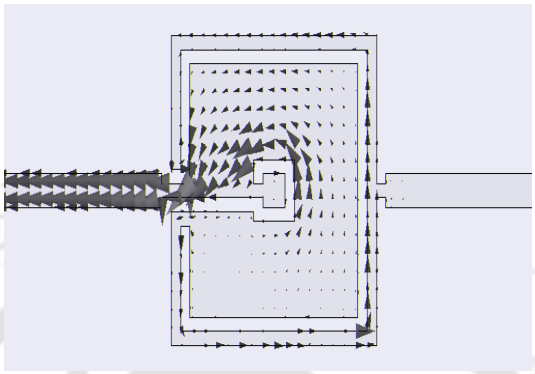

Figure 5.3: Simulated current distribution of the OCSRR at the resonant frequency 2.46 GHz.

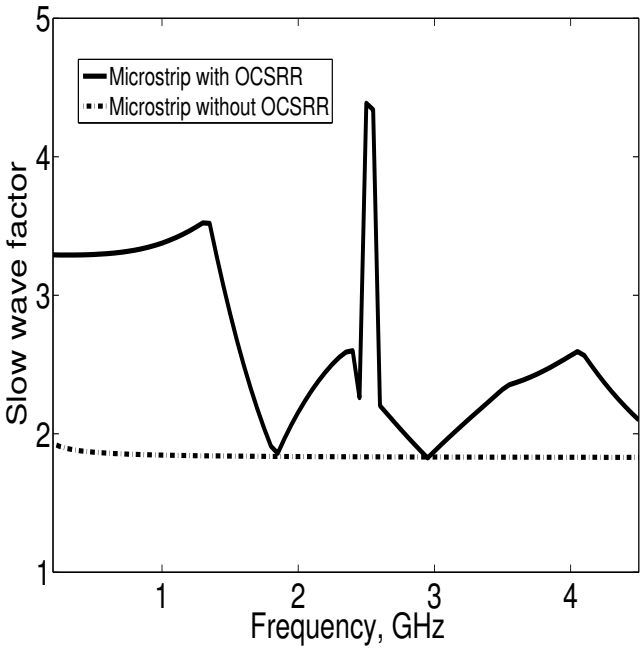

Figure 5.4: Slow-wave factor of the microstrip line.

to the transmission line theory [104], the propagation constant of a line without loss is,

$$\beta = \omega_0 \sqrt{LC} \tag{5.1}$$

where ω_0 is the angular frequency, and C and L are the distributed shunt capacitance and series inductance per unit length, respectively. It shows that slow-wave can be achieved by increasing C and L in the transmission line. Since the OCSRR is printed on the microstrip line, it will change the microstrip line inductance and capacitance, resulting in a slow-wave effect. The slow-wave factor (SWF) of the line loaded with the OCSRR is calculated by the method described in [105] using eqn. 5.2, and plotted in Fig. 5.4.

$$SWF = \frac{\lambda_0.\Delta\theta}{360L} + \sqrt{\varepsilon_{eff}} \tag{5.2}$$

where 'L' is the physical length of the line and $\Delta\theta$ is the phase difference between the microstrip line with OCSRR and without OCSRR. From the plot, it is observed that the SWF of the microstrip line loaded with the OCSRR is increased by 73% compared with the microstrip line without OCSRR. Further, SWF is increased up to 130 % near the resonant frequency. Thus, the increase in SWF validates the size reduction capability of the OCSRR for microwave applications.

In the previous section, we have seen that the OCSRR can be modeled as a parallel resonant circuit. To apply the proposed OCSRR section to a practical circuit design, it is necessary to extract the equivalent circuit parameters. From the scattering parameters of OCSRR shown in Fig. 5.2(b), it is observed that there exists a resonance frequency and a 3-dB cut-off frequency of OCSRR. This kind of characteristics can be obtained from a typical parallel LC tank circuit. The equivalent circuit parameters of OCSRR can be determined by the method described in [41]. The equivalent circuit of the OCSRR embedded microstrip line and one pole Butterworth lowpass filter prototype is shown in Fig. 5.5(a) & 5.5(b) respectively. The reactance value of the OCSRR unit can be expressed as follows,

$$X_{LC} = \frac{1}{\omega_0 C}\left(\frac{\omega_0}{\omega} - \frac{\omega}{\omega_0}\right) \tag{5.3}$$

where ω_0 is the resonant frequency of the parallel LC circuit, which is corresponding to the transmission zero location of the OCSRR. The series inductance of the one pole Butterworth lowpass filter is given as

$$X_L = \omega' Z_0 g_1 \tag{5.4}$$

where ω', g_1 and Z_0 are the normalized 3-dB cut-off frequency, prototype value of the one pole Butterworth LPF and port impedance respectively. At the cut-off frequency, two reactance value

must be equal, so

$$X_{LC}|_{\omega=\omega_c} = X_L|_{\omega'=1} \tag{5.5}$$

simplifying 5.3-5.5 the capacitance C and inductance L of the circuit can be deduced as follows

$$C = \frac{\omega_c}{2Z_0(\omega_0^2 - \omega_c^2)} \tag{5.6}$$

$$L = \frac{1}{4\pi^2 f_0^2 C} \tag{5.7}$$

where ω_c and ω_0 are the cut-off frequency and attenuation pole frequency respectively. The extracted

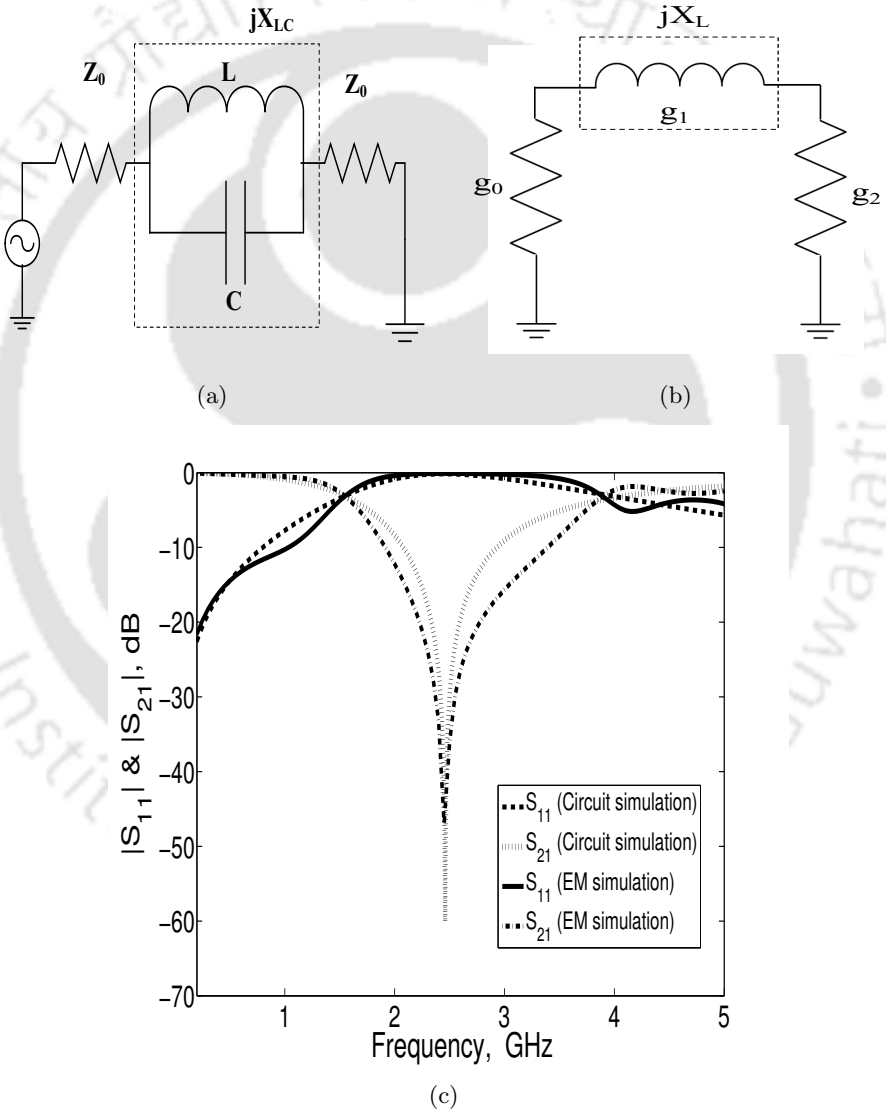

Figure 5.5: OCSRR a) Equivalent circuit of the microstrip line with OCSRR b) Butterworth prototype of one pole lowpass filter c) Simulated scattering parameters of OCSRR.

equivalent circuit values are C = 0.6664 pF and L = 6.2875 nH at the resonant frequency f_0 = 2.46 GHz. The equivalent circuit is simulated using Ansoft designer SV and results are plotted in Fig. 5.5(c). The small discrepancy between EM simulation and circuit simulation may be due to the negligence of capacitance to ground for microstrip implementation or other parasitic effects and losses in the resonant circuit.

5.4 Improved stopband lowpass filter using OCSRR

5.4.1 Introduction

The rapid development of commercial markets for wireless communication products over the past decade has led to an explosion of interest in size miniaturization and performance improvement of microwave circuit design. The design of compact lowpass filters with sharp cut-off and wide stopband is the present trend for the elimination of unwanted harmonics or spurious passband in microwave and wireless communication systems. Lowpass filter (LPF) design employing conventional structures such as stepped impedance and open stubs are suffering from either spurious passband or poor cut-off performance. Hence, many novel types of lowpass filters using defected ground structures (DGSs) and compact microstrip resonating cell (CMRC) have been proposed in various literature [41, 85, 86, 88–91, 106, 107]. Various DGS [41, 85, 86, 88, 89, 91] such as dumbbell, arrowhead, H shape, elliptical, complementary split ring resonator and open slot split ring resonator are employed to design a compact LPF and bandpass filter (BPF). A fractal shape DGS and modulated microstrip line [90] is used to obtain a good out-of-the-band filter performance and sharp cut-off in LPF design. A novel tapered CMRC and modified CMRC have been proposed to design a LPF with wide stopband [106], [107]. Even though, the performance is good, length of the filter is long due to the periodic arrangement of CMRCs. Recently, an open complementary split ring resonator has been proposed to design a compact lowpass filter in microstrip technology [36].

In this work, a compact, sharp cut-off and improved wide stopband lowpass filter is designed using OCSRR and open stub arrangement. The proposed filter offers a wide stop bandwidth than the conventional filter structure employing cascaded stages of OCSRR, and the length of the filter is approximately 73% shorter than the work reported in [36].

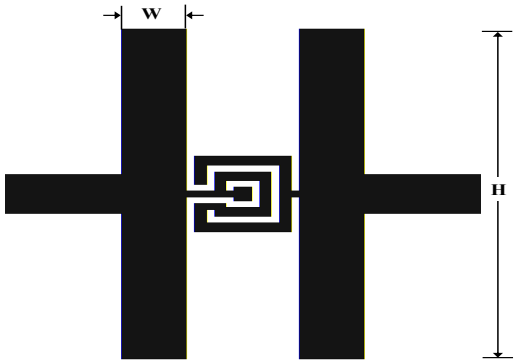

Figure 5.6: Proposed lowpass filter layout.

5.4.2 Lowpass filter design using OCSRR

As discussed in [36], the OCSRR based filter characteristic does not fall in any standard approximations such as Chebyshev, elliptic etc. Therefore, the lowpass filter is constructed using the cascaded stages of OCSRR. Since the OCSRRs are electrically small particles, filter dimensions can be made small. Thus, such filters are of interest in applications, where the main objective is to reduce the size of the filter. In the previous work [36], to obtain a spurious free stopband, additional cascaded stages of OCSRR, tuned to the spurious passband frequency is attached with the original filter. This will increase the length of the filter unnecessarily. Hence, in our proposed design, two open ended stubs are attached on both sides of the OCSRR to obtain a wide spurious free stopband. The layout of the proposed structure is shown in Fig. 5.6. The dimensions of OCSRR are as follows: $a = 6$ mm, $d = 0.4$ mm, $c = 1.45$ mm, $g = 0.4$ mm and $w = 0.4$ mm.

By keeping the width of the open stub constant, simulated transmission responses for stub lengths H = 10, 16, 20 and 26 mm are shown in Fig. 5.7(a). It is observed that by increasing the length of the stub, the cut-off frequency moves toward the lower end and sharp roll of rate is also achieved. Similarly, transmission responses of the structure for various stub widths W = 1 to 4 mm are plotted in Fig. 5.7(b). The increase in width of the stub causes an increased capacitive effect, due to which sharp transition from passband to stopband is achieved. Hence, suitable choice of device dimensions lead to a lowpass filter with the desired cut-off frequency.

For demonstration purpose, we have designed a lowpass filter with a 3 dB cut-off frequency of 1 GHz with more than 20 dB rejection level at 1.5 GHz. From the Figures 5.7(a) and 5.7(b), the length and width of the stub chosen are 26 mm and 4 mm respectively. The dimensions of OCSRR

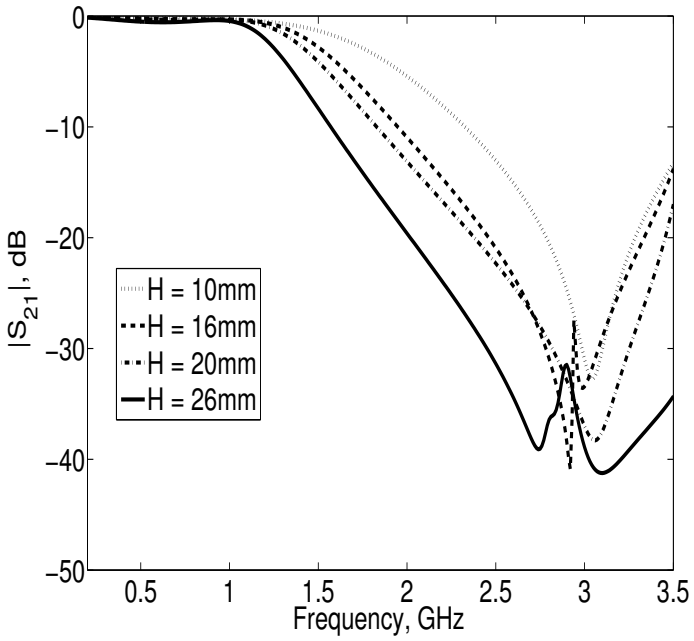

(a)

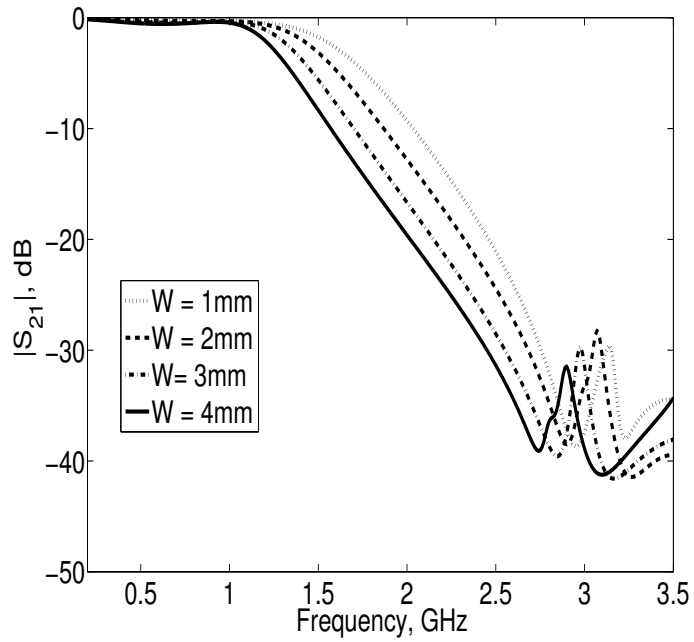

(b)

Figure 5.7: Proposed lowpass filter a) Transmission response for various heights 'H' for fixed width 'W'= 4 mm b) Transmission response for various widths 'W' for fixed height 'H' = 26 mm.

are same as mentioned above. However, the spurious passband is present near the cut-off frequency and the transition from passband to stopband performance is poor. Therefore, we have cascaded the

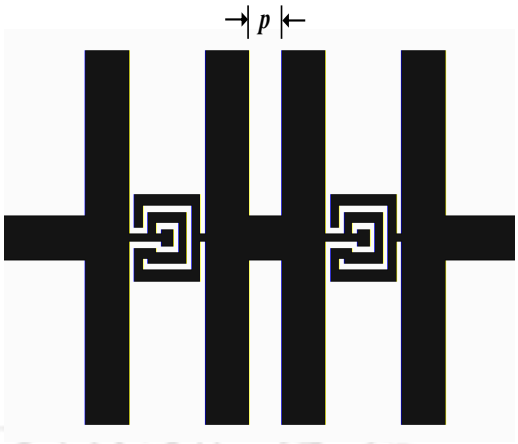

(a)

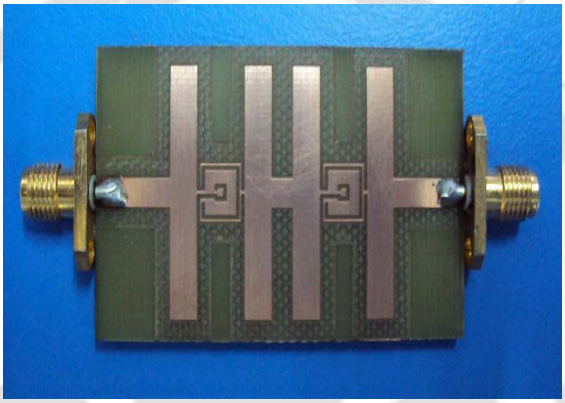

(b)

Figure 5.8: Proposed lowpass filter a) Layout b) Photograph.

two cells of OCSRR and open stub arrangement. The distances between the two cells are 3 mm, which is optimized using electromagnetic simulation. Fig. 5.8(a) and Fig. 5.8(b) depict the geometry and photograph of the proposed lowpass filter respectively. The prototype of the proposed filter is fabricated on the FR4 substrate with dielectric constant 4.4 and thickness 1.6 mm, and tested using Agilent 8753ES network analyzer. Simulated and experimental results of the proposed lowpass filter are illustrated in Fig. 5.9. The proposed filter has a 3 dB cut-off frequency of 1.08 GHz and low insertion loss of less than 0.66 dB in the passband. The insertion loss suddenly drops to 20 dB at 1.45 GHz that means the transition bandwidth is only 0.37 GHz. The selectivity of the proposed filter is 46 dB/GHz. The measured stopband rejection of the filter is better than 30 dB up to 6 GHz, which is nearly six times the cut-off frequency. The length of the filter is 32.6 mm excluding the

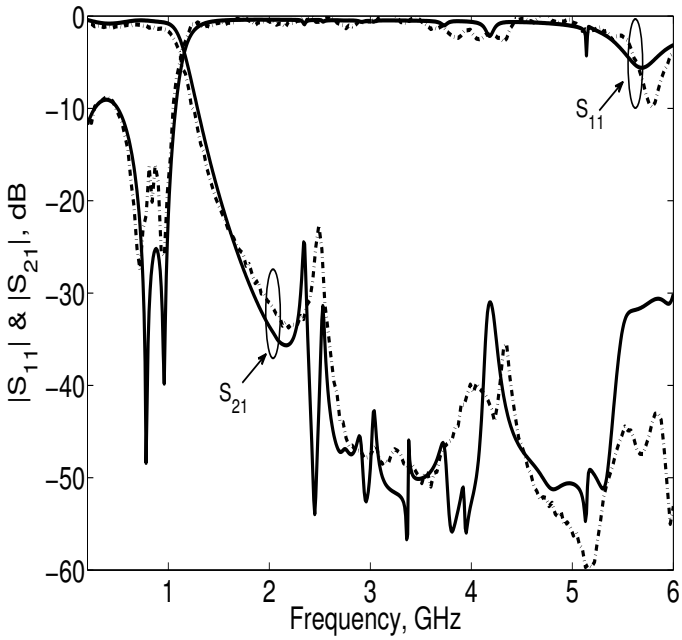

Figure 5.9: Simulated (solid line) and measured (dashed line) scattering parameters of proposed lowpass filter.

Table 5.1: Performance comparison of LPFs

Structure	Cut-off frequency (f_c)	Size	Stopbandwidth (up to)	Stopband rejection (more than 30 dB)
CSRR [88]	1.1 GHz	0.32 λ_g × 0.18 λ_g	5 f_c	Up to 4.4 f_c
Tapered CMRC [106]	1.3 GHz	0.62 λ_g × 0.19 λ_g	10 f_c	Up to 6 f_c
OCSRR only [36]	1.33 GHz	0.81 λ_g × 0.09 λ_g	4 f_c	Up to 2 f_c
Proposed work	1.08 GHz	0.22 λ_g × 0.18 λ_g	6 f_c	Up to 6 f_c

access line, which is 73% shorter than the work reported in [36]. The proposed lowpass filter result is compared with the some of the work already reported and tabulated in Table 5.1, where λ_g is the guided wavelength of the 50 Ω microstrip line at the cut-off frequency.

The proposed filter shows a very good performance in terms of low insertion loss, wide rejection bandwidth and compact design. Moreover, the fabrication of device is simple, since it does not involve any via holes.

5.5 Ultra-wide stopband lowpass filter using open complementary split ring resonator and defected ground structures

5.5.1 Introduction

As discussed in the previous section, the conventional filter design methods such as stepped impedance and open stub are suffering from poor skirt characteristics and spurious passband. Hence, over the past few years researchers have paid great attention for designing a compact and sharp cut-off lowpass filter with spurious free wide stopband. Various compact lowpass filters designs are referred in the previous section. In this section, a very small (0.16 λ_g × 0.08 λ_g) and ultra-wide stopband lowpass filter design using open complementary split ring resonator (OCSRR) and defected ground structure (DGS) is presented. A low pass filter is constructed using two cascaded stages of OCSRR. Since the rejection bandwidth of the OCSRR is narrow, tapered square dumbbell shaped DGS section is placed under the OCSRRs. The cut-off frequency of the proposed lowpass filter is 1.09 GHz. The rejection bandwidth of the filter covers the entire ultra wideband spectrum. Hence, the spurious passband suppression is achieved up to 10 f_c. The proposed lowpass filter is smaller and outperforming the existing filters in terms of insertion loss level, roll off rate and rejection bandwidth.

5.5.2 Lowpass filter with wide rejection bandwidth

From the scattering parameters of the OCSRR, we observe that the rejection bandwidth of the OCSRR is narrow and not suitable for lowpass filter application. So by cascading many numbers of OCSRRs, the required wide stop bandwidth can be achieved. In the previous section, the wide rejection bandwidth and compact size LPF is designed using open stubs attached on both sides of the OCSRR. In order to reduce the size of the filter further, tapered dumbbell shaped DGSs are placed underneath the OCSRR loaded microstrip line. Since DGSs are etched out from the ground plane, length of the filter is unaltered. Fig. 5.10(a) shows the schematic of the proposed LPF. The substrate used for simulation is Rogers/RT Duroid 5880 with dielectric constant $\varepsilon_r = 2.2$ and dielectric thickness of 0.381 mm. Here, we have cascaded the two OCSRR cells. The dark portion represents the top side and light portion represents the bottom side of the filter. The size of the OCSRR is same as mentioned in the section 5.3. The size of the DGS is optimized to overlap the stopband of DGS section with the OCSRR stopband to obtain a very wide stopband. Fig. 5.10(b) shows the simulated scattering parameters of the proposed LPF. The proposed filter has a 3 dB cut-off frequency of 1.09 GHz and low insertion loss of less than 0.25 dB in the passband. The insertion loss suddenly drops to 20 dB

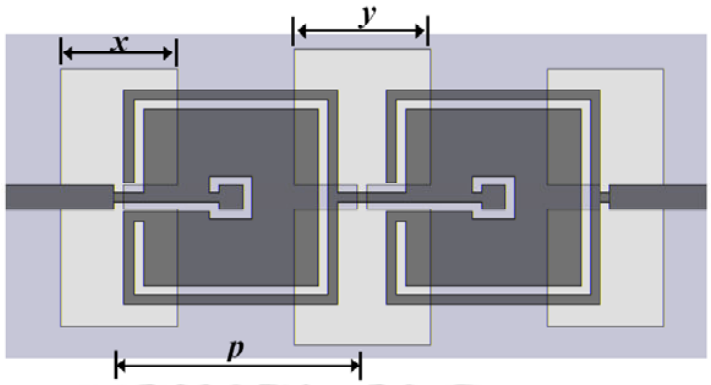

(a)

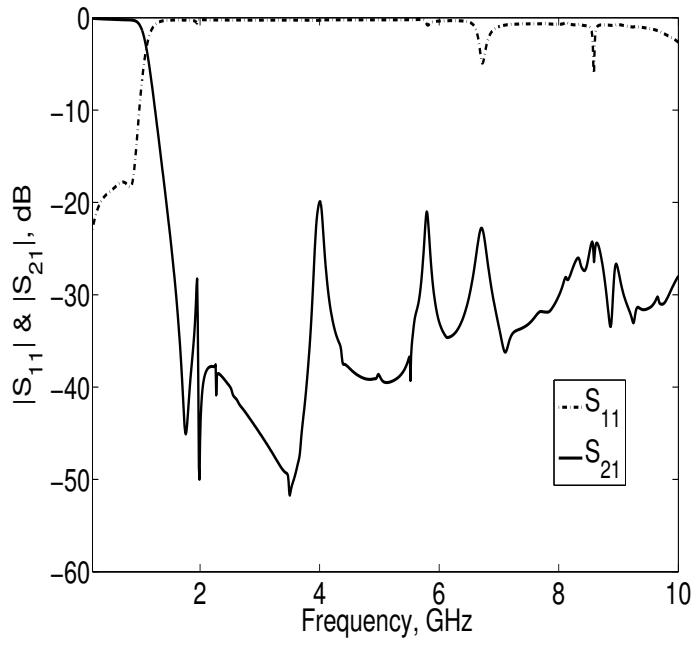

(b)

Figure 5.10: Proposed LPF a) Layout (x = 5.5 mm, y = 7.2 mm, p = 12.5 mm) b) Simulated scattering parameters.

at 1.43 GHz, which indicates that the transition bandwidth is only 0.34 GHz. The return loss in the passband is well above 15 dB. The simulated stopband rejection of the filter is better than 20 dB up to 10 GHz, which is nearly ten times the cut-off frequency. We have calculated the selectivity of the filter as 48.57 dB/GHz. Compared with the work already reported, the proposed filter size is compact and provides a wide stopband rejection. This proposed lowpass filter is much better than the existing highly efficient filters reported by Wu [88] and Aznar [36] in terms of stopband rejection width. Our

Table 5.2: Performance comparison of LPFs

Structure	Cut-off frequency (f_c)	Size	Stop bandwidth up to
CSRR [88]	1.1 GHz	0.32 λ_g × 0.18 λ_g	5 f_c
Tapered CMRC [106]	1.3 GHz	0.62 λ_g × 0.19 λ_g	10 f_c
OCSRR only [36]	1.33 GHz	0.81 λ_g × 0.09 λ_g	4 f_c
OCSRR & stub	1.08 GHz	0.22 λ_g × 0.18 λ_g	6 f_c
Proposed work	1.09 GHz	0.16 λ_g × 0.08 λ_g	10 f_c

lowpass filter has comparable rejection bandwidth with Li's lowpass filter [106]. Yet, it is much more compact as depicted in Table 5.2.

5.6 Compact, harmonic suppressed power divider using open complementary split ring resonator

5.6.1 Introduction

Microstrip power dividers are widely used in RF/Microwave front end systems such as power amplifiers, mixers, feed network of an antenna array system for distribution of low power signals and laboratory equipments. In order to meet the growing demands of size miniaturization and cost reduction of various communication systems many attempts have been made to reduce the size of the microwave circuits. Defected ground structures (DGSs) and photonic bandgap structures (PBGs) have been used to reduce the size of the power dividers and couplers [90, 99, 108–112]. In [108], a new type of compact microstrip ring hybrid incorporating PBG cells embedded in the ring is presented and 23 % size reduction is achieved. A 4:1 Wilkinson power divider with defected ground structure is proposed in [109]. An EBG embedded in-phase hybrid ring equal power divider providing a much broader bandwidth and occupying a smaller area with harmonic suppression characteristic is presented in [99]. A Wilkinson power divider using microstrip EBG cells for the suppression of harmonics and size reduction is presented in [110]. A metamaterial based T-junction power divider with considerable size reduction is discussed in [113] and [25]. Using an 'I' shaped DGS and CSRR DGS, compact power divider and branch line coupler (BLC) for wireless applications are presented in [111] and [112].

In this section, we propose a new compact T-junction power divider using an OCSRR for 900 MHz GSM operation with considerable size reduction. The proposed power divider occupies 47 % lesser

area than the conventional power divider and provides better third harmonic suppression.

5.6.1.1 The lossless power divider

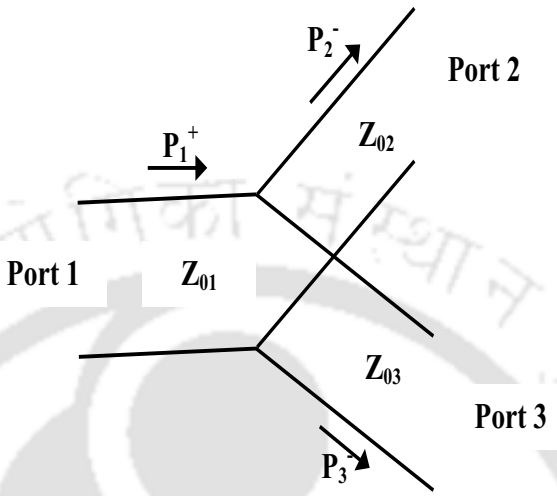

Figure 5.11: Transmission line model of a lossless T-junction.

The lossless T-junction can be modeled as as a junction of three transmission line as shown in Fig. 5.11. When ports 2 and port 3 are terminated in matched loads, the input impedance at port 1 must be equal to Z_{01}. This will only be true if the values Z_{02} and Z_{03} are selected such that:

$$Z_{01} = \frac{Z_{02}Z_{03}}{Z_{02} + Z_{03}} \tag{5.8}$$

Note however that this circuit is not symmetric, thus we find that $S_{22} \neq 0$ and $S_{33} \neq 0$. It is evident that this divider is lossless (no resistive components), so that:

$$P_1^+ = P_2^- + P_3^- \tag{5.9}$$

where P_1^+ is the power incident on port 1, and P_2^- and P_3^- is the power absorbed by the matched loads of ports 2 and 3. Unless $Z_{02} = Z_{03}$ the power will not be equally divide between the ports.

Power dividers can be implemented by means of a 90^0 impedance inverter. There are two different topologies of T-junction power divider as depicted in Fig. 5.12. We have used the first prototype for our design. The equal split conventional power divider is designed using two quarter wavelength transmission line with characteristics impedance of 70.7 Ω. The center frequency of the power divider

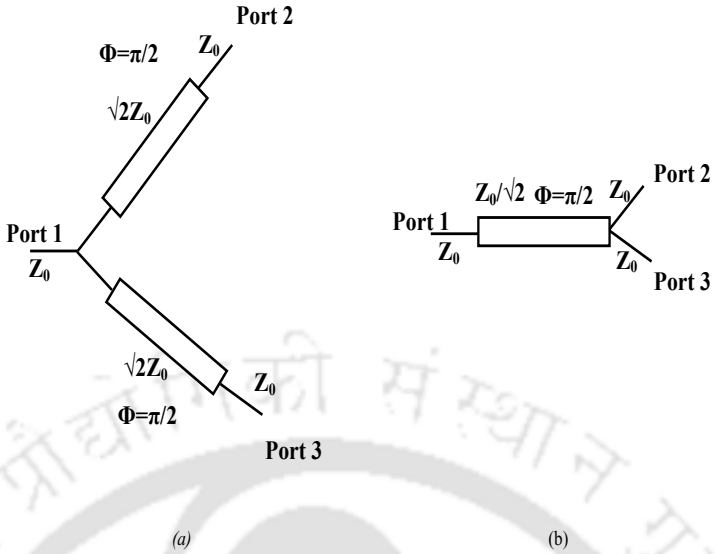

Figure 5.12: Basic topologies of power divider.

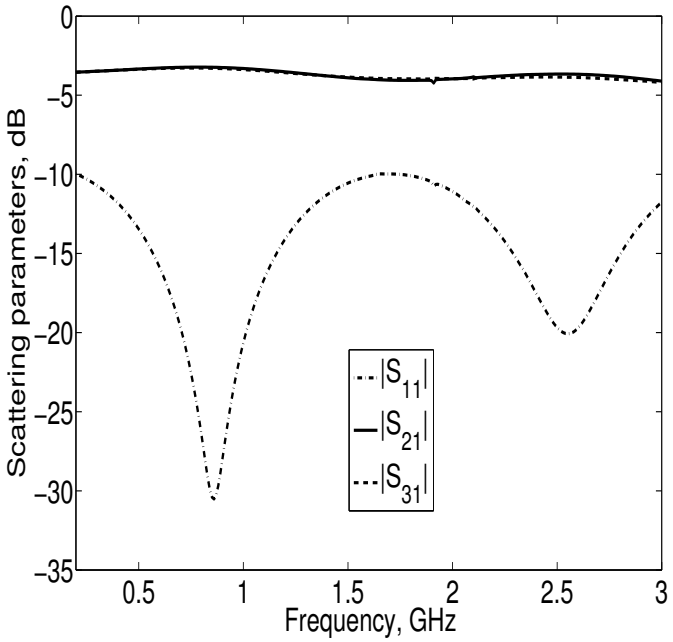

Figure 5.13: Simulated scattering parameters of conventional T-junction power divider.

is chosen as 900 MHz. The simulated results of the conventional equal split T-junction power divider is shown in Fig. 5.13

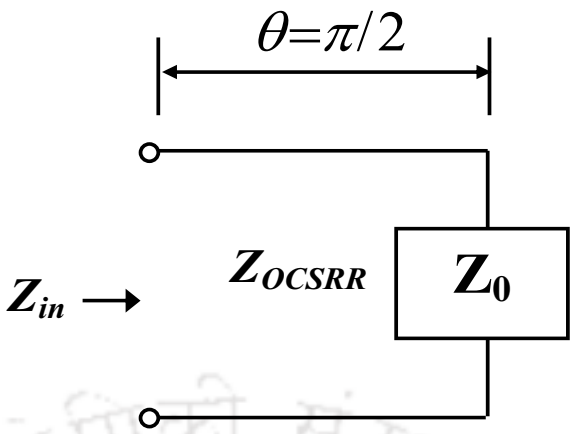

Figure 5.14: Simplified model to determine the characteristic impedance of OCSRR line.

5.6.2 Power divider using OCSRR

To design a OCSRR based power divider, the OCSRR is embedded in a 50 Ω microstrip line. The dimensions of the OCSRR are adjusted in such a way that to obtain a 70.7 Ω line impedance and 90^o phase shift at the center frequency. The characteristics impedance of the OCSRR embedded microstrip line is calculated using the method described in [109] as follows. Fig. 5.14 shows the simplified transmission line model to determine the characteristic impedance of OCSRR embedded microstrip line, where Z_0 is the port impedance. When $\theta = \pi/2$ at the center frequency, the magnitude of the reflection co-efficient (Γ) is maximum and it can be calculated from S_{11} by eq. 5.10. Once $|\Gamma|$ is known, Z_{in} is calculated by eq. 5.11. Finally, the impedance of OCSRR embedded line is calculated from eq. 5.12.

$$S_{11}[dB] = 20\log|\Gamma| \tag{5.10}$$

$$Z_{in} = Z_0\frac{1+|\Gamma|}{1-|\Gamma|} \tag{5.11}$$

$$Z_{OCSRR} = \sqrt{Z_{in}Z_0} = Z_0\sqrt{\frac{1+|\Gamma|}{1-|\Gamma|}} \tag{5.12}$$

Fig. 5.15 shows the simulated phase response of the OCSRR embedded microstrip line and conventional microstrip line. From the figure, it is observed that the phase of the OCSRR embedded line is -90^0 at 0.9 GHz and the phase of the conventional microstrip line is -90^0 at 1.3 GHz. The low resonant frequency shows that the OCSRR embedded microstrip lines generates the slow-wave effect.

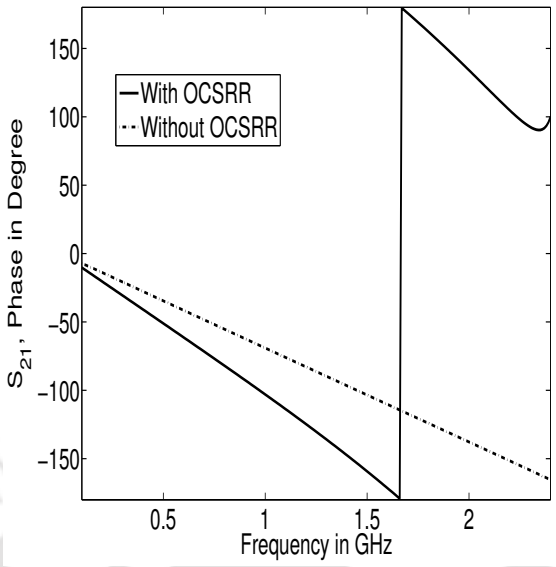

Figure 5.15: Simulated phase response of microstrip line with and without OCSRR.

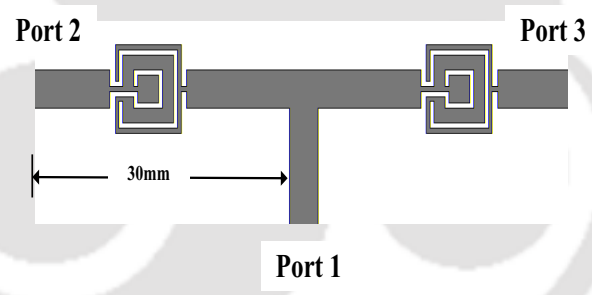

(a)

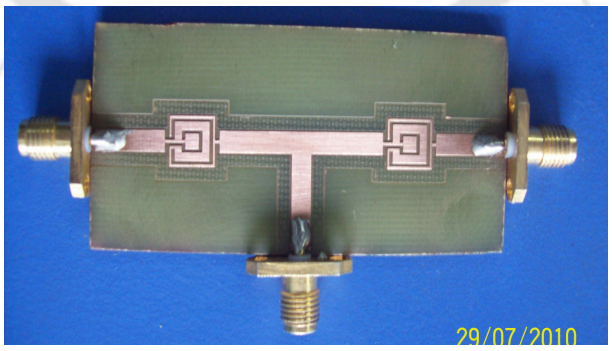

(b)

Figure 5.16: Proposed power divider a) Geometry b) Photograph.

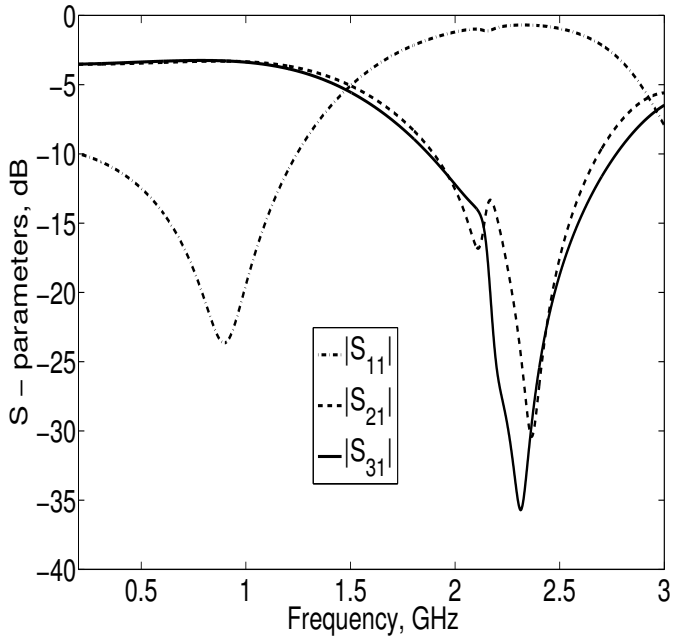

Figure 5.17: Proposed power divider simulated scattering parameters.

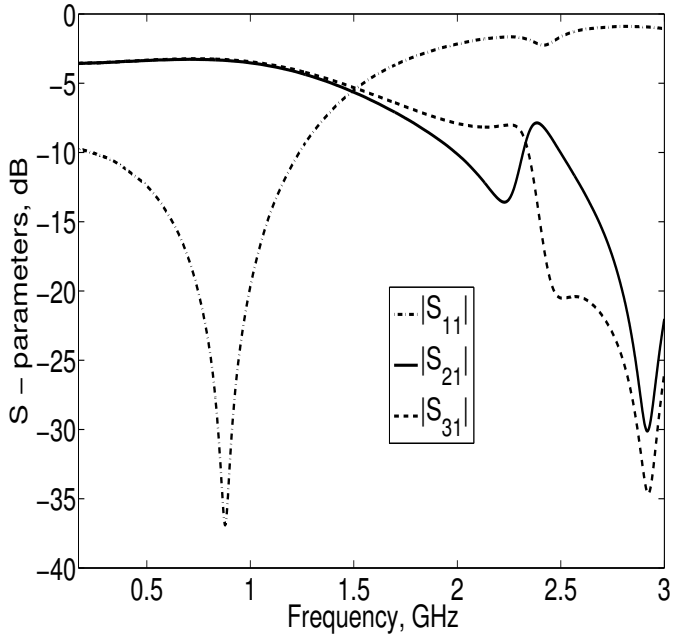

Figure 5.18: Proposed power divider measured scattering parameters.

To validate the proposed method, a T-junction power divider operating at 900 MHz GSM frequency is designed and fabricated. The layout and fabricated prototype of the proposed power divider are shown in Fig. 5.16(a) & 5.16(b). The dimensions of the OCSRR are adjusted to obtain the required

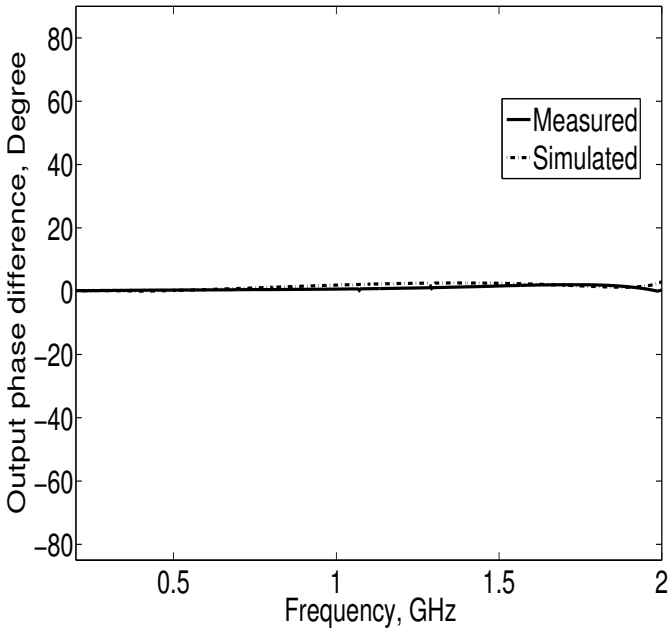

Figure 5.19: Simulated and measured output phase difference of the proposed power divider.

line impedance. The optimized dimensions of OCSRR used in the proposed power divider are $a = 7$ mm, $c = 0.9$ mm, $d = 0.4$ mm, $g = 0.4$ mm, and $w = 0.4$ mm.

The simulated and measured response of the proposed power divider are illustrated in Fig. 5.17 and Fig.5.18 respectively. As can be seen from the figures, the power is equally divided between the two output ports with measured insertion loss of 3.325 dB which is very close to the ideal 3 dB. The measured reflection co-efficient is more than 36 dB in the center frequency of the band and the third harmonic suppression is more than 22 dB. Fig. 5.19 shows the simulated and measured phase difference between the output ports of the developed power divider. It is observed that the two output port signals are in phase with each other around the center frequency with the maximum phase imbalance of 0.5^0. Table 5.3 gives a comparison between conventional power divider and proposed power divider.

Table 5.3: Comparison of conventional and proposed power dividers

Power divider	Circuit area (mm^2)	Relative area (%)	Third harmonic suppression (dB)
Conventional	3520	100	no
Proposed	1890	53	22

5.7 Size reduced and harmonic suppressed rat race coupler

5.7.1 Introduction

The rat-race coupler or 180^0 ring hybrid is one of the important component in the microwave/millimeter wave circuits. It is widely used in various applications such as mixer, multiplier, amplifier, etc. It is a four port network with a 180^0 phase shift between the two output ports. It can also be operated in in-phase operation. The schematic of rat-race coupler is shown in Fig. 5.20. The ports 4 and 3, 3 and 1, and 1 and 2 are separated by a electrical length of 90^0, and ports 2 and 4 are separated by a electrical length of 270^0. The signal applied to port 1 will be equally divided into two in-phase components at ports 2 and 3, and port 4 will be an isolated port. If the signal is applied to port 4, it will be divided into two components with a 180^0 phase difference at ports 2 and 3, and port 1 will be an isolated port. It can be also operated as a combiner. When input signals are applied at ports 2 and 3, sum of the input signals will be appeared at port 1 and the difference of the input signals will be observed at port 4. Hence, ports 1 and 4 are known as the sum and difference ports respectively. The important shortcoming of rat-race coupler is the size ($1.5\lambda_g$, where λ_g is the guided wavelength at the design frequency).

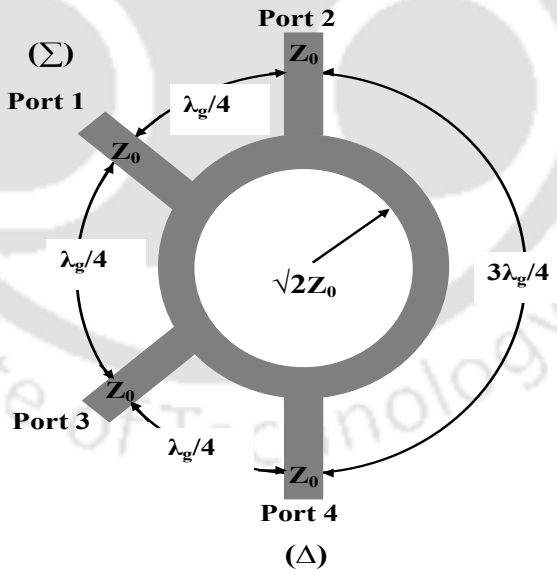

Figure 5.20: Schematic of conventional ring hybrid.

To overcome this limitation, several methods have been proposed [28, 108, 114–119]. By incorporating six evenly distributed PBG cells in the hybrid ring, 23% size reduction is achieved in [108]. The

space filling property of fractal curves are applied for the design of size reduced branch line coupler and rat race coupler [114]. Size reduction and harmonic suppression of ring hybrid using dumbbell shaped defected ground structure is presented in [115]. Miniaturized spurious passband suppressed rat-race coupler using compensated spiral compact microstrip resonant cell (C-SCMRC) resonator is demonstrated in [116]. The circuit area of the C-SCMRC rat-race coupler is only 45% of the conventional coupler. A very small hybrid ring coupler based on the periodic stepped-impedance ring resonator structure is reported in [117]. In [120], using CSRR based artificial transmission line, size miniaturized rat-race coupler is presented. However, this design involves via holes, which are difficult from the fabrication point of view. A novel LH-TL hybrid ring is proposed to realize a miniaturized hybrid ring [28], in which LH transmission line is produced by CSRRs. The occupied area of the ring hybrid can be reduced to 60% from that of the conventional one. In [119], it has been shown that a basic unit consisting of two shunt open-stubs separated by a transmission line section can be used to design a size reduced rat-race coupler with suppressed harmonics.

In our work, we have demonstrated a size reduced and harmonic suppressed ring hybrid using OCSRR. The slow-wave effect of the OCSRR embedded microstrip line is used to design such a compact ring hybrid. The proposed coupler is 37% smaller than the conventional coupler and offers a third harmonic suppression up to 33 dB.

5.7.2 Ring hybrid using OCSRR

As explained in previous section, the slow-wave effect caused by the OCSRR embedded microstrip line is used to design a compact and harmonic suppressed ring hybrid. Using the OCSRR embedded microstrip line with the characteristic impedance of 50 Ω, the required microstrip line of characteristic impedance 70.7 Ω is realized and it is applied for the design of a ring hybrid. The length of the microstrip line is 20 mm, which is approximately equal to the $\lambda_g/4$ at 2 GHz. The dimensions of the OCSRR are as follows: $a = 4$ mm, $c = 0.4$ mm, $d = 0.5$ mm, $g = 0.3$ mm, and $w = 0.4$ mm. Fig. 5.21 shows the simulated phase response of the microstrip line with OCSRR and without OCSRR. From the diagram, it is evident that the phase of the OCSRR embedded microstrip line is -90^0 at 1.5 GHz, whereas 2 GHz in microstrip line without OCSRR. The slow-wave effect of the OCSRR embedded line is also plotted in Fig. 5.22. The slow-wave factor of the OCSRR embedded line is more than the conventional microstrip line. This property helps us to design a size reduced ring hybrid.

The configuration of the proposed rectangular shaped ring hybrid operating at 1.5 GHz is shown

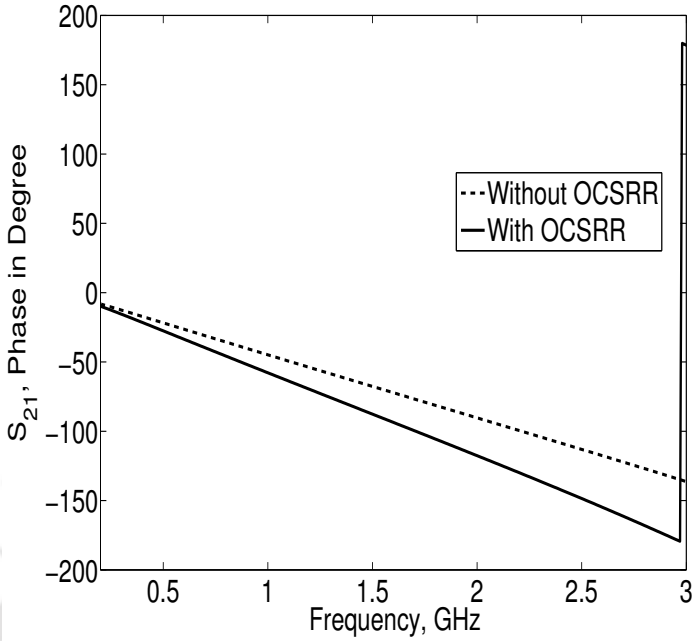

Figure 5.21: Simulated phase response of microstrip line with and without OCSRR.

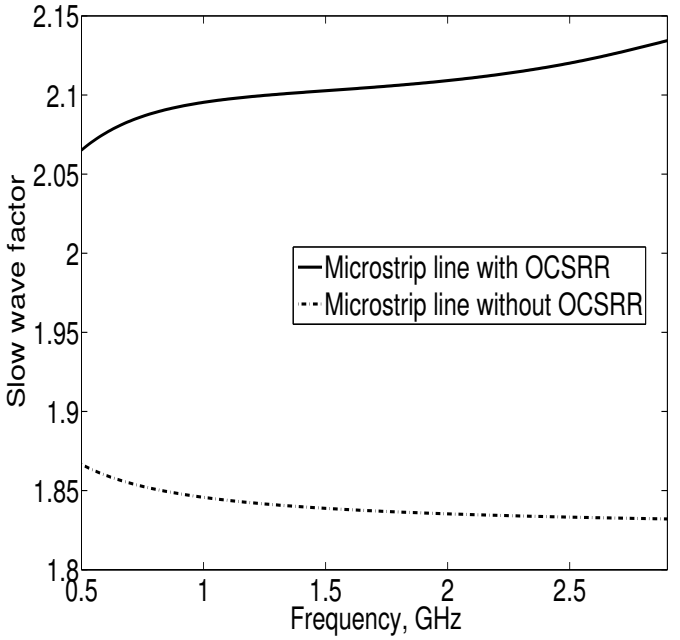

Figure 5.22: Slow-wave factor of the microstrip line loaded with OCSRR.

in Fig. 5.23(a). The conventional 70.7 Ω microstrip line is replaced with the OCSRR embedded microstrip line. The substrate used for simulation and fabrication is FR4 substrate with relative permittivity of 4.4 and thickness 1.6 mm. The photograph of the fabricated ring hybrid is shown in

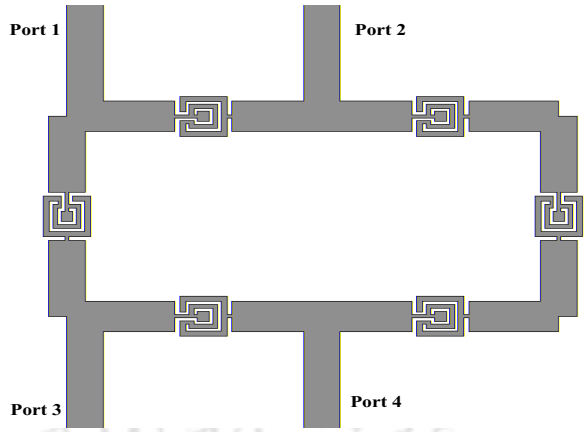

(a)

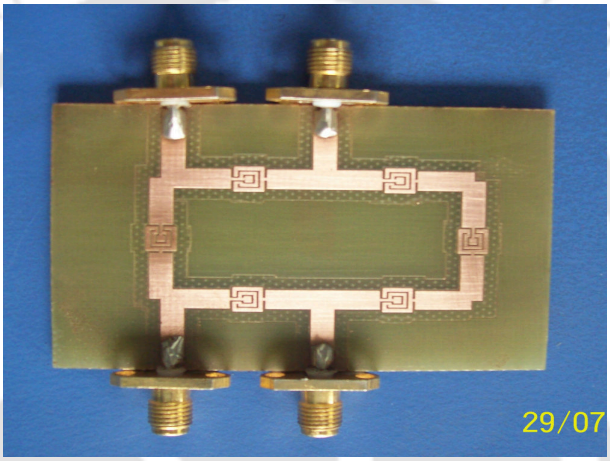

(b)

Figure 5.23: Proposed ring hybrid a) Geometry b) Fabricated prototype.

Fig. 5.23(b). Simulated and measured S-parameters of the proposed ring hybrid are shown in Fig. 5.24. Simulation and measurement are in good agreement. In Fig. 5.24(a), frequency variation of the input matching (S_{11}) and the output at port 2 (S_{21}) are shown and in Fig. 5.24(b), the output at port 3 (S_{31}) and the isolation (S_{41}) are shown. Measurements have been carried out using Rohde & Schwarz vector network analyzer. The measured output $|S_{21}|$ is -3.508 dB and $|S_{31}|$ is -3.398 dB at 1.5 GHz. The measured return loss $|S_{11}|$ is -43.53 dB and isolation $|S_{41}|$ is better than -39 dB.

The measured phase response of the proposed ring hybrid for the port 1 and port 4 excitations are shown in Fig. 5.25 and Fig. 5.26 respectively. The phase difference between S_{21} and S_{31} is 0.9^0. The phase difference between S_{34} and S_{24} is 183.15^0. The proposed coupler offers the third harmonic suppression up to 35 dB and 37% smaller than the conventional ring hybrid. The measured amplitude

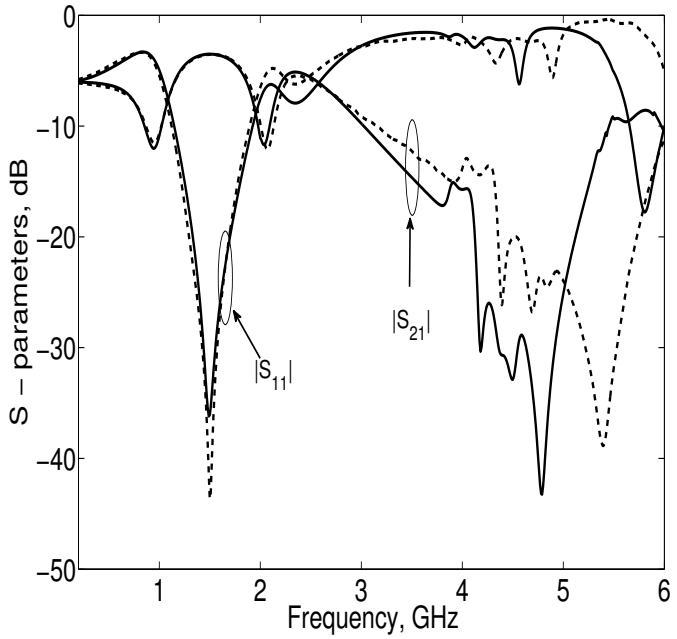

(a)

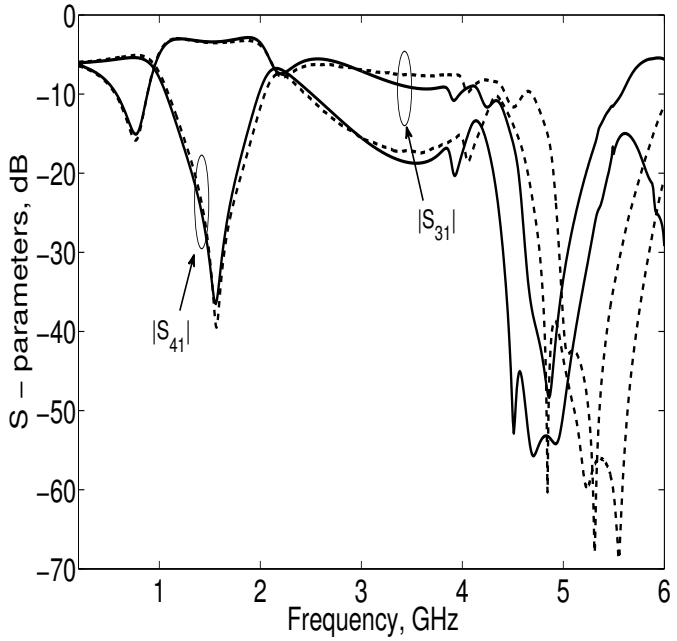

(b)

Figure 5.24: Proposed rat-race coupler a) Simulated (solid line) and measured (dashed line) scattering parameters ($|S_{11}|$, $|S_{21}|$) b) Simulated (solid line) and measured (dashed line) scattering parameters ($|S_{31}|$, $|S_{41}|$).

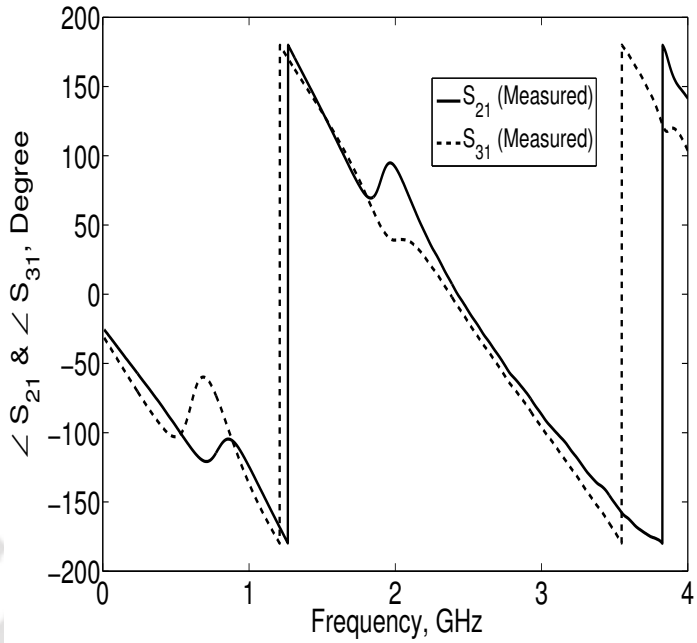

Figure 5.25: Phase response for the sum port excitation.

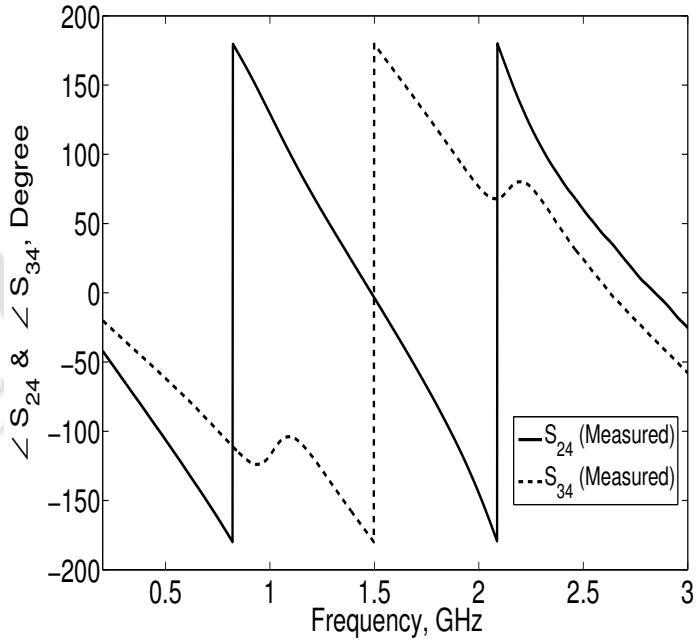

Figure 5.26: Phase response for the difference port excitation.

imbalance for the ring hybrid is 0.11 dB. The isolation and matching are better than 20 dB from 1.33 GHz to 1.7 GHz and 1.32 GHz to 1.77 GHz respectively for the proposed ring hybrid. These values are, respectively from 1.24 GHz to 1.75 GHz and 1.32 GHz to 1.72 GHz for the conventional

Table 5.4: Performances of the proposed ring hybrid

	Simulation	Measurement
Operating frequency	1.5 GHz	1.544 GHz
Return loss (S_{11})	36.08 dB	43.53 dB
Isolation (S_{41})	36.5 dB	39 dB
Output 1 (S_{21})	3.506 dB	3.508 dB
Output 2 (S_{31})	3.39 dB	3.398 dB
Amplitude imbalance	0.116 dB	0.11 dB
Phase difference (Sum port)	1.6^0	0.9^0
Phase difference (Difference port)	184.4^0	183.15^0

ring hybrid and these values are comparable to the proposed ring hybrid. The performances of the proposed ring hybrid are summarized in Table 5.4.

5.8 Summary

This chapter dealt with the modeling and applications of sub-wavelength resonator viz. open complementary split ring resonator. Some of the performance enhanced filters and couplers have been presented. Compact and improved stopband lowpass filters are designed using OCSRR, open stub and DGS combination. Size miniaturized and third harmonic suppressed T-junction power divider and rat-race coupler have been designed using OCSRR and verified with the fabricated prototypes.

6

Conclusions and future work

Contents

6.1 Conclusions

The main objective of this thesis is to explore the usage of metamaterial based sub-wavelength resonators: CSSRR, CSRR, OSSRR and OCSRR for performance enhancement of microwave devices such as filters, coupler, power divider, etc. The lumped element model of these resonators have been developed and equivalent circuit parameters are extracted to support this study. Detailed parametric study has been carried out to investigate the relation between the dimensions and resonant frequency of these sub-wavelength resonators. Several size miniaturized lowpass filters, bandpass filter, stopband extended bandstop and lowpass filters and miniaturization of power divider and ring hybrid with harmonic suppression are presented in this thesis. Commercial full wave simulators (IE3D and CST Microwave Studio) have been used for the design and analysis purpose. Several size miniaturized and performance enhanced planar microwave components have been developed during the course of study.

- Various wide rejection bandwidth bandstop filters have been developed using CSSRR, CSRR, open stub and spurline. The proposed BSFs occupy lesser area than the conventional open stub BSF and provide enhanced rejection bandwidth. By cascading the proposed BSFs with LPFs and BPFs, harmonic suppression of stepped impedance lowpass filter and PCML bandpass filters have been achieved.

- UWB bandpass filter with notch frequency characteristics is desirable to avoid the interference between the UWB systems and the WLAN radio devices. In our work, we have presented an UWB bandpass filter with notch function using CSSRR. Compared with the conventional CSRR, CSSRR has sharp cut-off and flat insertion loss after the stopband. Hence, it is utilized to introduce a sharp rejection band in the WLAN frequency region. To design the UWB bandpass filter with notch function, UWB BPF is designed using ground plane aperture technique. The CSSRR resonating at 5.5 GHz is designed and placed underneath the parallel coupled microstrip lines around the ground plane aperture. The proposed filter is capable of suppressing the interference from IEEE 802.11a WLAN signals effectively. Compared with the work reported in [57] and [64], the proposed method provides better FBW in the notch band and does not require any via holes which are used in [57] and [60].

- A novel and size miniaturized sub-wavelength resonator known as OSSRR, exhibiting negative permittivity is proposed. For the same resonant frequency, the size of the OSSRR is smaller than

the conventional CSRR. Hence, compact composite right/left handed planar transmission line is synthesized by OSSRR and interdigital capacitor. Compared with the work reported in [81], the proposed structure does not involve any via holes. So complexity is reduced from fabrication point of view.

- A wide fractional bandwidth (FBW) bandpass filter is designed by cascading highpass (HPF) and lowpass (LPF) filters realized using OSSRR and compact microstrip resonating cell (CMRC), respectively. The fractional bandwidth of the filter can be easily varied by varying the cut-off frequencies of LPF and HPF sections. For demonstration purpose, two BPF with different FBW is presented. Type 1 filter has 29.2% FBW and is 20% smaller in size than the conventional third order PCML bandpass filter. Type 2 BPF has 76% FBW and occupies 47% smaller area than the traditional PCML BPF.

- A compact lowpass filter is designed using periodic array of OSSRR and open stubs. The proposed filter has sharp cut-off characteristics and 17.5% smaller than the conventional stepped impedance lowpass filter and 8% smaller than the CSRR DGS LPF.

- A wide stopband, sharp cut-off and compact lowpass filter is designed using open complementary split ring resonator (OCSRR) and open stub. The proposed lowpass filter consist of two OCSRR connected in series. The open stubs are attached on both sides of the OCSRR. At the 3 dB cut-off frequency of 1.08 GHz, the proposed filter offers a sharp and wide rejection bandwidth of more than 20 dB up to six times the cut-off frequency. The filter size is very small (0.22 λ_g $\times$ 0.18λ_g, where λ_g is the guided wavelength at the cut-off frequency).

- A very small (0.16 λ_g $\times$ 0.08 λ_g) and ultra wide stopband lowpass filter has been developed using open complementary split ring resonator and defected ground structure. Lowpass filter is constructed using two cascaded stages of OCSRR. Since the rejection bandwidth of the OCSRR is narrow, tapered square dumbbell shaped DGS section is placed under the OCSRRs. The cut-off frequency of the proposed lowpass filter is 1.09 GHz. The rejection bandwidth of the filter covers the entire ultra wideband spectrum. Hence the spurious passband suppression is achieved up to 10 f_c.

- The slow-wave effect and the stopband effect of the OCSRR have been utilized for the size miniaturization and harmonic suppression of power divider and ring hybrid. OCSRR embedded

microstrip line is used for the design of a T-junction power divider and 180^0 ring hybrid. For the T-junction power divider third harmonic is suppressed up to 22 dB, and device area is just 53% of a conventional power divider. For the ring hybrid, third harmonic is suppressed up to 35 dB and device area is 37% smaller than the conventional one.

6.2 Suggestions for future work

In this section, some suggestions for further research are proposed.

- The effect of applying fractal technique, in reducing the size of the resonators can be further investigated.
- The potential for use of OSSRR in the design of dual band components such as, dual band power divider, branch line coupler and ring hybrid should also be investigated.
- The use of OSSRR to minimize the size of couplers can be studied.
- Other compact sized resonators such as spiral and triangular shaped resonators, should be explored in further attempt to reduce the size of the microwave devices.
- In this study, performance enhancement of microwave devices using metamaterial based subwavelength resonators have been investigated. This approach can be further extended to enhance antenna gain, bandwidth, etc.
- Here, the open complementary split resonators are used to design compact lowpass filters. Studies of use of such resonators for designing bandstop and bandpass filters would also be beneficial.

Bibliography

[1] V. G. Veselago, "Electrodynamics of substances with simultaneously negative values of ε and μ," *Sov. Phys.-Usp.*, vol. 10, pp. 509–514, Jan.-Feb. 1968.

[2] J. B. Pendry, A. J. Holden, W. J. Stewart, and I. Young, "Extremely low frequency plasmons in metallic mesostructures," *Phys. Rev. Lett*, vol. 76, pp. 4773–4776, 1996.

[3] J. B. Pendry, A. J. Holden, D. J. Robbins, and W. J. Stewart, "Magnetism from conductors and enhanced linear media," *IEEE Trans. Microwave Theory Tech.*, vol. 47, no. 11, pp. 2075–2084, Nov. 1999.

[4] R. A. Shelby, D. R. Smith, and S. Schultz, "Experimental verification of a negative index of refraction," *Science*, vol. 292, pp. 77–79, Apr. 2001.

[5] C. Caloz and T. Itoh, *Electromagnetic metamaterials : Transmission line theory and microwave applications.* Wiley Interscience, 2006.

[6] A. Iyer and G. Eleftheriades, "Negative refractive index metamaterials supporting 2-D waves," in *Proceedings of IEEE-MTT International Microwave Symposium Digest*, vol. 2, Seattle, WA, 2002, pp. 412–415.

[7] A. Oliner, "A periodic-structure negative-refractive-index medium without resonant elements," in *URSI Digest*, San Antonio, TX, Jun. 2002.

[8] C. Caloz and T. Itoh, "Application of the transmission line theory of left-handed (LH) materials to the realization of a microstrip LH transmission line," in *Proceedings of IEEE-AP-S USNC/URSI National Radio Science Meeting*, vol. 2, San Antonio, TX, Jun. 2002, pp. 412–415.

[9] F. Falcone, T. Lopetegi, J. D. Baena, R. Marques, F. Martin, and M. Sorolla, "Effective negative-ε stop-band microstrip lines based on complementary split ring resonators," *IEEE Microwave and Wireless Components Letters*, vol. 14, pp. 280–282, 2004.

[10] J. Garcia, F. Martin, F. Falcone, J. Bonache, I. Gil, T. Lopetegi, M. A. G. Laso, M. Sorolla, and R. Marques, "Spurious passband suppression in microstrip coupled line band pass filters by means of split ring resonators," *IEEE Microwave Wireless Compon. Lett.*, vol. 14, no. 9, pp. 416–418, Sep. 2004.

[11] J. Garcia, F. Martin, F. Falcone, J. Bonache, J. D. Baena, I. Gil, E. Amat, T. Lopetegi, M. A. G. Laso, J. A. M. Iturmendi, M. Sorolla, and R. Marques, "Microwave filters with improved stopband based on sub-wavelength resonators," *IEEE Trans. Microw. Theroy Tech.*, vol. 53, no. 6, pp. 1997–2006, Jun. 2005.

[12] J. J. Garcia-Garcia, J. Bonache, F. Falcone, J. D. Baena, F. Martin, I. Gil, T. Lopetegi, M. A. G. Laso, A. Marcotegui, R. Marques, and M. Sorolla, "Stepped-impedance lowpass filters with spurious passband suppression," *Electronics Letters*, vol. 40, pp. 881–883, Jul. 2004.

[13] H.-W. Wu, M.-H. Weng, Y.-K. Su, R.-Y. Yang, and C.-Y. Hung, "Propagation characteristics of complementary split-ring resonator for wide bandgap enhancement in microstrip bandpass filter," *Microwave and Optical Technology Letters*, vol. 49, no. 2, pp. 292–295, Feb. 2007.

[14] M. K. Mandal, P. Mondal, S. Sanyal, and A. Chakrabarty, "Low insertion-loss, sharp-rejection and compact microstrip low-pass filters," *IEEE Microwave and Wireless Components Letters*, vol. 16, no. 11, pp. 600–602, Nov. 2006.

[15] P. Mondal, M. K. Mandal, A. Chakrabarty, and S. Sanyal, "Compact bandpass filters with wide controllable fractional bandwidth," *IEEE Microwave and Wireless Components Letters*, vol. 16, no. 10, pp. 540–542, Oct. 2006.

[16] J. Bonache, I. Gil, J. Garcia-Garcia, and F. Martin, "Novel microstrip bandpass filters based on complementary split ring resonators," *IEEE Transactions on Microwave Theory and Techniques*, vol. 54, no. 1, pp. 265–271, Jan. 2006.

[17] M. Gil, J. Bonache, J. Garcia-Garcia, J. Martel, and F. Martin, "Composite right/left handed metamaterial transmission lines based on complementary split ring resonators and their applications to very wideband and compact filter design." *IEEE Transactions on Microwave Theory and Techniques*, vol. 55, no. 6, pp. 1296–1304, Jun. 2007.

[18] P. Mondal and A. Chakrabarty, "Compact highpass filter using complementary split ring resonator," *Microwave and Optical Technology Letters*, vol. 49, no. 10, pp. 2470–2472, Oct. 2007.

[19] P. Mondal, M. K. Mandal, and A. Chakrabarty, "Compact ultra-wideband bandpass filter with improved out-of-band rejection," *Microwave and Optical Technology Letters*, vol. 50, no. 3, pp. 758–761, Mar. 2008.

[20] S. Dwari and S. Sanyal, "Compact sharp cut-off wide stopband microstrip low-pass filter using complementary split ring resonator," *Microwave and Optical Technology Letters*, vol. 49, no. 11, pp. 2865–2867, Nov. 2007.

[21] B. Wu, J. W. Fan, L. P. Zhao, and C. H. Liang, "Design of dual band filter using defected split ring resonator combined with interdigital capacitor," *Microwave and Optical Technology Letters*, vol. 49, no. 9, pp. 2104–2106, Sep. 2007.

[22] S. N. Burokur, M. Latrach, and S. Toutain, "A novel type of microstrip coupler utilizing a slot split ring resonators defected ground plane," *Microwave and Optical Technology Letters*, vol. 48, no. 1, pp. 138–141, Jan. 2006.

[23] K.-Y. Liu, C. Li, and F. Li, "A new type of microstrip coupler with complementary split-ring resonator," *Microwave and Optical Technology Letters*, vol. 49, no. 7, pp. 1613–1616, Jul. 2007.

[24] F. Aznar, J. Bonache, A. Valcarcel, and F. Martin, "Miniaturization of narrow-band power dividers by using CPW metamaterial transmission lines," *Microwave and Optical Technology Letters*, vol. 51, no. 4, pp. 926–929, Apr. 2009.

[25] M. Gil, J. Bonache, I. Gil, J. Garcia-Garcia, and F. Martin, "Miniaturization of planar microwave circuits by using resonant-type left handed transmission lines," *IET Microw. Antennas Propag.*, vol. 1, no. 1, pp. 73–79, Feb. 2007.

[26] M. Gil, J. Bonache, and F. Martin, "Synthesis and applications of new left handed microstip line with complementary split ring resonators etched on the signal strip," *IET Microw. Antennas Propag.*, vol. 2, no. 4, pp. 324–330, 2008.

[27] H. Okabe, C. Caloz, and T. Itoh, "A compact enhanced-bandwidth hybrid ring using an artificial lumped-element left-handed transmission-line section," *IEEE Transactions on Microwave Theory and Techniques*, vol. 52, pp. 798–804, 2004.

[28] J.-X. Niu and X.-L. Zhou, "A novel miniaturized hybrid ring using complementary split ring resonators," *Microwave and Optical Technology Letters*, vol. 50, no. 3, pp. 632–635, Mar. 2008.

[29] I.-H. Lin, M. DeVincentis, C. Caloz, and T. Itoh, "Arbitrary dual-band components using composite right/left-handed transmission lines," *IEEE Transactions on Microwave Theory and Techniques*, vol. 52, pp. 1142–1149, 2004.

[30] J.-X. Niu and X.-L. Zhou, "A novel dual-band branch line coupler based on strip-shaped complementary split ring resonators," *Microwave and Optical Technology Letters*, vol. 49, no. 11, pp. 2859–2862, Nov. 2007.

[31] J. Bonache, G. Siso, M. Gil, A. Iniesta, J. Garcia-Rincon, and F. Martin, "Application of composite right/left handed (CRLH) transmission lines based on complementary split ring resonators (CSRRs) to the design of dual-band microwave components," *IEEE Microwave Wireless Compon. Lett.*, vol. 18, no. 8, pp. 524–526, Aug. 2008.

[32] J. Selga, G. Siso, M. Gil, J. Bonache, and F. Martin, "Microwave circuit miniaturization with complementary spiral resonators: Application to high-pass filters and dual-band components," *Microwave and Optical Technology Letters*, vol. 51, pp. 2741–2744, 2009.

[33] J. Martel, R. Marques, F. Falcone, J. D. Baena, F. Medina, F. Martin, and M. Sorolla, "A new LC series element for compact bandpass filter design," *IEEE Microwave and Wireless Components Letters*, vol. 14, no. 14, pp. 210–212, May 2004.

[34] A. Velez, F. Aznar, J. Bonache, M. C. Velazquez-Ahumuda, J. Martel, and F. Martin, "Open complementary split ring resonators (OCSRRs) and their application to wideband CPW bandpass fitlers," *IEEE Microwave and Wireless Components Letters*, vol. 19, no. 4, pp. 197–199, Apr. 2009.

[35] M. Duran-Sindreu, A. Velez, F. Aznar, G. Siso, J. Bonache, and F. Martin, "Applications of open split ring resonators and open complementary split ring resonators to the synthesis of artificial transmission lines and microwave passive components," *IEEE Transactions on Microwave Theory and Techniques*, vol. 57, no. 12, pp. 3395–3403, Dec. 2009.

[36] F. Aznar, A. Velez, J. Bonache, J. Menes, and F. Martin, "Compact lowpass filters with very sharp transition bands based on open complementary split ring resonators," *Electronics Letters*, vol. 45, no. 6, pp. 316–317, 2009.

[37] J. Kim, C. Cho, and J. Lee, "5.2 GHz notched ultra-wideband antenna using slot-type SRR," *Electronics Letters*, vol. 42, pp. 315–316, 2006.

[38] J. Liu, S. Gong, Y. Xu, X. Zhang, C. Feng, and N. Qi, "Compact printed ultra-wideband monopole antenna with dual band-notched characteristics," *Electronics Letters*, vol. 44, no. 12, pp. 710–711, Jun. 2008.

[39] Y. Lee and Y. Hao, "Characterization of microstip patch antennas on metamaterial substrate loaded with complementary split ring resonators," *Microwave and Optical Technology Letters*, vol. 50, no. 8, pp. 2131–2135, Aug. 2008.

[40] D. R. Smith, D. C. Vier, T. Koschny, and C. M. Soukoulis, "Electromagnetic parameter retrieval from inhomogeneous metamaterials," *Physical Review E*, vol. 71, no. 3, pp. 036 617(1)–036 617(11), 2005.

[41] D. Ahn, J. S. Park, C. S. Kim, J. Kim, Y. Qian, and T. Itoh, "A design of the low-pass filter using the novel microstrip defected ground structure," *IEEE Trans. Microw. Theory and Tech.*, vol. 49, no. 1, pp. 86–93, Jan. 2001.

[42] H.-W. Wu, M.-H. Weng, Y.-K. Su, C.-Y. Hung, and R.-Y. Yang, "Spurious suppression of a dual mode bandpass filter using simple c-shaped electromagnetic bandgap cells," *Microwave and Optical Technology Letters*, vol. 48, no. 10, pp. 2090–2093, Oct. 2006.

[43] J. D. Baena, J. Bonache, F. Martin, R. M. Sillero, F. Falcone, T. Lopetgi, M. A. L. J. Garcia-Garcia, I. Gil, M. F. Portillo, and M. Sorolla, "Equivalent circuit models for split-ring resonators and complementary split-ring resonators coupled to planar transmission lines," *IEEE Trans. Microw. Theory and Tech.*, vol. 53, no. 4, pp. 1451–1461, Apr. 2005.

[44] D. M. Pozar, *Microwave Engineering*, 2nd ed. Addision-Wesley, 1998.

[45] G. Matthaei, L. F. Young, and E. M. T. Jones, *Microwave Filters, Impedance-Matching Networks and Coupling Structures*. Artech, 1980.

[46] J.-S. Hong and M. J. Lancaster, *Microstrip filters for RF/Microwave Applications*. Wiley, 2001.

[47] T. Lopetegi, M. A. G. Laso, J. Hernandez, M. Bacaicoa, D. Benito, M. J. Garde, M. Sorolla, and M. Guglielmi, "New microstrip "wiggly-line" filters with spurious passband suppression," *IEEE Trans. Microw. Theroy Tech.*, vol. 49, no. 9, pp. 1593–1598, Sep. 2001.

[48] J.-T. Kuo, W.-H. Hsu, and W.-T. Huang, "Parallel coupled microstrip filters with suppression of harmonic response," *IEEE Microwave Wireless Compon. Lett.*, vol. 12, no. 10, pp. 383–385, Oct. 2002.

[49] B. S. Kim, J. W. Lee, and M. S. Song, "An implementation of harmonic-suppression microstrip filters with periodic grooves," *IEEE Microwave Wireless Compon. Lett.*, vol. 14, no. 9, pp. 413–415, Sep. 2004.

[50] J. Garcia, F. Martin, F. Falcone, J. Bonache, J. D. Baena, I. Gil, E. Amat, T. Lopetegi, M. A. G. Laso, J. A. M. Iturmendi, M. Sorolla, and R. Marques, "Microwave filters with improved stopband based on sub-wavelength resonators," *IEEE Trans. Microw. Theroy Tech.*, vol. 53, no. 6, pp. 1997–2004, Jun. 2005.

[51] W.-H. Tu and K. Chang, "Compact microstrip bandstop filter using open stub and spurline," *IEEE Microwave and Wireless Components Letters*, vol. 15, no. 4, pp. 268–270, Apr 2005.

[52] Y.-Z. Wang and M.-L. Her, "Compact microstrip bandstop filter using stepped impedance resonator (SIR) and spurline," *IEE Proc.-Microw. Antennas Propagation*, vol. 153, no. 5, pp. 435–440, Oct. 2006.

[53] R. N. Bates, "Design of microstrip spurline bandstop filters," *IEE J. Microw. Optics, Acoustics*, vol. 1, pp. 209–214, Nov 1977.

[54] D.-J. Woo, T.-K. Lee, J.-W. Lee, C.-S. Pyo, and W.-K. Choi, "Novel U-slot and V -slot DGSs for bandstop filter with improved Q factor," *IEEE Transactions On Microwave Theory And Techniques*, vol. 54, no. 6, pp. 2840–2847, Jun. 2006.

[55] M. Mandal and S. Sanyal, "Compact bandstop filter using signal interference technique," *Electronics Letters*, vol. 43, no. 2, pp. 110 – 111, Jan. 2007.

[56] N. C. Karmakar, "Theoretical investigations into binomial distributions of photonic bandgaps in microstripline structures," *Microwave and Optical Technology Letters*, vol. 33, pp. 191–196, 2002.

[57] H. Shaman and J.-S. Hong, "Ultra-wideband (UWB) bandpass filter with embedded band notch structures," *IEEE Microwave Wireless Compon. Lett.*, vol. 17, no. 3, pp. 193–195, Mar. 2007.

[58] S. W. Wong and L. Zhu, "Implementation of compact UWB bandpass filter with a notch-band," *IEEE Microwave Wireless Compon. Lett.*, vol. 18, no. 1, pp. 10–12, Jan. 2008.

[59] G.-M. Yang, R. Jin, C. Vittoria, V. G. Harris, and N. X. Sun, "Small ultra-wideband (UWB) bandpass filter with notched band," *IEEE Microwave Wireless Compon. Lett.*, vol. 18, no. 3, pp. 176–178, Mar. 2008.

[60] A. Ali and Z. Hu, "Metamaterial resonator based wave propagation notch for ultrawideband filter applications," *IEEE Antennas and Wireless Propagation Letters*, vol. 7, pp. 210–212, 2008.

[61] L. Qi, L. Chang-Hong, Z. Wei, and X. Wei-Feng, "Novel compact UWB bandpass filter with notched band," *Microwave and Optical Technology Letters*, vol. 52, no. 2, pp. 280–283, Feb. 2010.

[62] P. Mondal and Y. L. Guan, "A coplanar stripline ultra-wideband bandpass filter with notch band," *IEEE Microwave and Wireless Components Letters*, vol. 20, no. 1, pp. 22–24, Jan. 2010.

[63] L. Zhu, H. Bu, and K. Wu, "Broadband and compact multi-pole microstrip bandpass filters using ground plane aperture technique," *IEE Proceedings on Microwave, Antennas and Propagation*, vol. 149, no. 1, pp. 71–77, Feb. 2002.

[64] L. Zhu, S. Sun, and W. Menzel, "Ultra-wideband (UWB) bandpass filters using multiple mode resonator," *IEEE Microwave Wireless Compon. Lett.*, vol. 15, no. 11, pp. 796–798, Nov. 2005.

[65] F. Falcone, T. Lopetegi, M. A. G. Laso, J. D. Baena, J. Bonache, M. Beruete, R. Marques, F. Martin, and M. Sorolla, "Babinet principle applied to metasurface and metamaterial design," *Physics Review Letters*, vol. 93, pp. 197 401(1)–197 401(4), 2004.

[66] F. R. Yang, K. P. Ma, Y. Qian, and T. Itoh, "A uniplanar compact photonic-bandgap (UC-PBG) structure and its applications for microwave circuits,," *IEEE Transactions on Microwave Theory and Techniques*, vol. 47, no. 8, pp. 1509–1514, Aug. 1999.

[67] J.-T. Kuo, M. Jiang, and H.-J. Chang, "Design of parallel coupled microstrip filters with suppression of spurious resonances using substrate suspension," *IEEE Transactions on Microwave Theory and Techniques*, vol. 52, no. 1, pp. 83–89, Jan. 2004.

[68] J. T. Kuo and M. Jiang, "Enhanced microstrip filter design with a uniform overlay for suppressing the second harmonic response," *IEEE Microwave and Wireless Components Letters*, vol. 14, no. 9, pp. 419–421, Sep. 2004.

[69] M. C. V. Ahumada, J. Martel, and F. Medina, "Parallel coupled microstrip filters with ground-plane aperture for spurious band suppression and enhanced coupling," *IEEE Transactions on Microwave Theory and Techniqus*, vol. 52, no. 3, pp. 1082–1086, Mar. 2004.

[70] ——, "Parallel coupled microstrip filters with floating ground-plane conductor for spurious band suppression," *IEEE Transactions on Microwave Theory and Techniques*, vol. 53, no. 5, pp. 1823–1828, May 2005.

[71] C.-Y. Cheng and R. W. Ziolkowski, "Tailoring double-negative metamaterial responses to achieve anomalous propagation effect along microstrip transmission lines," *IEEE Transactions on Microwave Theory and Techniques*, vol. 51, no. 12, pp. 2306–2314, Dec. 2003.

[72] L. Huangfu, L. Ran, H. Chen, X. Zhang, K. Chen, T. M. Grzegorczyk, and J. A. Kong, "Experimental confirmation of negative refractive index of a metamaterial composed of omega-like metallic patterns," *Applied physics Letter*, vol. 84, pp. 1537–1539, 2004.

[73] V. Crnojevic-Bengin, V. Radonic, and B. Jokanovic, "Left-handed microstrip lines with multiple complementary split-ring and spiral resonators," *Microwave and Optical Technology Letters*, vol. 49, no. 6, pp. 1391–1395, Jun. 2007.

[74] N. T. Messiha, A. M. Ghuniem, and H. M. EL-Hennawy, "Planar transmission line medium with negative refractive index based on complementary omega-like structure," *IEEE Microwave Wireless Compon. Lett.*, vol. 18, no. 9, pp. 575–577, Sep. 2008.

[75] D. Hyun and W. S. Park, "Extraction of effective permitivity and permeability of periodic metamaterial cells," *Microwave and Optical Technology Letters*, vol. 51, no. 8, pp. 1824–1830, Aug. 2009.

[76] C. Zhu, J.-J. Ma, L. Chen, and C.-H. Liang, "Negative index metamaterial composed of triangular open-loop resonator and wire structure," *Microwave and Optical Technology Letters*, vol. 51, no. 9, pp. 2022–2025, Sep. 2009.

[77] M. B. Manapati and R. S. Kshetrimayum, "SAR reduction in human head from mobile phone radiation using single negative metamaterials," *Journal of Electromagnetic Waves and Applications*, vol. 23, no. 10, pp. 1385–1395, 2009.

[78] M. Palandoken and H. Henke, "Fractal spiral resonator as magnetic metamaterial," in *IEEE Applied Electromagnetic conference*, Kolkatta, 2009.

[79] J. Bonache, M. Gil, I. Gil, J. Garcia-Garcia, and F. Martin, "On the electrical characteristics of complementry metamaterial resonators," *IEEE Microwave and Wireless Components Letters*, vol. 16, no. 10, pp. 543–545, Oct. 2006.

[80] I. Gil, J. Bonache, M. Gil, J. Garcia-Garcia, and F. Martin, "Left-handed and right-handed transmission properties of microstrip lines loaded with complementary split rings resonators," *Microwave and Optical Technology Letters*, vol. 48, pp. 2508–2511, 2006.

[81] M.-Sindreu, F. Aznar, A. Velez, J. Bonache, and F. Martin, "New composite right/left handed transmission lines based on electrically small open resonators," in *Microwave Symposium Digest*, 2009, pp. 45–48.

[82] X.Ying and A. Alphones, "Propagation characteristics of complementary split ring resonator (CSRR) based EBG structure," *Microwave and Optical Technology Letters*, vol. 47, pp. 197–199, 2005.

[83] C.-S. Kim, J.-S. Lim, S. Nam, K.-Y. Kang, and D. Ahn, "Equivalent circuit modeling of spiral defected ground structure for microstrip line," *Electronics Letters*, vol. 38, pp. 1109–1111, Sep. 2002.

[84] J. S. Park, J. S. Yun, and D. Ahn, "A design of the novel coupled line bandpass filter using defected ground structure with wide stopband performance," *IEEE Tran. Microw. Theory Tech.*, vol. 50, no. 9, pp. 2037–2043, Sep. 2002.

[85] A. B. A. Rahman, A. K. Verma, A. Boutejdar, and A. S. Omar, "Control of bandstop response of hi-lo microstrip low-pass filter using slot in ground plane," *IEEE Transactions on Microw. Theory and Techniques*, vol. 52, no. 3, pp. 1008–1013, Mar. 2004.

[86] M. K. Mandal and S. Sanyal, "A novel defected ground structure for planar circuits," *IEEE Microwave and Wireless Components Letters*, vol. 16, no. 2, pp. 93–95, Feb. 2006.

[87] S.-W. Ting, K.-W. Tam, and R. P. Martins, "Miniaturized microstrip lowpass filter with wide stopband using double equilateral U-shaped defected ground structure," *IEEE Microwave and Wireless Components Letters*, vol. 16, no. 5, pp. 240–242, May 2006.

[88] R. Li and L. Zhu, "Compact UWB bandpass filter using stub loaded multiple mode resonator," *IEEE Microwave Wireless Compon. Lett.*, vol. 17, no. 1, pp. 40–42, Jan. 2007.

[89] X. Chen, L. Wang, L. Weng, and X. Shi, "Compact lowpass filter using novel elliptic shape DGS," *Microwave and Optical Technology Letters*, vol. 51, no. 4, pp. 1088–1091, Apr. 2009.

[90] P. Kurgan and M. Kitlinski, "Novel doubly perforated broadband microstrip branchline couplers," *Microwave and Optical Technology Letters*, vol. 51, no. 9, pp. 2149–2152, Sep. 2009.

[91] S. S. Karthikeyan and R. S. Kshetrimayum, "Compact wideband bandpass filter using open slot split ring resonator and CMRC," *Progress In Electromagnetics Research Letters*, vol. 10, pp. 39–48, 2009.

[92] C.-L. Hsu, F.-C. Hsu, and J.-T. Kuo, "Microstrip bandpass filters for ultra-wideband (UWB) wireless communications," in *Proceedings of IEEE MTT-S International Conference*, 2005, pp. 679–682.

[93] G. M. Yang, R. H. Jin, and J. P. Geng, "Planar microstrip UWB bandpass filter using U-shaped slot coupling structure," *Electronics Letters*, vol. 42, no. 25, pp. 1461–1463, Dec. 2006.

[94] M. Shobeyri and M. H. V. Samiei, "Compact ultra-wideband bandpass filter with defected ground structure," *Progress In Electromagnetics Research Letters*, vol. 4, pp. 25–31, 2008.

[95] J. An, G.-M. Wang, W.-D. Zeng, and L.-X. Ma, "UWB filter using defected ground structure of von koch fractal shape slot," *Progress In Electromagnetics Research Letters*, vol. 6, pp. 61–66, 2009.

[96] S. Sun, L. Zhu, and H.-H. Tan, "A compact wideband bandpass filter using transversal resonator and asymmetrical interdigital coupled lines," *IEEE Microwave and Wireless Components Letters*, vol. 18, no. 3, pp. 173–175, Mar. 2008.

[97] C. Li, K.-Y. Liu, and F. Li, "Design of microstrip highpass filters with complementary split ring resonators," *Electronics Letters*, vol. 43, no. 1, pp. 35–36, Jan. 2007.

[98] Q. Xue, K. M. Shum, and C. H. Chan, "Novel 1-D microstrip PBG cells," *IEEE Microwave and Wireless Components Letters*, vol. 10, no. 10, pp. 403–405, Oct. 2000.

[99] B.-L. Ooi, "Compact EBG in-phase hybrid-ring equal power divider," *IEEE Trans. Microw. Theory Tech.*, vol. 53, no. 7, pp. 2329–2324, 2005.

[100] F. Martin, J. Bonache, F. Falcone, M. Sorolla, and R. Marques, "Split ring resonator based left-handed coplanar waveguide," *Applied physics Letter*, vol. 83, no. 22, pp. 4652–4654, Dec. 2003.

[101] M. Gil, J. Bonache, J. Garcia-Garcia, J. Martel, and F. Martin, "Composite right/left handed (CRLH) metamaterial transmission lines based on complementary split rings resonators (CSRRs) and their applications to very wide band and compact filter design," *IEEE Transactions on Microwave Theory and Techniques*, vol. 55, no. 6, pp. 1293–1304, Jun. 2007.

[102] S. S. Karthikeyan and R. S. Kshetrimayum, "Composite right/left handed transmission line based on open slot split ring resonator," *Microwave and Optical Technology Letters*, vol. 52, no. 8, pp. 1729–1731, Aug. 2010.

[103] F. Aznar, A. Velez, M. Duran-Sindreu, J. Bonache, and F. Martin, "Elliptic-function CPW low-pass filters implemented by means of open complementary split ring resonators (OCSRRs)," *IEEE Microwave and Wireless Components Letters*, vol. 19, no. 11, pp. 689–691, Nov. 2009.

[104] R. E. Collin, *Foundations for Microwave Engineering*. New York: McGraw-Hill, 1996.

[105] H.-W. Li, Z.-F. Li, X.-W. Sun, S. Kurachi, J. Chen, and T. Youhimasu, "Theoretical analysis of dispersion characteristics of microstrip lines with defected ground structure," *Journal of Active and Passive Electronic Devices*, vol. 2, no. 3, pp. 315–322, 2007.

[106] L. Li, Z.-F. Li, and Q.-F. Wei, "Compact and selective lowpass filter with very wide stopband using tapered compact microstrip resonant cells," *Electronics Letters*, vol. 45, no. 5, pp. 267–268, 2009.

[107] K. Deng, Q. Xue, and W. Che, "Improved compact microstrip resonance cell lowpass filter with wide stopband characteristics," *Electronics Letters*, vol. 43, no. 8, pp. 46–464, 2007.

[108] K. M. Shum, Q. Xue, and C. H. Chan, "A novel microstrip ring hybrid incorporating a PBG cell," *IEEE Microwave and WirelessComponents Letters*, vol. 11, no. 6, pp. 258–260, Jun. 2001.

[109] J.-S. Lim, S.-W. Lee, J.-S. Park, D. Ahn, and S. Nam, "A 4:1 unequal wilkinson power divider," *IEEE Microwave and Wireless Components Letters*, vol. 11, no. 3, pp. 124–126, Mar. 2001.

[110] C.-M. Lin, H.-H. Su, J.-C. Chiu, and Y.-H. Wang, "Wilkinson power divider using microstrip EBG cells for the suppression of harmonics," *IEEE Microwave and Wireless Components Letters*, vol. 17, no. 10, pp. 700–702, Oct. 2007.

[111] D. Packiaraj, A. Bhargavi, M. Ramesh, and A. T. Kalghatgi, "Compact power divider using defected ground structure for wireless applications," in *IEEE-International Conference on Signalprocessing, Communications and Networking*, Chennai, 2008, pp. 25–29.

[112] M. Ramesh, D. Packiaraj, and A. T. Kalghatgi, "A compact branch line coupler using defected ground structure," *Journal of Electromagnetic Waves and Applications*, vol. 22, no. 2-3, pp. 267–276, 2008.

[113] E. Saenz, A. Cantora, I. Ederra, R. Gonzalo, and P. de Maagt, "A metamaterial T-junction power divider," *IEEE Microwave and Wireless Components Letters*, vol. 17, no. 3, pp. 172–174, Mar. 2007.

[114] H. Ghali and T. A. Moselhy, "Miniaturized fractal rat-race, branch-line, and coupled-line hybrids," *IEEE Transcation on Microwave Theory and Techniques*, vol. 52, no. 11, pp. 2513–2520, Nov. 2004.

[115] Y. J. Sung, C. S. Ahn, and Y.-S. Kim, "Size reduction and harmonic suppression of rat-race hybrid coupler using defected structure," *IEEE Microwave and Wireless Components Letters*, vol. 14, no. 1, pp. 7–9, Jan. 2004.

[116] J. Gu and X. Sun, "Miniaturization and harmonic suppression rat-race coupler using C-SCMRC resonators with distributive equivalent circuit," *IEEE Microwave and Wireless Components Letters*, vol. 15, no. 12, pp. 880–882, Dec. 2005.

[117] J.-T. Kuo, J.-S. Wu, and Y.-C. Chiou, "Miniaturized rat race coupler with suppression of spurious passband," *IEEE Microwave and Wireless Components Letters*, vol. 17, no. 1, pp. 46–48, Jan. 2007.

[118] G. Siso, M. Gil, J. Bonache, and F. Martin, "Application of metamaterial transmission lines to design of quadrature phase shifters," *Electronics Letters*, vol. 43, no. 20, pp. 1098–1100, 2007.

[119] P. Mondal and A. Chakrabarty, "Design of miniaturised branch-line and rat-race hybrid couplers with harmonics suppression," *IET Microw. Antennas Propag.*, vol. 3, no. 1, pp. 109–116, 2009.

[120] G. Siso, J. Bonache, M. Gil, J. Garcia-Garcia, and F. Martin, "Compact rat-race hybrid coupler implemented through artificial left handed and right handed lines," in *IEEE/MTT-S International Microwave Symposium*, 2007, pp. 25–28.

List of Publications

Journal Papers:

1. S. S. Karthikeyan and R. S. Kshetrimayum, "Compact, harmonic suppressed power divider using open complementary split ring resonator," *submitted to Microwave and Optical Technology Letters.*

2. S. S. Karthikeyan and R. S. Kshetrimayum, "Size miniaturized rat-race coupler using open complementary split ring resonator," *submitted to IEICE Transaction on Electronics.*

3. S. S. Karthikeyan and R. S. Kshetrimayum, "Compact lowpass filter design using open slot split ring resonator," *submitted to AEU International Journal of Electronics and Communication.*

4. S. S. Karthikeyan and R. S. Kshetrimayum, "Compact, deep and wide rejection bandwidth lowpass filter using open complementary split ring resonator," *Microwave and Optical Technology Letters*, vol. 53, no. 4, pp. 845-848, Apr. 2011.

5. S. S. Karthikeyan and R. S. Kshetrimayum, "Notched UWB bandpass filter using complementary single split ring resonator," *IEICE Electronics Express*, vol. 7, pp. 349–355, Sep. 2010.

6. S. S. Karthikeyan and R. S. Kshetrimayum, "Composite right/left handed transmission line based on open slot split ring resonator," *Microwave and Optical Technology Letters*, vol. 52, no. 8, pp. 1729-1731, Aug. 2010.

7. S. S. Karthikeyan and R. S. Kshetrimayum, "Compact wideband bandpass filter using open slot split ring resonator and CMRC," *Progress in Electromagnetics Research Letters*, vol. 10, pp. 39-48, 2009.

8. S. S. Karthikeyan and R. S. Kshetrimayum, "Harmonic suppression of parallel coupled microstrip line bandpass filter using CSRR," *Progress in Electromagnetics Research Letters*, vol. 7, pp. 193-201, 2009.

9. R. S. Kshetrimayum, S. S. Karthikeyan and D. Dey, "Band gap determination of triangular lattice EBGs in the ground plane," *AEU International Journal of Electronics and Communication*, vol. 63, no. 8, pp. 699-702, Aug. 2009.

10. S. S. Karthikeyan and R. S. Kshetrimayum, "A parametric study on the stopband characteristics of CSRRs," *International Journal of Recent Trends in Engineering*, vol. 1, no. 3, pp. 274-276, 2009.

11. R. S. Kshetrimayum, K. Sridhar and S. S. Karthikeyan, "Stop band characteristics for periodic patterns of CSRRs in the ground plane and its applications in harmonic suppression of bandpass filters," *International Journal of Microwave and Optical Technology*, vol. 3, no. 2, pp. 88-95, Apr. 2008.

12. R. S. Kshetrimayum, K. Sridhar and S. S. Karthikeyan, "Stopband characteristics for periodic patterns of CSRRs in the ground plane," *IETE Technical Review*, vol. 24, no. 6, pp. 449-460 , Dec. 2007.

Conference Papers:

1. S. S. Karthikeyan and M. Arulvani, "Double negative metamaterial design using open split ring resonator," *in Proc. IEEE Tech. Sym.*, Kharagpur, India, Apr. 3-4, 2010.

2. S. S. Karthikeyan, and R. S. Kshetrimayum, "Performance enhancement of microstrip bandpass filter using CSSRR," *in Proc. International Conference on Advances in Computing, Control, and Telecommunication Technologies*, Trivandrum, India, Dec. 28-29, 2009.

3. S. S. Karthikeyan and R. S. Kshetrimayum, "Slot split ring resonators and its applications in performance enhancement of microwave filter," *in Proc. IEEE Applied Electromagnetics Conference*, Kolkata, India, Dec. 14-16, 2009. (**Student Author Award**)

4. R. S. Kshetrimayum, V. K. Reddy and S. S. Karthikeyan, "Novel wide stopband filter using CSRR and open stubs," *in Proc. IEEE INDICON*, Bangalore, India, Sep. 6-8, 2007.